PRECISION WAVELENGTH MEASUREMENTS OF THE ANNIHILATION

RADIATION FROM COPPER 64 AND GAMMA-RADIATION

FOLLOWING DECAY OF GOLD 198 AND TANTALUM 182

Thesis by

Harry Charles Hoyt

In Partial Fulfillment of the Requirements

for the Degree of

Doctor of Philosophy

California Institute of Technology

Pasadena, California

1952

ACKNOWLEDGMENTS

The author wishes to express his gratitude to Dr. J.W.M. DuMond, who suggested the research topics described here, and whose guidance and advice have been invaluable. The assistance of Dr. David E. Muller in making the measurements and his part in the endless discussions of the results and their interpretation are gratefully acknowledged.

ABSTRACT

The geometry, kinematics, and operation of the curved crystal gamma-ray spectrometer are briefly described. The effect of a recently discovered systematic non-linearity is discussed in some detail. A new calibration of the instrument and the means taken to correct for the non-linearity are described. Error-contributing factors are analyzed, and their contributions to the final error are estimated. The three principal components of the observed line profile are discussed.

A new measurement of the annihilation radiation is reported. The relation of this measurement to the determination of the mass of the positron is discussed. Measurements of the wavelength of the 411 Kev gamma-ray line following the decay of Au^{198} are given. Wavelengths of sixteen gamma-ray lines following decay of Ta^{182} are tabulated. The formulation of an energy level scheme for its daughter W^{182} is discussed.

TABLE OF CONTENTS

I. THE GAMMA-RAY SPECTROMETER

A. Geometry and Kinematics

The principles regarding the use of bent crystal laminae for the focussing of x-rays have been known for some time and have been discussed extensively in the literature.[1,2] The comparatively recent application of these concepts to gamma-ray spectroscopy has given the field of nuclear physics a new and powerful tool for the precision study of nuclear spectra. Prior to the development of the focussing curved crystal gamma-ray spectrometer, the determination of nuclear energy level schemes was at best an uncertain process; now for the first time it is possible to determine all or parts of nuclear energy level schemes with (near) absolute certainty. Another very important application of the spectrometer lies in the field of fundamental constants of physics. Two combinations of these constants, h/e and $h/m_o c$, can be and have been studied with the curved crystal spectrometer; one of these experiments ($h/m_o c$) will be discussed in detail in this thesis.

Crystal spectrometers utilizing single bent crystal laminae may be divided into two types: reflection spectrometers and transmission spectrometers. Although the fundamental concepts are the same for these two types, the particular application for which a spectrometer is designed will determine which type is more advantageous. In the present case, where measurement of very short gamma-ray wavelengths is the goal, the transmission spectrometer is the more suitable instrument. Subsequent discussion shall be limited to this case.

There are two requirements which must be satisfied in order to produce the proper focussing action in the spectrometer. The first of

these, governing the location of the reflecting planes, is that at all of the reflecting planes the angle of deviation of the reflected beam from the direction of the incident beam must be the same. This angle is given by the well-known Bragg equation

$$\phi = 2 \sin^{-1}\left(\frac{n\lambda}{2d}\right)$$

This condition can be satisfied by placing the reflecting planes of the lamina so that they lie on a circle passing through the focal (source) point. The second requirement, governing the orientation of the reflecting planes, states that the angle of incidence at the reflecting plane must equal the angle of reflection. These angles must be the same for all the reflecting planes. Hence the reflecting planes must, when extended, intersect at a common point lying on the circle through the focal point and the reflecting planes. The resulting situation (transmission case only) is shown in Fig. 1.

Inspection of Fig. 1 brings to light some interesting facts regarding the preparation of the crystal lamina. Both of the conditions require that the lamina be bent, but the bending required is different in the two cases. For all of the reflecting planes to lie on the focal circle, a flat lamina must be bent so that its radius of curvature is r, the radius of the focal circle. For the reflecting planes to be properly oriented (so that their extensions intersect at the point β) the lamina must be bent to a radius of curvature equal to the diameter, 2r, of the focal circle. The solution of this apparent dilemma lies in the fact that the two conditions for focussing do not require that the reflecting planes maintain a constant angle with the surfaces of entrance and exit to the

crystal lamina. Thus by a combination of profiling the surfaces and bending, the lamina can be brought to the desired state for proper focussing action.

Curved crystal spectrometers have been constructed by first profiling the unstressed crystal lamina to a radius of curvature equal to the diameter of the focal circle and then bending it until the spectra focus on the focal circle. Fortunately, however, there is a more practical solution to the problem than the difficult profiling of the lamina. Cauchois[3] was the first to point this out. She showed that the condition on the orientation of the reflecting planes (our second condition) is the more stringent; and if the arc of the focal circle covered by the crystal is not too large, the aberrations of focussing can be kept small enough for practical purposes without necessitating profiling the surfaces of the lamina. Another important observation made by Cauchois concerned the variation of grating space from front to rear of the lamina when bent. Her considerations showed that in the transmission spectrometer, it is the neutral axis (or median plane) of the lamina which must be placed tangent to the focal circle when the lamina is bent. The geometry of the practical solution of the transmission spectrometer is shown in Fig. 2. This is the actual geometry of the curved crystal gamma-ray spectrometer. The crystal lamina used is 2 mm thick and has an area of about 2" x 1.75". It is clamped between two accurately cylindrically profiled stainless steel blocks so as to have a radius of curvature of 2 meters. The blocks are provided with holes through which the radiation can pass. The lamina is of quartz, cut so that the reflection (310) planes are normal to the surfaces.
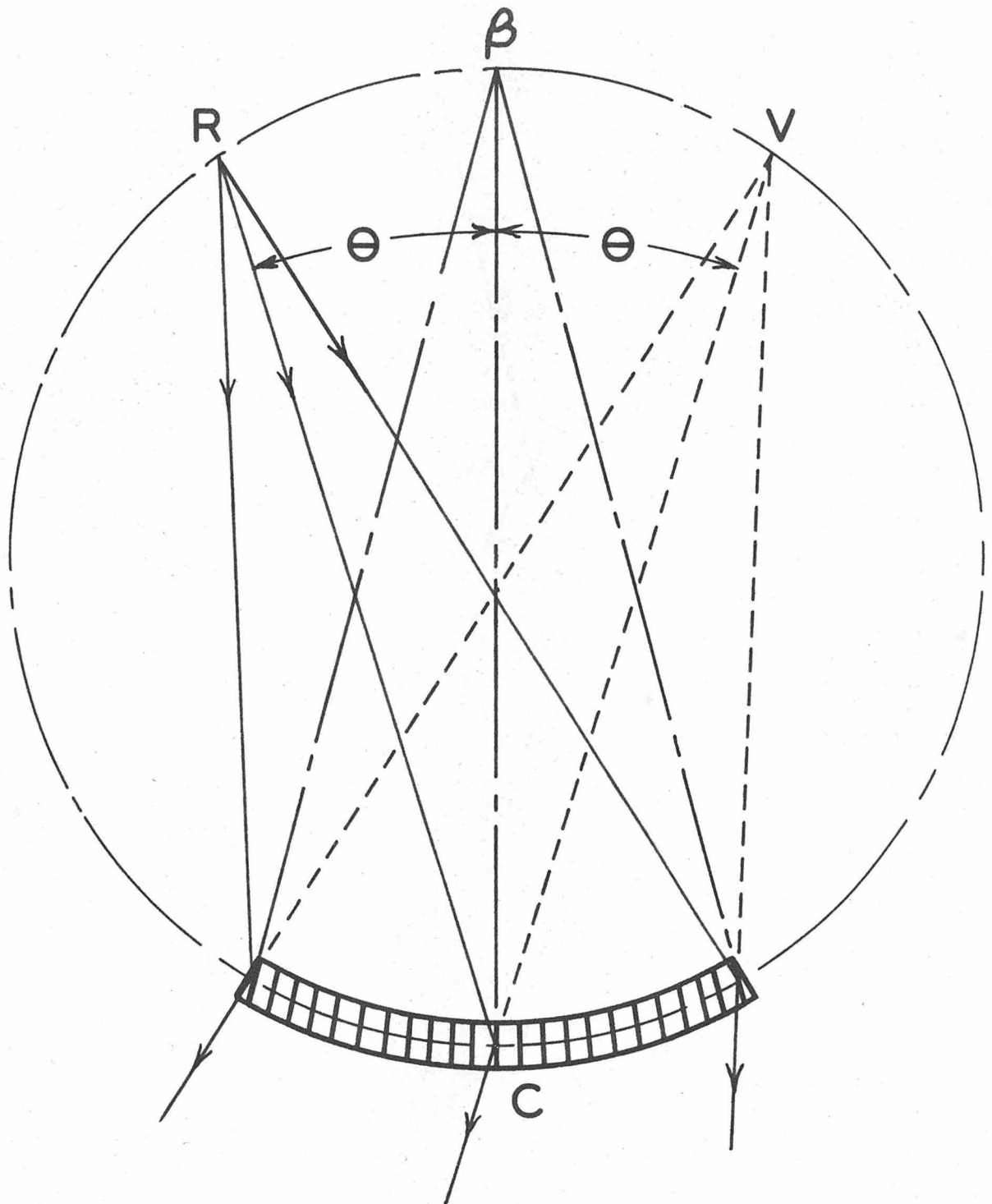
FIG. 1 - THE EXACT SOLUTION FOR THE
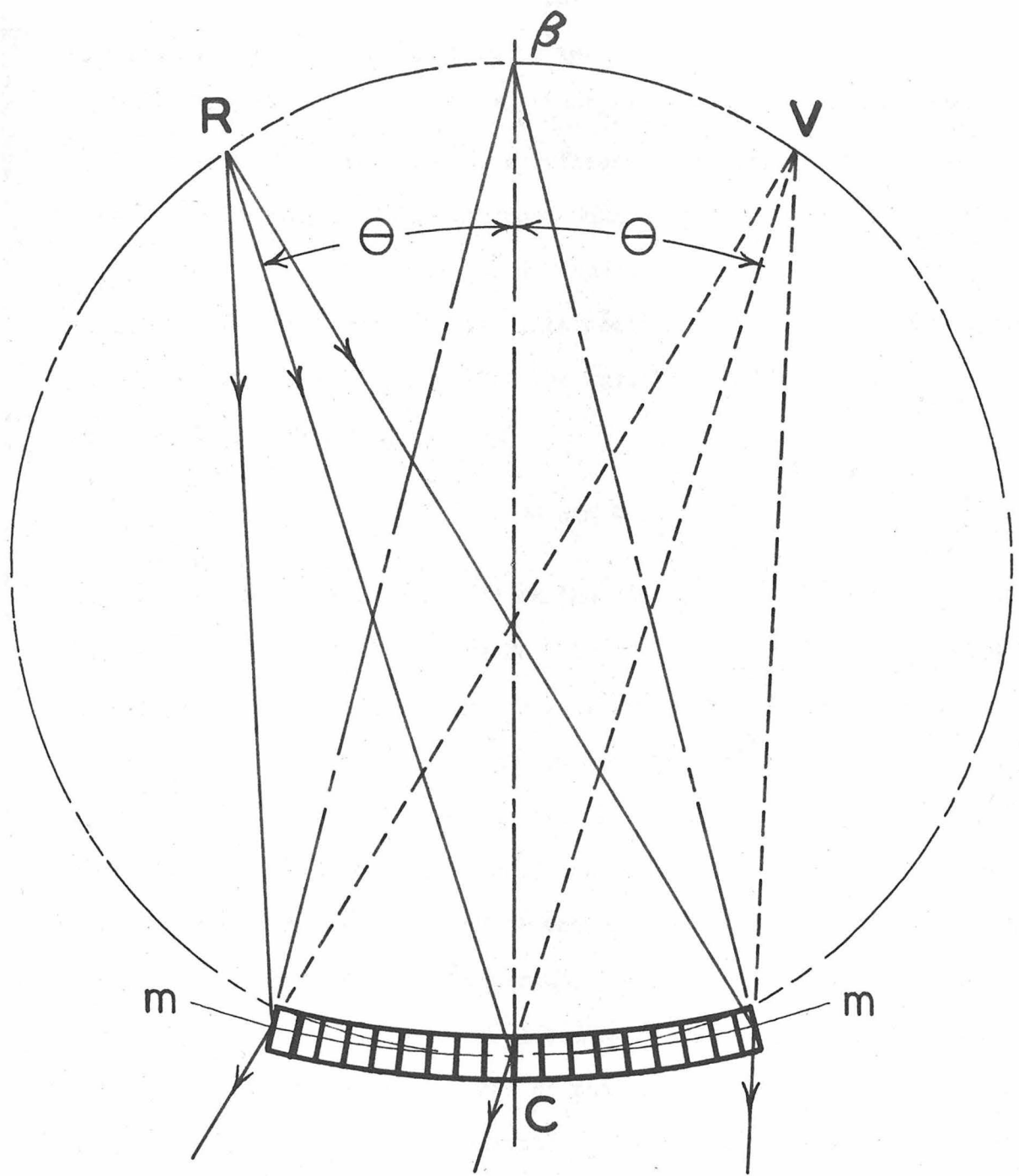TRANSMISSION SPECTROMETER

FIG. 2- THE PRACTICAL SOLUTION FOR THE
TRANSMISSION SPECTROMETER

It is readily apparent from both Fig. 1 and Fig. 2 that the transmission spectrometer may be used in two ways. First, a source of radiation may be placed at R on the focal circle. When the proper (Bragg) angle is set on the instrument, a reflected beam appears on the opposite side of the crystal. This divergent beam appears to come from V. The virtual focus V and the real focus R are symmetrically located on the focal circle with respect to the intersection of the reflecting planes of the crystal, the "β- point". The wavelength of the reflected radiation is given by the Bragg equation.

$$n\lambda = 2d \sin \Theta .$$

Second, the source may be placed on the opposite side of the crystal. In this case a beam converging toward V is reflected so as to focus at R. The Bragg equation applies here as well as in the preceding case. The requirements of the experiment dictate the way the spectrometer is to be used. A source at R must be confined to a small volume or be defined by a slit (the ideal is a line source), whereas a source on the opposite side of the crystal must be extended if the entire area of the crystal is to be used. Use of radioactive materials as sources of gamma-radiation is more practical if the source is placed at R. Unfortunately, however, the gain in luminosity due to use of the entire crystal is partially cancelled by the high specific activity of the source required by the small focal volume. This difficulty can be alleviated only by the use of sensitive detecting devices.

The actual measurement of a gamma- or x-ray wavelength involves the measurement of the Bragg angle Θ corresponding to this wavelength. Rather than measure this angle itself, which requires accurate knowledge

of the position of intersection of the extended reflecting planes (the
β- point), reflections from opposite sides of the reflecting planes may
be studied. The angular difference between the two positions of the
source, which correspond to the interchange of R and V in Figures 1 and
2, gives twice the Bragg angle Θ. A further refinement may be intro-
duced by measuring the sine of the angle instead of the angle itself. In
this case the difference reading gives 2 sin Θ, which is precisely the
factor which must be inserted in the Bragg equation

$$n\lambda = 2d \sin \Theta .$$

In addition, the wavelength is proportional to sin Θ, and consequently
the measuring device for sin Θ may be calibrated directly in terms of
wavelength if the grating space d or a reference wavelength is known.
Thus the spectrometer becomes a direct reading instrument. In actual
practice a reference wavelength, that of the tungsten $K\alpha_1$ x-ray line, is
used for calibration.

The kinematic design of the gamma-ray spectrometer is shown in Fig.
3. The crystal C is mounted so as to have its median plane (neutral
axis) tangent to the 2 meter diameter focal circle F. The source R is
constrained to move on the circumference of the focal circle by means of
a rigid radius bar OR. The sine of the Bragg angle Θ is measured by two
precision screws located in a travelling carriage Q which moves along a
swinging track T. A second carriage L moves along Q. The crystal C, the
center of the focal circle O, and the β - point are rigidly connected
together and to the screw carriage Q by a steel beam terminated by a $1\frac{1}{4}$
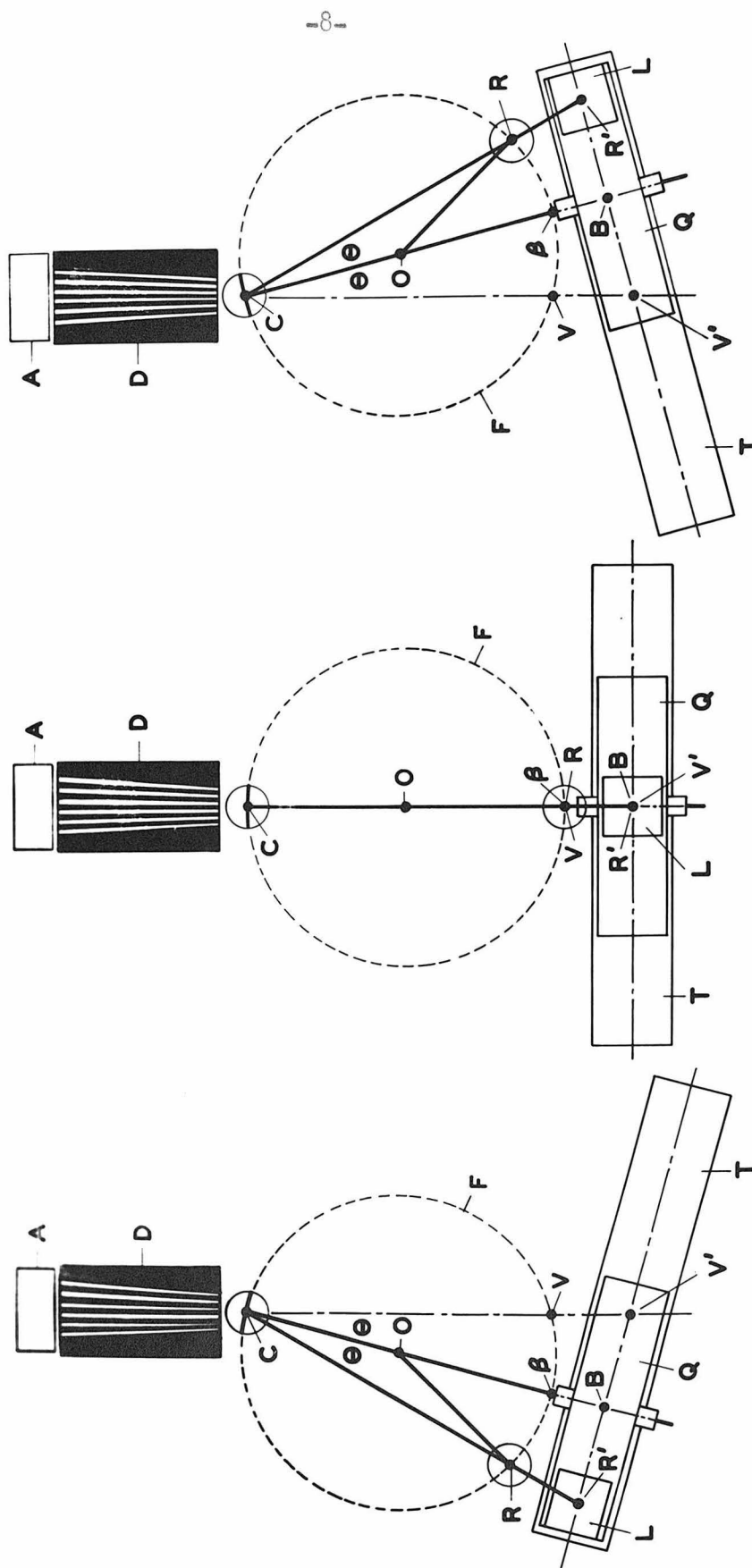inch steel rod which runs through the center of Q. The source R is

Fig. 3 — Illustrating the kinematics of the curved crystal gamma-ray spectrometer. The central (zero) position and settings of the instrument for the same wavelength are shown.

connected to the crystal pivot (not the crystal) and the upper carriage L by a steel beam, and is allowed to run back and forth along this beam so that it may remain on the focal circle. The upper screw in carriage Q is attached to L by a nut; the lower screw is attached to the pivot V' of the swinging track T by a nut. Thus the motions of L relative to Q and of Q relative to T are coupled by the two long precision screws located in Q. A more detailed drawing of the arrangement of the swinging track, carriages, screws and nuts is given in Section C (Fig. 10). The two screws have the same pitch; consequently the distances R'B and BV' are always equal. And since CR' and CV' are fixed lengths, both R'B and BV' are a measure of $\sin \theta$. In actual practice the distance R'B is used, dimensions of the instrument being so chosen that one revolution of the screws moves L relative to Q and Q relative to T a distance of about one millimeter, this distance corresponding to a wavelength change of about one x.u. (Siegbahn scale). The distance through which R' moves relative to Q (or the point B) in going from reflection on one side of the crystal reflection planes to reflection on the other side is proportional to $2 \sin \theta$, or twice the wavelength of the radiation being studied. The central position of the instrument and corresponding wavelength settings on either side of center are shown in the figure.

At settings for very short wavelengths the direct beam which passes through the crystal without reflection tends to obscure the reflected beam, since the angular separation of the two beams is small (about 20 minutes of arc for 1 Mev radiation). Any detecting device placed behind the crystal must have a fairly large entrance aperture due to the divergence of the reflected beam, and hence is bound to intercept a fraction

of the direct beam at small reflection angles. Consequently auxiliary means for separating the reflected and direct beams must be used. Such a separation is achieved by use of a baffle, commonly called the collimator, consisting of tapered lead sheets held apart by similarly tapered spacers. The collimator, D in Fig. 3, allows radiation up to about 1.5 Mev in energy (corresponding to $\sim$ 15 minutes of arc) to be studied. Above this energy radiation scattered from the tapered lead sheets in the collimator obscures the reflected beam. It should be emphasized that the collimator has nothing to do with the resolution of the instrument, but serves merely to separate direct and reflected beams. The radiation detector A is placed behind the collimator.

There are two feasible methods available for carrying out the motions necessary to the measurement of wavelengths. The first of these, employed in the present gamma-ray spectrometer and indicated in Fig. 3, is to fix the direction of the reflected beam (i.e., the collimator) and to move crystal and source. The second is to fix the source position and move the crystal and collimator. The first method requires elaborate mechanical methods for accurately determining the relative positions and orientations of crystal and source; the second requires that only the crystal orientation be known accurately, since the collimator has nothing to do with the reflection and focussing properties of the spectrometer. Thus the second method conceivably can eliminate a large number of the sources of error present in the first method because of the large number of moving parts coupled to the crystal and source. A new spectrometer utilizing the second method is being designed at the present time. A considerable increase in precision is expected.

B. Operation

As mentioned in the previous section, the confinement of the radiation source to a small focal volume necessitates (1) use of high specific activities and (2) development of a sensitive detector. Because of the limitations imposed on the use of high specific activities by the low neutron absorption cross-sections for many of the materials studied (the spectrometer is limited to use of sources made by neutron bombardment or naturally radioactive substances for economic and other reasons) and by radiation hazards, the development of a sensitive detector is a very real problem and one of the most important problems connected with the use of the spectrometer.

The first solution of the detector problem was a multicellular Geiger counter. Briefly, this counter consisted of a large metal tube (either round or square in cross-section) closed at one end and placed so that the radiation passed axially down the tube. The front of the tube was covered and sealed by a thin metal window. Inside the tube a number of disks of some metallic material were evenly spaced and oriented so as to be normal to the radiation path. Anode collecting wires placed in each cell were attached to a central rod passing down the axis of the tube through holes in the disks. The gamma-ray beam ejected photoelectrons, Compton electrons and, for high energy radiation, pair electrons from the disks, and these particles triggered the counter. Use of several cells in this manner is equivalent to placing several conventional counters in the beam. Background due to cosmic radiation was reduced by means of appropriate anti-coincidence circuits; background due to scattered radiation by shielding the counter in all directions with at least $2\frac{1}{2}$ inches

of lead. Use of this multicellular counter and many variations of the basic design showed conclusively that the curved crystal gamma-ray spectrometer was capable of high precision work in nuclear spectroscopy. However, many disenchanting problems were encountered during the construction and use of these counters, and it was realized that a significant increase in luminosity must come through use of an entirely different type of detector. The multicellular counters have been described in more detail by Lind[4] and Brown.[5]

The development of the scintillation counter as a radiation detector provided the next approach to the specific problems of the gamma-ray spectrometer. The choice of phosphor and design and construction of the scintillation detector have been described in detail by D. E. Muller in his thesis[6]; consequently only a rudimentary description of the device will be given here. The scintillation crystal used is a large (3" x 3" x 1") single crystal of sodium iodide activated by a small amount of thallium impurity. This crystal is placed with its large faces normal to the radiation beam. The light pulses produced by interaction of the radiation with the matter of the crystal are observed from opposite sides of the crystal by two RCA 5819 photomultiplier tubes, which are optically joined to the glass crystal box by lucite light cones. The resultant signals from the photomultiplier tubes are then fed through separate preamplifiers to a coincidence circuit, and thence to the main amplifier, pulse height discriminators and scaler. Cosmic ray background is reduced appreciably by (1) presenting small crystal area in the vertical direction and (2) using a pulse height discriminator to eliminate abnormally large pulses such as are produced by cosmic rays. Noise from the

photomultiplier tubes is reduced by (1) the coincidence circuit and (2) a pulse height discriminator. Background due to scattered radiation is eliminated by thick lead shielding as before. A line drawing of the scintillation counter and a block diagram of the entire detector circuit are given in Figs. 4 and 5.

Installation of the scintillation counter in the spectrometer immediately showed a remarkable increase in the over-all luminosity of the instrument. As a result, sources as low as 10 millicuries can at times be used with satisfactory results; formerly about 100 millicuries was regarded as a lower limit. The energy range which can be studied has been extended down to about 50 Kev; the previous low energy limit was above 100 Kev. An interesting by-product of this extension of the energy range is that it permits the use of radioactive materials - namely, the WK_{α_1} x-ray line produced by internal conversion following decay of Ta^{182} - to calibrate the wavelength scale of the spectrometer. This elimination of the heavy x-ray tube (and its stiff high tension cables) formerly used for calibration has removed a possible source of error in the conversion factor from screw divisions to milliangstroms due to mechanical flexures in the spectrometer. The scintillation crystal has been in almost continuous use for over 18 months and there has been no detectable loss in sensitivity.

During a "run" of the spectrometer on a given gamma-ray line produced by radioactive decay in the source being studied, a pair of profiles corresponding to this gamma-ray line are obtained. The two members of this pair of profiles correspond to reflections from opposite sides of the crystal planes. The central position of the profile (usually an axis of

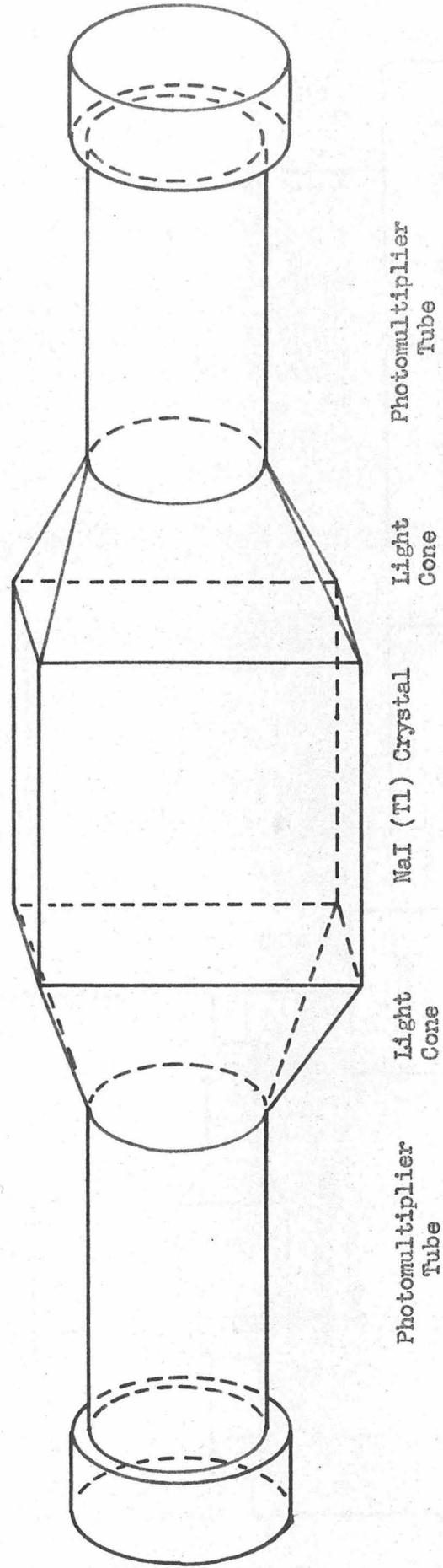Photomultiplier Tube   Light Cone   NaI (Tl) Crystal   Light Cone   Photomultiplier Tube

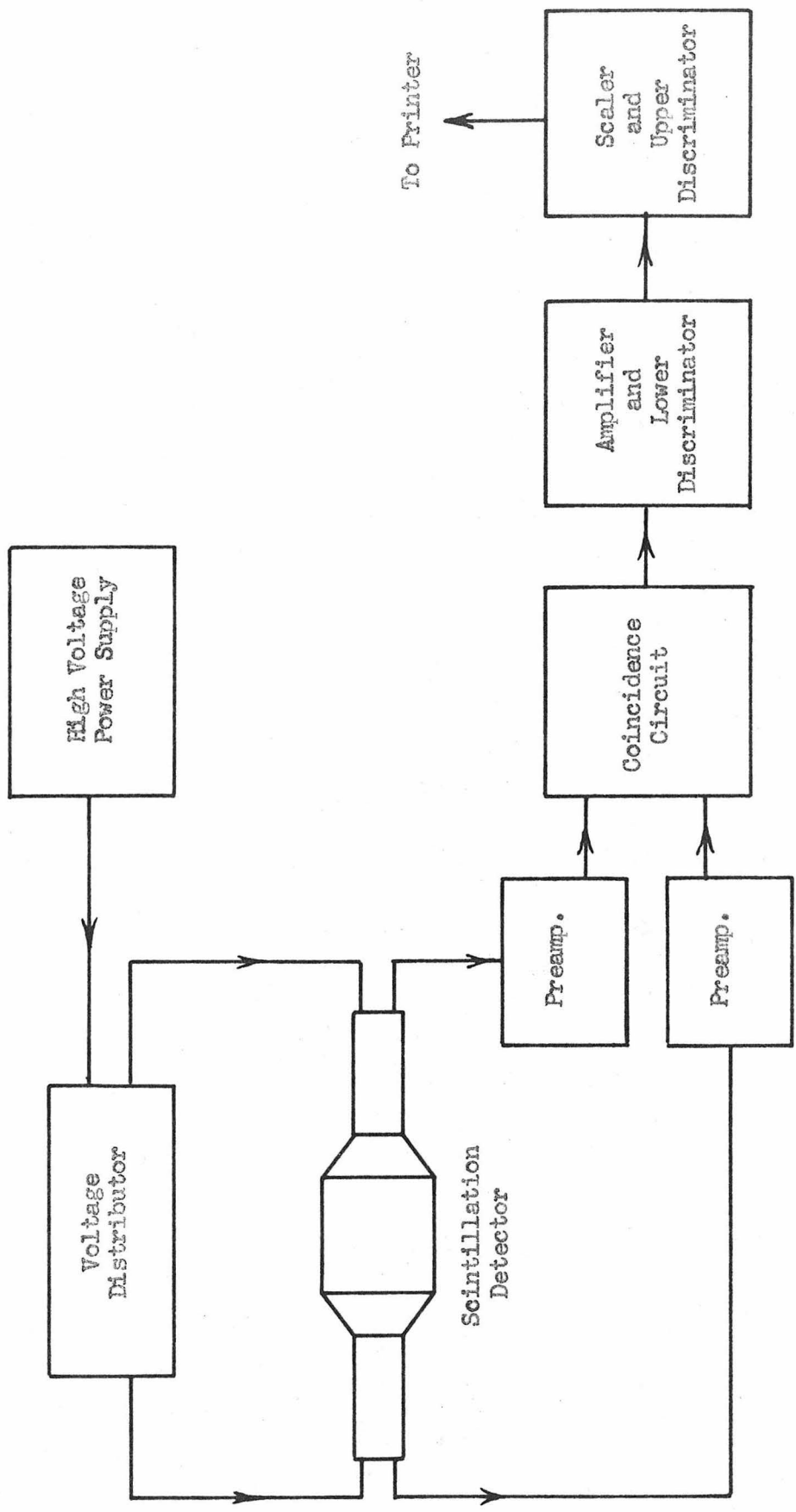Fig. 4 - Line Drawing of Scintillation Counter

Fig. 5 - Block Diagram of Entire Detector Circuit

symmetry) corresponds to the wavelength of the gamma-ray line. A typical pair of profiles is shown in Part II, Section B (Fig. 31). To obtain a profile, which may be from 0.3 to 0.6 x.u. (0.3 to 0.6 revolution of the screw) wide at its base, it is necessary to record counts at more than 20 different wavelength settings of the instrument. The counting interval at each point varies from one to thirty minutes, depending on the strength of the source and the counting statistics desired. A plot of counts per arbitrary unit time interval for the different wavelength settings then gives the desired profile. It is clear that if the spectrometer is to be operated manually, almost constant attendance by the experimenter is required. With continuous operation, as is necessary with short-lived sources, considerable wear-and-tear of personnel results. Hence it was deemed highly desirable to design and build an automatic observer to operate the instrument. This was done by James Kohl.

The following operations are carried out during a run across a profile: (1) the spectrometer is set to the desired wavelength position, (2) counts are accumulated for a given time interval, (3) a background count is taken with lead intercepting the gamma-ray beam, (4) total counts, time interval, and wavelength setting are recorded. The "robot" was built to perform all of these operations.

The timer is the basic unit of the robot, and is used to initiate each of the four operations. A clock motor trips a microswitch every minute, and the resultant signal produces a forward step in the cycle of operations. Counting intervals might conceivably be selected in two different ways: (1) to give the same number of counts, and thus the same statistical accuracy, at each wavelength setting or (2) to give the same

counting interval for all points. The second of these was chosen for the present robot. The size of counting interval used for a given run is a compromise value, usually chosen to give 1% statistics or slightly better at the peak of the profile. This counting interval is set on the robot and is thereafter repeated at each wavelength setting; the actual counting of the time spent at each setting is accomplished by means of telephone type stepping relays. The use of two stepping relays in series allows the counting interval to be divided into sub-intervals, total accumulated counts being recorded at the end of each sub-interval. In this way a continuous check on the behavior of the detector is possible. At the end of the counting interval signals are transmitted to the screw-set mechanism to move the spectrometer to the next wavelength position and to the printer to record the time and accumulated counts.

Accurate setting of the spectrometer is accomplished with a precisely machined wheel, divided into 100 alternate conducting and insulating sectors, which is attached to the screws. A contact riding on this wheel alternately makes and breaks contact in the circuit supplying power to the set motor. Breaking contact causes the spectrometer to stop at the wavelength position corresponding to the insulated section of the sector wheel. In order to permit skipping certain settings when desired, a programming mechanism is included in the screw-set circuit. This consists of a microswitch riding on a punched tape. The punched tape is projected forward by a small ratchet motor which is synchronized with the rotation of the sector wheel. As long as the microswitch contact rides on the tape the set motor continues to rotate the screws. When the contact drops through a hole in the tape, the next insulating section of the sector

wheel is selected as the stopping point. In this way an entire program
of pre-selected wavelength settings can be carried out. An additional
circuit has been added to insert about 5 inches of lead in the gamma-ray
beam at regular intervals to check the stability of the detector. When
these background readings are taken the set motor does not receive its
starting signal; thus no points on the profile are skipped.

The remainder of the robot is concerned with the recording of data.
There are four data which must be recorded for each point on the profile.
These are (1) the screw setting, (2) the time corresponding to the begin-
ning of the counting interval, (3) the time at which the counting inter-
val is ended, and (4) the accumulated counts. The screw settings are
transmitted to the recording unit, called the printer, by a selsyn arrange-
ment connected to the screw. The selsyns are not connected to the screw-
set circuit and therefore give the actual screw setting; this prevents
erroneous interpretation of data should the programming tape skip a setting.
Time is recorded on a set of counting wheels operated by a ratchet motor,
which in turn is operated by the clock signals. The desired times are re-
corded by causing the printer to print at both beginning and end of the
counting interval. The printed information gives the accumulated time in
minutes from the beginning of the run (or runs). Thus information necessary
for decay corrections, if any, is available. Counts are recorded on still
another set of counting wheels, which are operated by signals from the
scaler. As mentioned previously the printer prints at sub-intervals of
the chosen counting interval, recording accumulated counts each time.
Total counts are recorded at the end of the counting interval, and the
counting wheels are then reset to zero in preparation for the next counting

interval. An odd minute is provided between successive counting intervals; this allows ample time for screw-setting, to reset the counting wheels to zero, etc.

C. Calibration

In any experiment the presence of errors in the equipment used and in the judgment of the observer will affect the final results of the experiment. If the "true" value of the quantity being measured is to be ascertained with any certainty, these errors must be carefully analyzed by the experimenter. The result of such an analysis is to divide the errors into two general classes: (1) systematic errors and (2) random errors. The systematic errors are such that, if recognized, their effects can be determined and thereby eliminated from the final results by the application of appropriate correction factors. Random errors, on the other hand, are (or are assumed to be) of a statistical nature, and the experimenter can only estimate their magnitude. This estimate, however, when stated in the form of a standard deviation or a probable error gives an idea of how close to the "true" value the experimental result is, and therefore is a measure of the precision of the experiment. This section will be concerned only with systematic errors; discussion of random errors and precision will be deferred until the next section.

Systematic errors, once recognized, can be evaluated by either calculation or calibration. The particular circumstances of a given experiment will determine which method is to be used. In the case of the gamma-ray spectrometer calibration techniques are used exclusively. This is felt to be the safest approach, since some of the sources of systematic error are not completely understood.

The most obvious place to look for a systematic error is in the precision screws used to drive the two carriages and to measure the sine of the Bragg angle. First, the pitch of the screws, although intended to

correspond to one x.u. per revolution, does not do this exactly. This is corrected for by using the tungsten $K\alpha_1$ x-ray line to fix a point on the screws. It is then a simple matter to compute the x.u. per screw division, assuming the screws to be perfectly uniform helices. Actually, however, the screws are not perfect. For example, any periodic error in the lathe on which the screws were turned will be reflected in the screws themselves. There may also be other errors due to the machining processes. The existence of errors in the screws was recognized at the outset, and the screws were calibrated shortly after the spectrometer was put into operation.

Reference to Fig. 3, Section A, shows that the important quantity in the measurement of the sine of the Bragg angle is the position of the upper (source) carriage with respect to the lower (screw) carriage. To determine these positions accurately, a glass decimeter scale calibrated at the National Bureau of Standards was attached to the source carriage at the same level as the carriage and directly above the screw. A 100 power microscope, attached to the screw carriage, allowed the observer to look at the scratches on the glass scale. These scratches, whose positions with respect to the zero of the scale are accurately known, were made to coincide in position with the cross-hairs of the microscope, and the corresponding screw settings were noted. In this way a correspondence between screw settings and distances on the glass scale was obtained. By making observations every 5 mm over the useful (600 cm) length of the one meter screw, a satisfactory calibration curve was obtained. In addition, the quasi-periodic error was determined at appropriate positions by taking readings at 0.1 mm intervals over a 1 mm range. Now the correction

curve corresponding to the scale readings every 5 mm contained the periodic error; hence it was necessary to subtract the periodic error from each reading before plotting the final over-all screw correction curve. Otherwise, in adding the periodic error correction to a screw correction one would in effect be applying the periodic correction twice, once for the calibration points and once for the wavelength position. Since determining the periodic error over the entire length of the screw is a Herculean task (over 10^4 readings would be necessary, if taken every 0.1 mm, just to cover the screw once), it was deemed sufficient to determine the periodic errors at 10 mm intervals over the interesting portion of the wavelength scale. In applying corrections at any given point the closest periodic correction curve was used. This is a justifiable procedure on the grounds that (1) the periodic error curves vary slowly over a large distance and (2) the periodic correction is always much smaller than the other corrections. Typical correction curves will be shown later, when a more recent calibration is discussed.

During the calibration described above it was noticed that even with this calibration the corrected screw reading might not correspond exactly to the source position. The "new" source of systematic error lay in the fact that minute flexures (twisting) of the beam resting on the source carriage, and on which the lead source bomb rests, would cause undesired displacements of the source relative to the source carriage, the two being separated by a vertical distance of about 12 inches (see Figs. 7 and 8). This effect was easily detected by placing a sensitive level on the source beam. Also, slight deflections due to imperfections in the ways on which the source carriage moved could be detected with the

level. The motion of the source due to these causes could be calculated from the level readings. The level was left on the instrument after the calibration, and level readings were taken during all subsequent wavelength measurements and the necessary corrections were included in the final wavelength values.

For several years it was believed that all appreciable systematic errors had been accounted for, although this could not be stated with absolute certainty. The first indication of still another systematic error came with the measurement of the annihilation radiation produced during the decay of Cu^{64}.[7] Comparison of the experimental value of the wavelength, 24.271 ± 0.010 mÅ, with the value of the Compton wavelength of the electron, 24.265 ± 0.0037 mÅ, computed by DuMond and Cohen[8] showed a discrepancy of 0.006 mÅ, corresponding to 0.006 revolution of the screw. This is of the same order of magnitude as most of the calibration corrections, and so could conceivably be due to an unknown systematic error. In view of this possibility the large error of 0.010 mÅ (4 times the actual experimental standard deviation found from agreement of several different measurements) was assigned to the measurement. However, this evidence was hardly conclusive, and the rather exciting possibility of a difference in the masses of positron and electron accounting for the discrepancy tended to obscure the situation even more. Fortunately additional evidence appeared in the spring of 1951 from an unexpected source.

During measurements of gamma radiation following decay of a very active source of Ir^{192}, D. E. Muller[6,9] found that he could detect three different orders of reflection for four different gamma-rays, and two orders for the $IrK\alpha_1$ x-ray produced after photoelectric absorption

in the source. The results of these measurements are summarized in the
table below. It will be noticed that with one exception the measured

Table I

Muller's Wavelength Values (in mÅ) for Reflection in
Different Orders for γ - and X-rays Following Decay of Ir^{192}

Line	Wavelength		
	1st Order	2nd Order	3rd Order
295.79 Kev	41.909	41.894	41.898
308.26 Kev	40.214	40.205	40.191
316.28 Kev	39.197	39.183	39.174
467.53 Kev	26.515	26.503	26.496
Ir Kα_1	191.025	190.993	

value of the wavelength for a given line decreases as the order of reflec-
tion increases. Since a higher order of reflection corresponds to a
greater distance measured with the screw, these data constitute rather
overwhelming evidence for presence of a systematic non-linearity in the
spectrometer. Additional confirmation comes from the fact that the
observed trend is of the correct magnitude and in the right direction to
account for the discrepancy in the annihilation radiation measurement.

The discovery of this systematic error made it advisable to launch
an investigation as to its nature and source. It was decided to include
this investigation as part of a new complete calibration of the instru-
ment. Accordingly, the new calibration was begun by David Muller and John

Helmer in July 1951, upon completion of investigations of gamma-radiation following decay of Ta^{182}. By this time it was suspected that the motion of the crystal, which is supposed to rotate on its pivot so as always to point at the center of the screw carriage, was not as it should be. To test this motion a six inch diameter concave mirror was mounted on the pivot in place of the crystal. The radius of curvature of the mirror was chosen so that the center of curvature was directly above the center of the screw. A point source of light was placed slightly above the center of curvature, and a microscope attached to the screw carriage was placed below the center of curvature so as to view the image of the point source. An elbow in the microscope permitted the observer to occupy a more comfortable viewing position. The image of small cross-hairs in front of the light source was formed on a scale placed at the focus of the microscope objective. Thus a quantitative description of the motion could be obtained. The mirror mounted on the crystal pivot is shown in Fig. 6; the "mirror" microscope and light source can be seen in Figs. 7 and 8.

Studies using the mirror and microscope arrangement showed that the crystal did not always point at the same (center) point of the screw carriage. Instead, the crystal seemed to lead the screw carriage in a non-linear manner, or turn through a greater angle than was indicated by the reading of the screw. The net result is that the screw must turn farther for the source to catch up with the crystal, and the resultant wavelength value is too large. The effect also was found to have a fair amount of hysteresis, that is, the amount by which the crystal leads the screw carriage depends on the previous history of settings made on the instrument. The presence of the hysteresis makes any correction for this
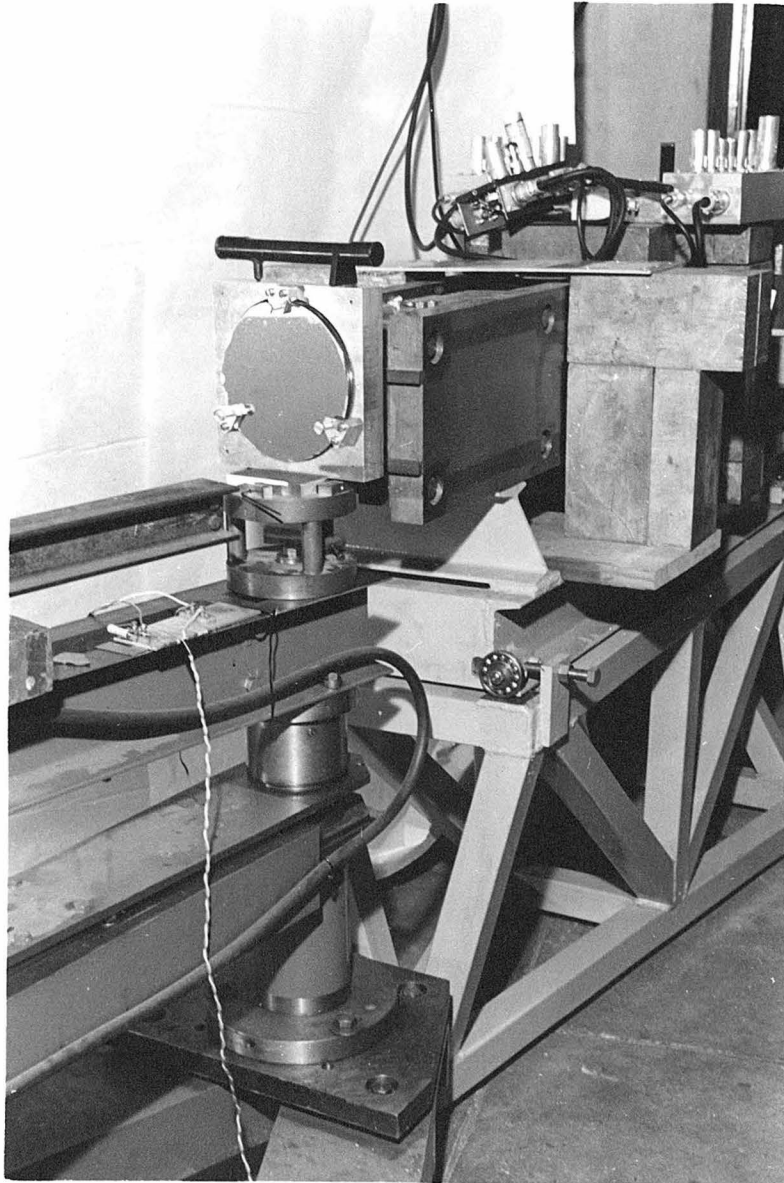
Fig. 6 - Showing the 6" precision-figured concave mirror mounted on the crystal pivot where it served, along with the elbow microscope and light source, to check the fidelity with which the turning of the crystal pivot followed the motion of the long screw carriage.
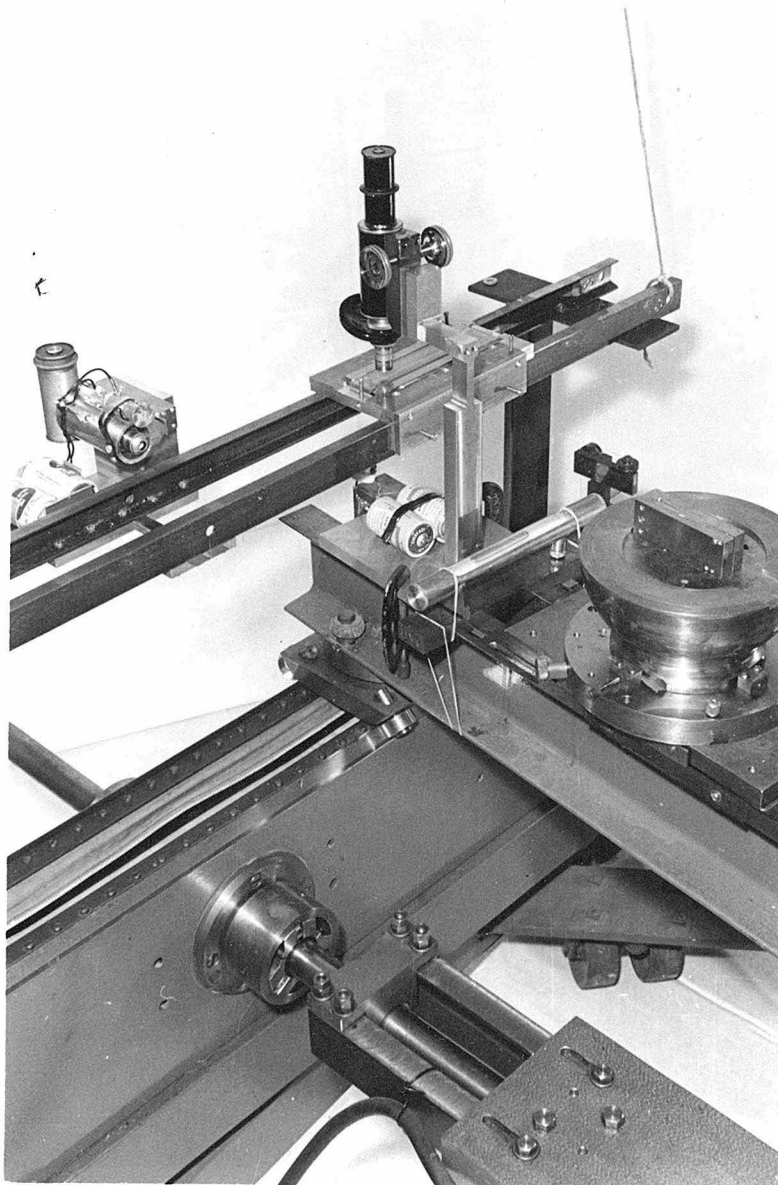
Fig. 7 - Showing arrangements for the calibration of the spectrometer.
A pair of rails rigidly supported on the long screw carriage
carry a small carriage provided with a Bureau of Standards
calibrated precision glass scale. A vertical microscope,
rigidly attached to the upper (source supporting) beam, views
the glass scale. The focus of the microscope is at the same
height as the source and is directly above the pivot of the
small carriage supporting the upper beam. The horizontal
elbow microscope and tiny light source used in conjunction
with the 6" concave mirror to detect any anomalies in the
motion of the crystal pivot are mounted at the center of the
rails. The source holder, standing on the lower half of the
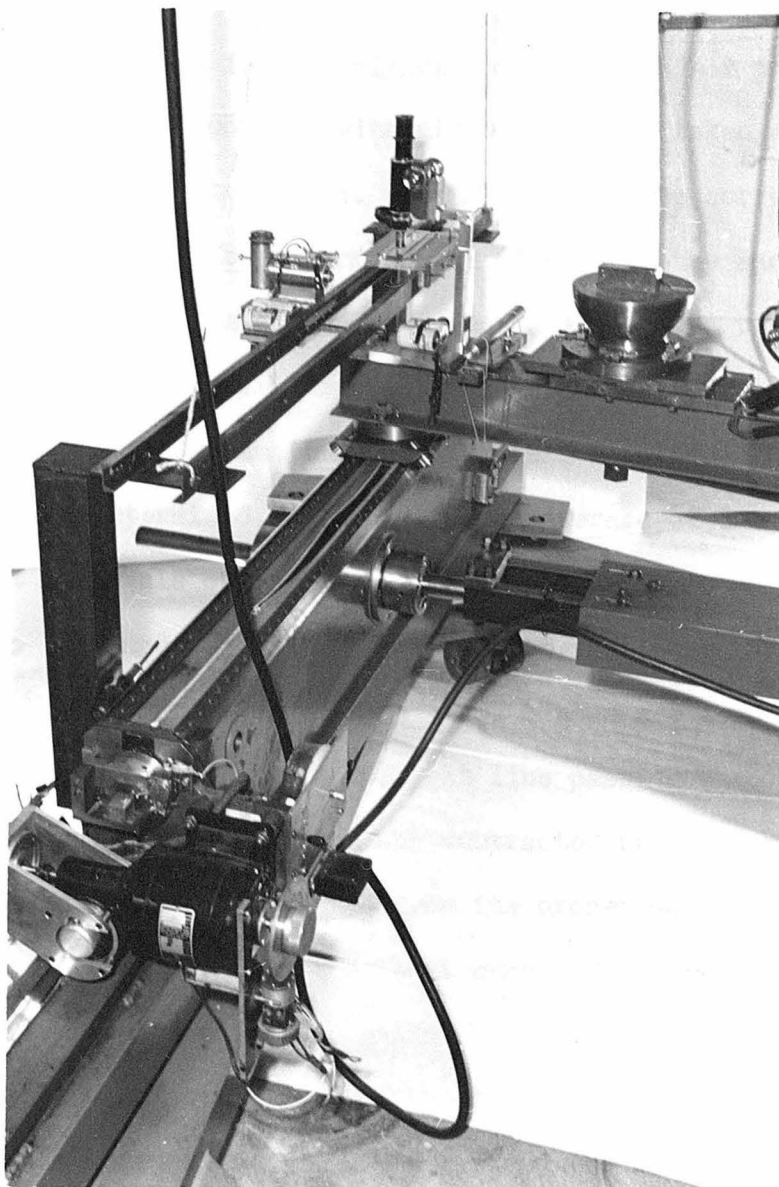lead bomb used for shielding, can be seen at the right center.

Fig. 8 - Another view of the set-up for the calibration of the
curved crystal gamma-ray spectrometer. The $1\frac{1}{4}$ inch
round steel bar which terminates the lower beam, and
which passes through the center of the long screw
carriage, can be clearly seen. It is the minute bending
of this bar, primarily caused by the weight of the
driving motor at the lower left, which is responsible
for the newly discovered systematic non-linearity.

non-linear crystal motion from a calibration curve subject to more un-
certainty than a correction made with mirror readings taken at the time
the wavelength measurement is made. The mirror and the corresponding
microscope therefore have been permanently mounted on the spectrometer,
and have been used in all measurements made subsequent to the calibration.
This correction henceforth will be referred to as the "mirror" correction.

To correct previous measurements for this non-linearity, a cali-
bration curve was determined. This curve, an average of 6 individual
curves made at intervals over a period of 6 months, is shown in Fig. 9.
This curve has been made to conform to the fact that there are two fixed
points at which the correction must be zero. These are zero and the
$WK\alpha_1$ x-ray calibration point. A straight line passing through zero and
the $WK\alpha_1$ x-ray wavelength position was subtracted from the original curve
showing the deviation of the crystal from its proper position in terms of
screw divisions (or mÅ) to give the final curve of Fig. 9.

Muller has succeeded in explaining most of the non-linearity in
terms of a slight bending of the $1\frac{1}{4}$ inch steel bar which passes through
the center of the screw carriage. This bar and the lower beam, of which
it is an extension, serve to couple the crystal to the screw carriage and
are the means by which the crystal is constrained so as always to point
at the center of the screw carriage. It is clear that if the bar is sub-
ject to any bending which has a horizontal component, this will indeed
result in the crystal moving with respect to the screw carriage so as to
point away from the center of the carriage. Reference to Fig. 10 will
enable us to visualize the situation more clearly and to formulate an
analytical expression for the deflection. The lower beam and $1\frac{1}{4}$" bar

can be seen in the photographs of Figs. 7 and 8. The cause of the deflection, the driving motor and selsyn unit attached to the end of the screw carriage can also be seen in Fig. 8. The unbalanced weight of this motor produces a clockwise torque about the center of the lower screw, as is shown in the end view of Fig. 10. The geometry of the tracks on which the ball bearing wheels run was chosen so that for small virtual displacements the carriage rotates about an axis coinciding with lower screw. The action of the horizontal bar, however, opposes such motion. Now, to find out what axis the carriage might rotate about when under the influence of an applied torque, one must look for those points of the screw carriage which are <u>fixed</u> in space at that instant. A little reflection with the aid of the figure shows that there are two such points, viz., the two nuts riding on the screws. The upper nut is fixed to the source carriage L, which is in turn connected to the long beam on which the source bomb rests; the lower nut is connected to the supporting frame (base) of the instrument. These two points fix an axis A-A, which passes through the center line of the horizontal bar, about which the carriage can rotate. We are now ready to derive the analytic expression for the deflection of $1\frac{1}{4}$" bar.

· Let x be the displacement of the source carriage L with respect to the center of the screw carriage Q, s be the perpendicular distance between the axes of the two screws, Θ the angle which the axis A-A makes with the axes of the screws, δ the <u>horizontal</u> component of the deflection of the $1\frac{1}{4}$" bar from its true position at the center of the screw carriage, $\mathcal{L}$ the applied torque, and k the elastic constant of proportionality for the bar. Now $\mathcal{L}$, according to the usual conventions, is a

vector directed along the axis of the lower screw from left to right.
The component of $\mathcal{L}$ along the axis A-A, which is the one which produces
the rotation about this axis, is $\mathcal{L}\cos\Theta$. The deflection produced by this
component is $k\mathcal{L}\cos\Theta$, and hence the horizontal component δ is given by
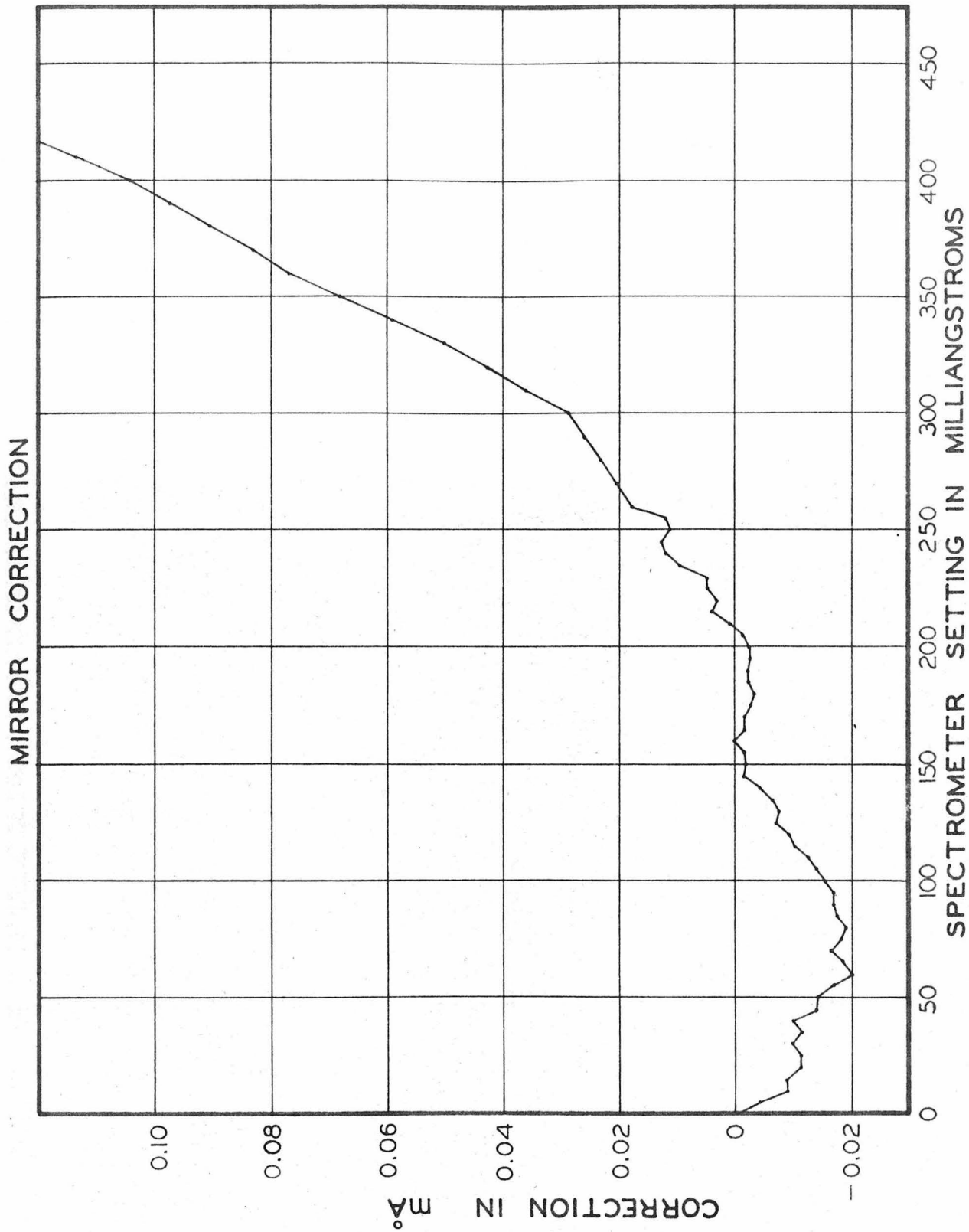
$$\delta = k\,\mathcal{L}\cos\Theta\,\sin\Theta \tag{1}$$

The angle Θ may be found from

$$\cot\Theta = \frac{2x}{s}\quad, \tag{2}$$

and using this equation to eliminate Θ, (1) becomes

$$\delta = \frac{k\mathcal{L}\left(\dfrac{2x}{s}\right)}{1+\left(\dfrac{2x}{s}\right)^2} \tag{3}$$

The units of k may be chosen so that δ is given in milliangstroms (m$\overset{\circ}{A}$).
The independent variable x may also be stated in terms of wavelength units.
A plot of (3) with an arbitrary ordinate scale is given in Fig. 11. Also
shown is the straight line passing through zero and the $WK\alpha_1$ x-ray cali-
bration point which must be subtracted from the curve of (3) to give the
proper correction curve. The result of the subtraction is shown in Fig.
12. Actually this curve gives corrections for readings taken on both
sides of center of the instrument. The difference between values for the
wavelength (but with opposite signs) is used to correct 2λ (twice the
wavelength) or the value on the right-hand side alone is used to correct
λ. In Fig. 13, the curve of Fig. 12 has been superimposed on the
experimental curve of Fig. 9 for comparison. The ordinate scale of Fig. 12

MIRROR CORRECTION
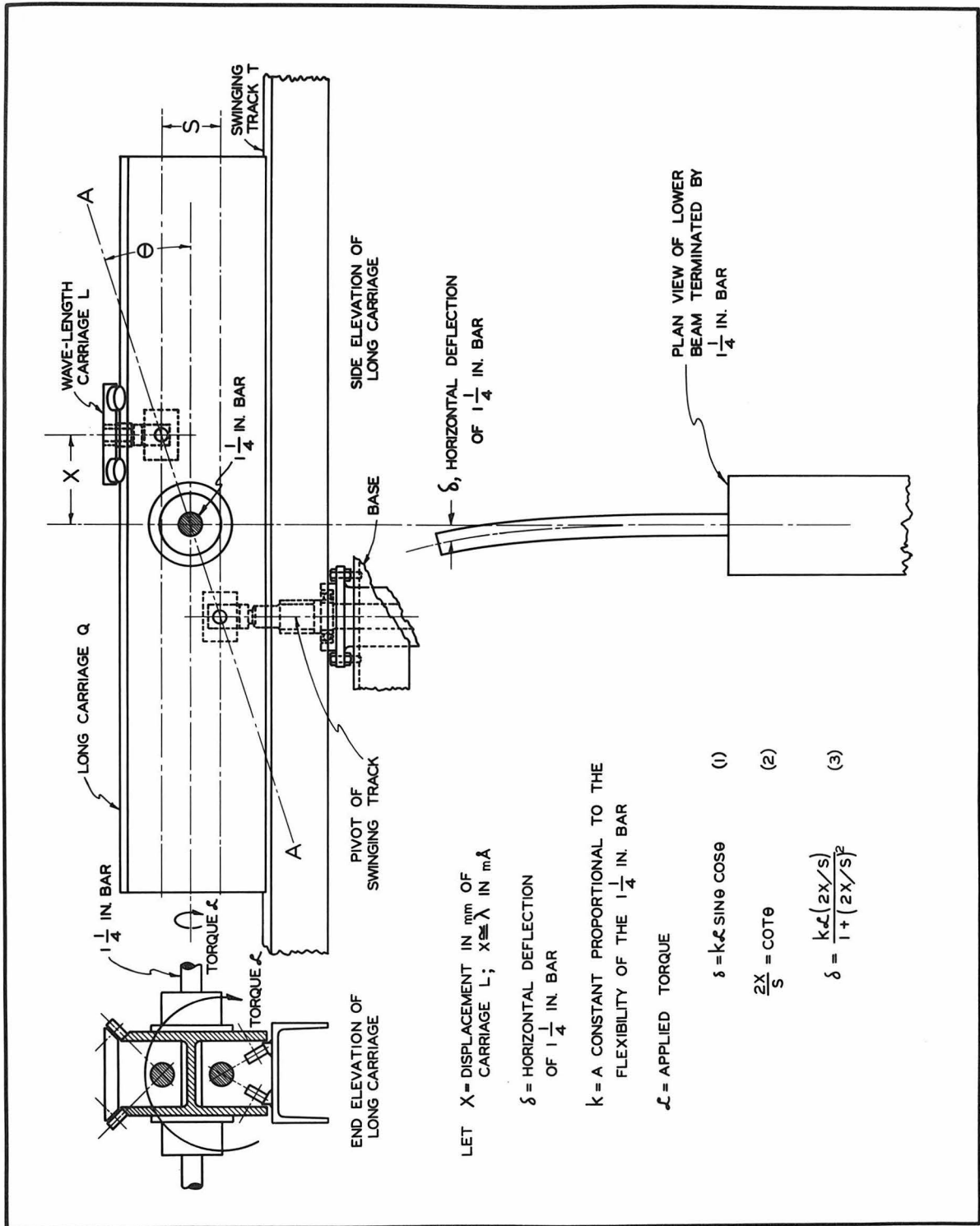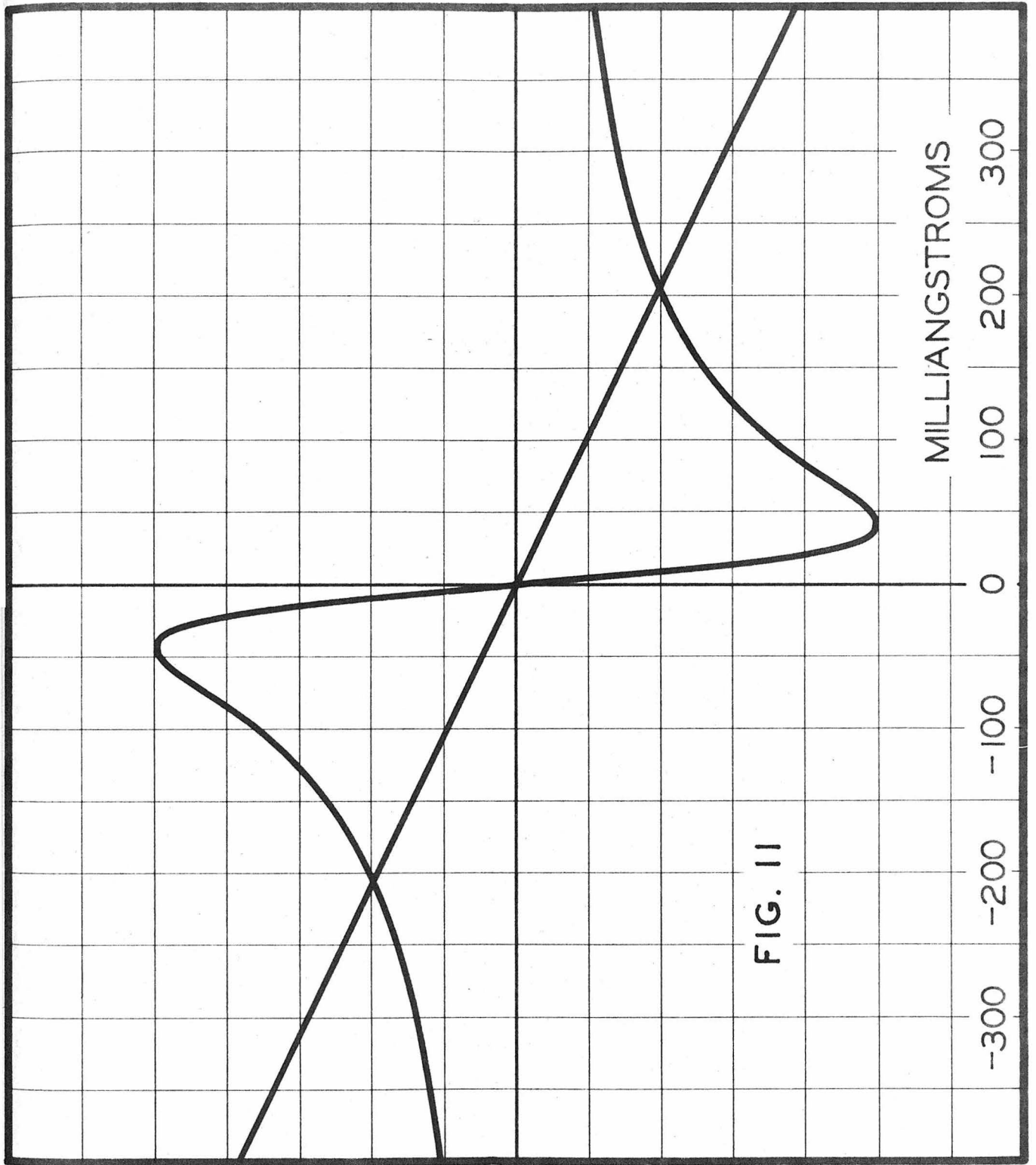
CORRECTION IN mÅ

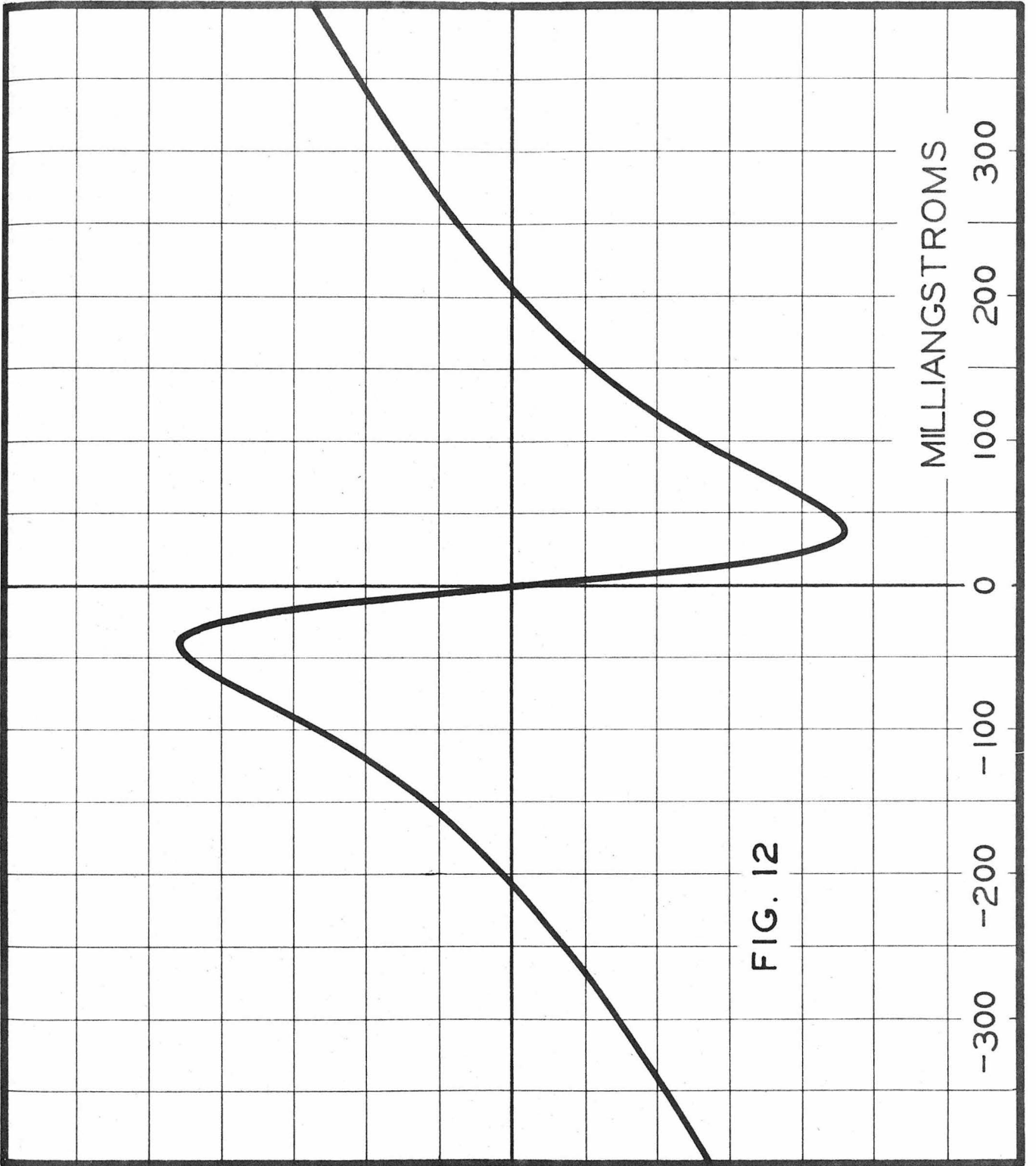SPECTROMETER SETTING IN MILLIANGSTROMS
FIG. 9

Fig. 10

LET X = DISPLACEMENT IN mm OF
CARRIAGE L; X ≅ λ IN mÅ

δ = HORIZONTAL DEFLECTION
OF 1¼ IN. BAR

k = A CONSTANT PROPORTIONAL TO THE
FLEXIBILITY OF THE 1¼ IN. BAR

$\mathcal{L}$ = APPLIED TORQUE

$$\delta = k\mathcal{L}\sin\theta\cos\theta \qquad (1)$$

$$\frac{2X}{s} = \cot\theta \qquad (2)$$

$$\delta = \frac{k\mathcal{L}(2X/s)}{1+(2X/s)^2} \qquad (3)$$

FIG. 11

MILLIANGSTROMS

FIG. 12

MILLIANGSTROMS

MIRROR CORRECTION

CORRECTION IN mÅ

SPECTROMETER SETTING IN mÅ

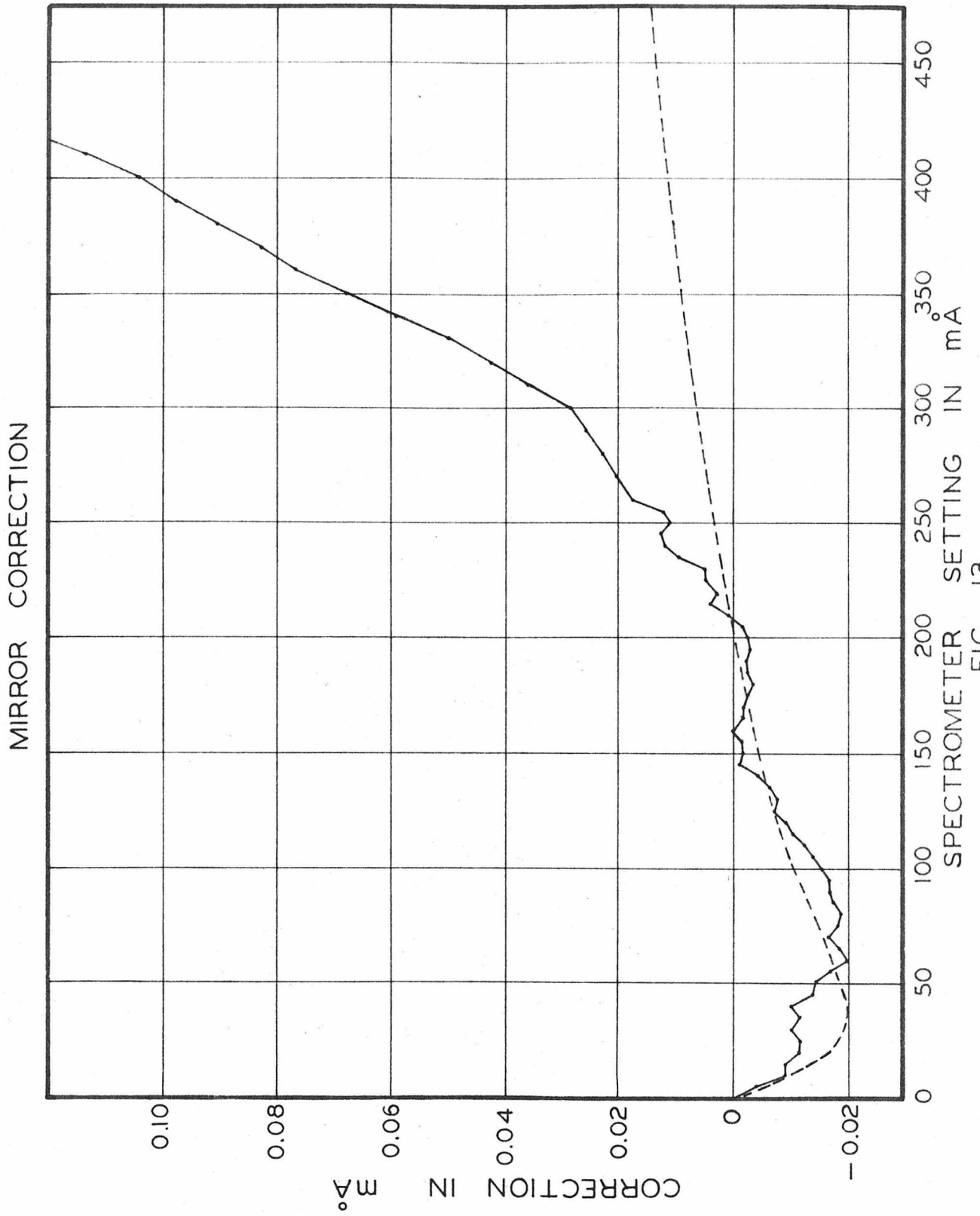FIG. 13

was adjusted for the minimum to have the arbitrary value of -0.02 mÅ.
From this comparison it can be seen that although the bending of the
$1\frac{1}{4}$" bar seems to account for a good deal of the non-linearity between
zero and 200 mÅ, beyond 200 mÅ it definitely accounts for only a small
part of the mirror correction. Other sources of this non-linearity are
yet to be determined.

Muller's results of Table I have been corrected for this non-
linearity with the aid of the calibration curve of Fig. 9. The corrected
results are given in Table II. The striking agreement of these corrected
values shows that this motion of the crystal relative to the screw
carriage is indeed the source of the non-linearity.

Table II

Muller's Ir^{192} Results After The Mirror

Correction Has Been Applied

Line	Wavelength in mÅ		
	1st Order	2nd Order	3rd Order
295.95 Kev	41.887	41.891	41.885
308.45 Kev	40.191	40.187	40.190
316.45 Kev	39.175	39.172	39.172
467.95 Kev	26.495	26.486	26.491
Ir $K\alpha_1$	191.031	191.041	

For the remainder of the calibration, i.e., the calibration of
the screw, it was decided to set up the calibration equipment so as to

view the motion as the source would see it. In essence, this meant

mounting the Bureau of Standards calibrated glass scale at the height

of the source. In this calibration the scale was mounted on the screw

carriage. The scale was placed in a special aluminum holder which was

then placed on a pair of steel rails at source level. The steel rails

were rigidly supported on two end plates, made of angle iron, attached to

the screw carriage. By means of suitable adjustments, the rails were

aligned so that the scale was directly above the screws and could be

moved parallel to them.

A microscope which could be focussed on the glass scale was

mounted on the source beam so as to be directly above the pivot connect-

ing the source beam to the source carriage (the small carriage riding on

top of the long screw carriage). This arrangement is shown in Figs. 7

and 8.

The first step in the screw calibration was to establish a series

of base points along the screw at 10 cm intervals. This was done by

setting the microscope on the first mark of the Bureau of Standards 10 cm

glass scale, noting the screw reading, and then moving the microscope

to the other end of the scale and noting the corresponding reading at

that point. Then, without touching either microscope or screw, the scale

was moved along the rails until the microscope cross-hairs coincided with

the initial mark on the scale, and the process was repeated. A large

number of these "over-all" calibrations was made, and the averages of the

results were used to give the base points. The chief advantage of this

initial procedure was that it could be completed in a short time, and any

effects due to accidentally bumping the instrument, temperature changes

from day to day, etc., then would not affect the calibration or cause undue loss of time.

Following the over-all calibration, an intensive calibration was made over each 10 cm region. The first mark on the glass scale was set to coincide with the screw setting (base point) beginning one of the 10 cm sections, as found in the over-all calibration. Then screw readings were taken every 5 mm over the entire length of the scale. The difference, scale reading (in mm) multiplied by the appropriate factor to give screw divisions minus the number of revolutions through which the screw has turned, gives the desired correction curve when plotted against screw reading. The final correction curve for each 10 cm section of the screw was the average of 4 runs. The observations for a typical section and their average are shown in Fig. 14. The manner in which the readings spread out as the screw setting is increased will be discussed in Section D.

As was mentioned earlier in connection with the first calibration of the screws, the quasi-periodic error of the screws is contained in the readings taken for the intensive calibration. The procedure used in determining periodic error was the same as that followed before. The periodic error was determined over a one mm range at intervals of 10 mm along the screw. Only the interesting portion of the screw, that between the $WK\alpha_1$ x-ray calibration points on either side of the instrument, was covered. The periodic error correction applied at any given point is that given by the closest periodic error curve. This correction must be subtracted from the intensive calibration curve to get the proper correction curve; then the proper periodic correction is added to this curve to get the

final wavelength value. 3 or 4 runs were made to determine each periodic correction curve. A typical curve is shown in Fig. 15.

Although level readings were meticulously taken throughout the calibration, a level correction is not necessary with the new calibration. This is because the glass calibrating scale was mounted at the same height as the source, and therefore the effects of minute twisting of the source beam are already included in the readings of the scale as seen by the microscope mounted on the source beam.

The final correction curve for the screw, without periodic error, is given in Fig. 16. Fig. 17 shows the combined mirror and screw correction, found by adding the curves of Figs. 9 and 16. All of these curves have been adjusted to pass through zero at the $WK\alpha_1$ x-ray point.

Upon completion of the calibration it was felt that the mirror correction would be more accurate if mirror readings were actually taken at the time of the wavelength measurements. Such a procedure eliminates the large uncertainty due to hysteresis effects in the instrument, since these effects are automatically included in the mirror readings. The permanent mirror and microscope arrangement is shown in Figs. 18 and 19. Still another amendment to the normal operating procedure is concerned with the removal of the backlash in the screws. During the calibration it was found that almost 20 cm of travel is needed to remove completely the effects of backlash. Previously it had been thought that 1 to 2 cm was sufficient. Accordingly, prior to running a pair of line profiles the wavelength carriage is run to the end of the screw (-470 x.u.) and then brought to the proper setting. This procedure guarantees the complete removal of the backlash, and also that all pairs of profiles are begun in
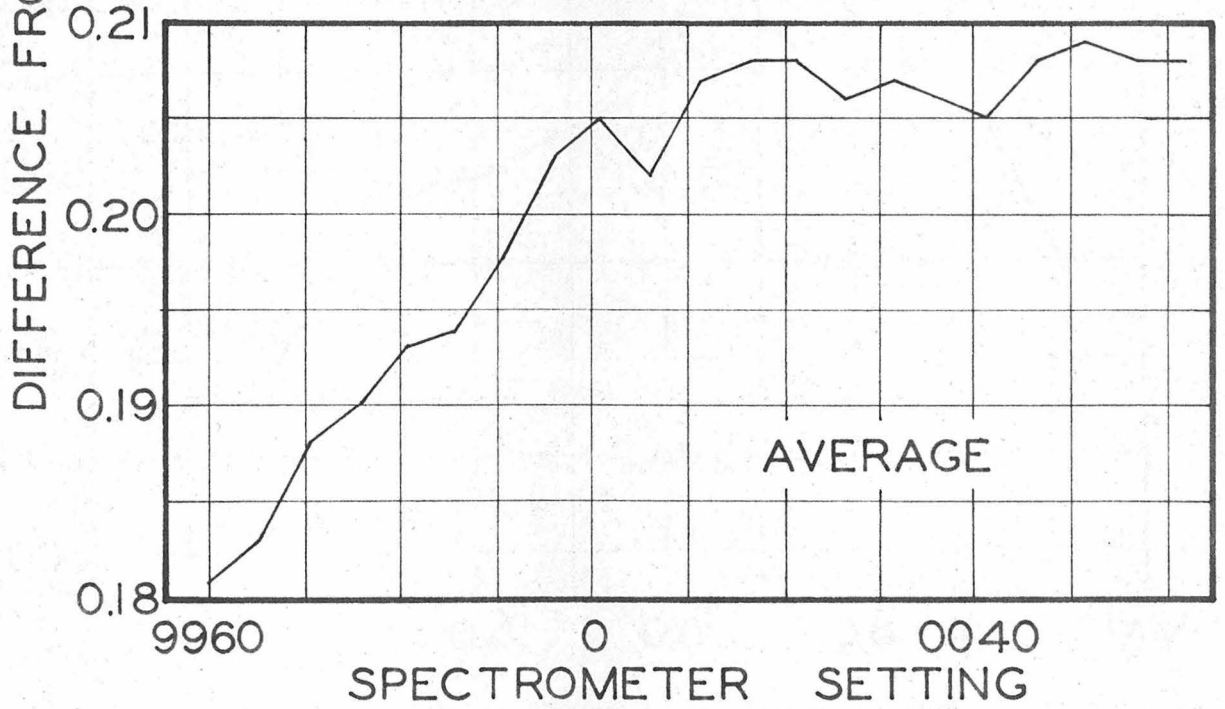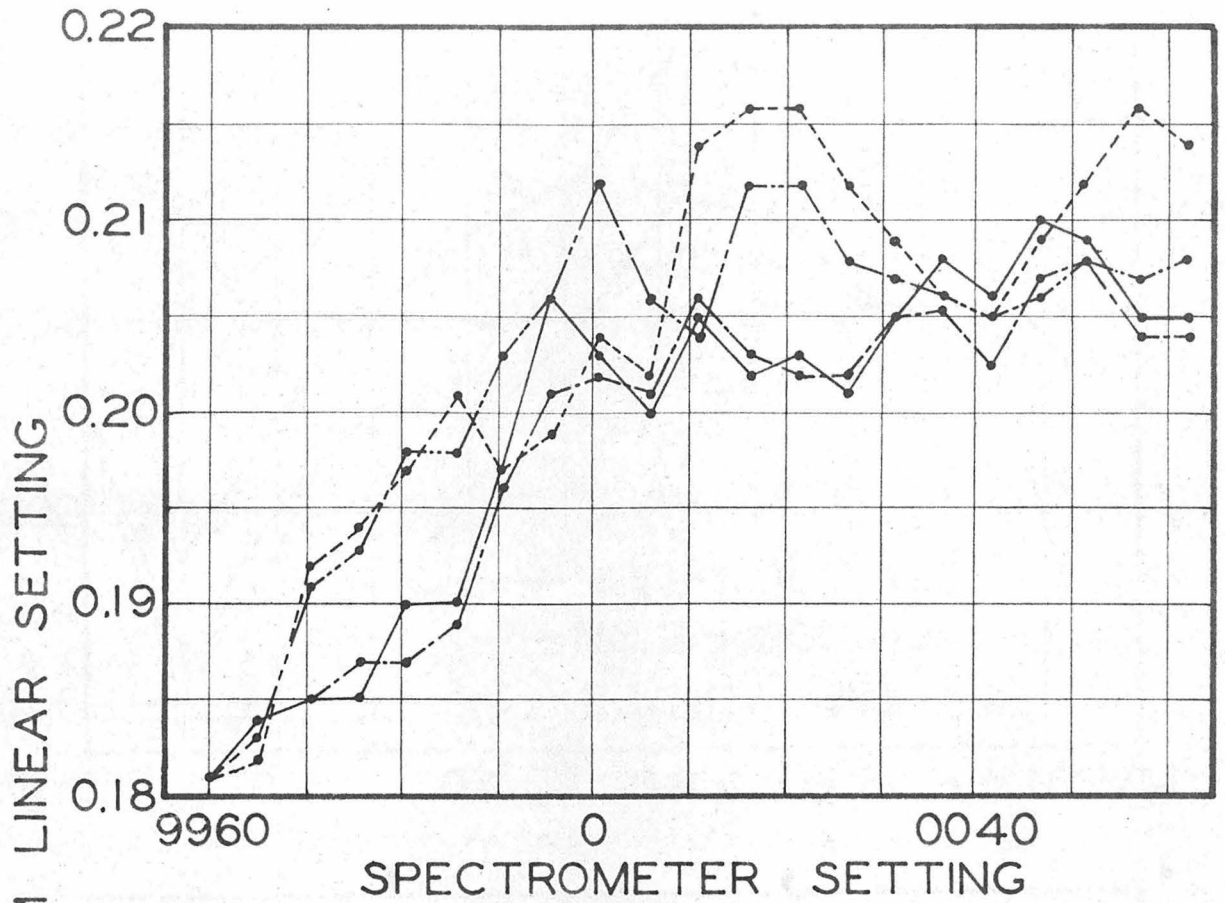
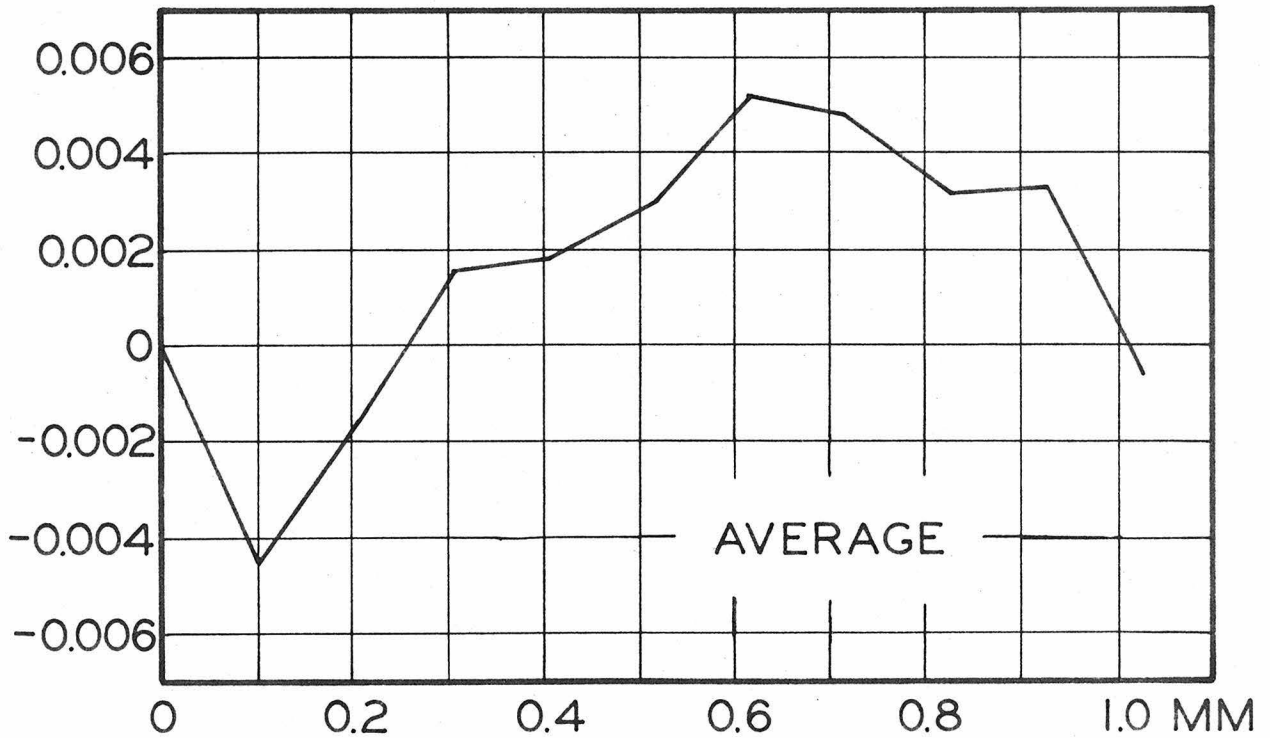FIG. 14 - INTENSIVE CALIBRATION CURVES FOR
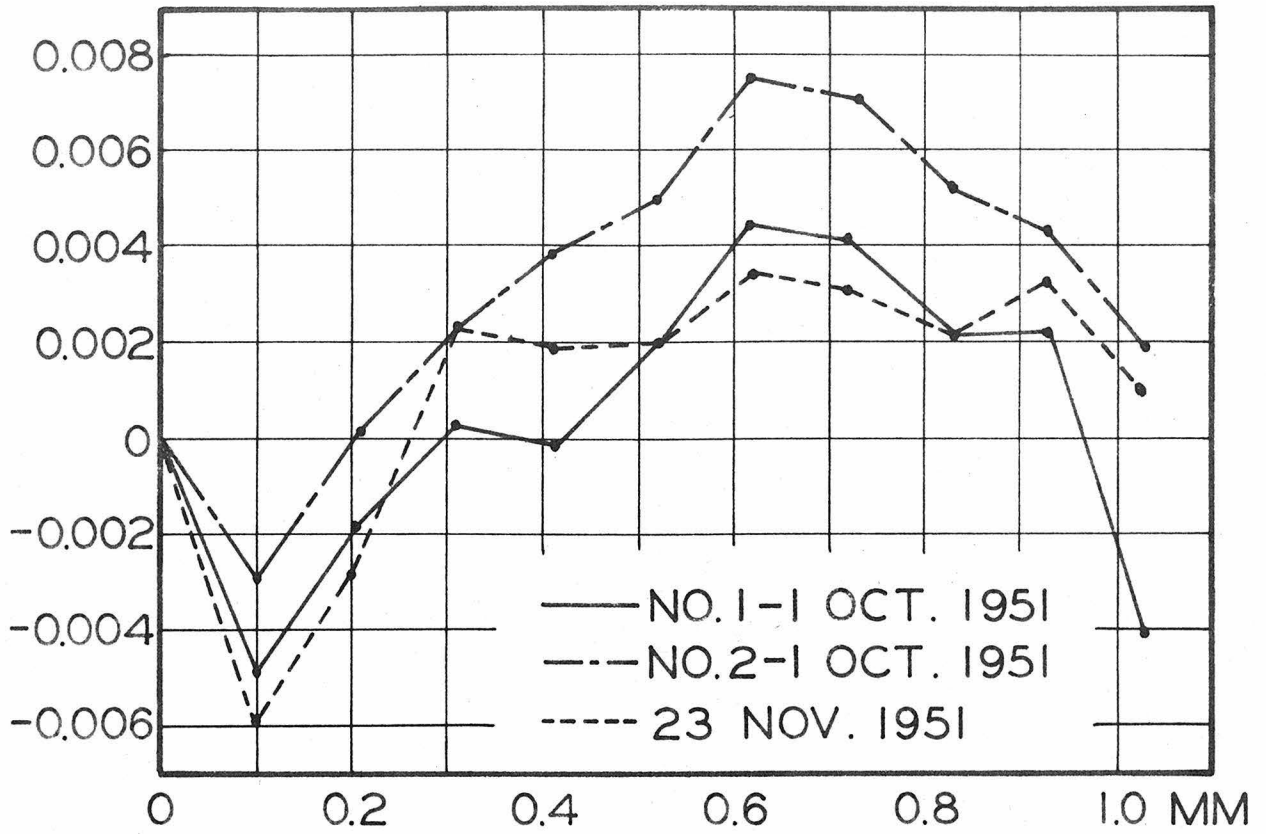A TYPICAL 10 CM REGION

FIG. 15 - A TYPICAL PERIODIC ERROR CURVE

SCREW CORRECTION

FIG. 16

TOTAL CORRECTION (MIRROR + SCREW)

CORRECTION IN mÅ
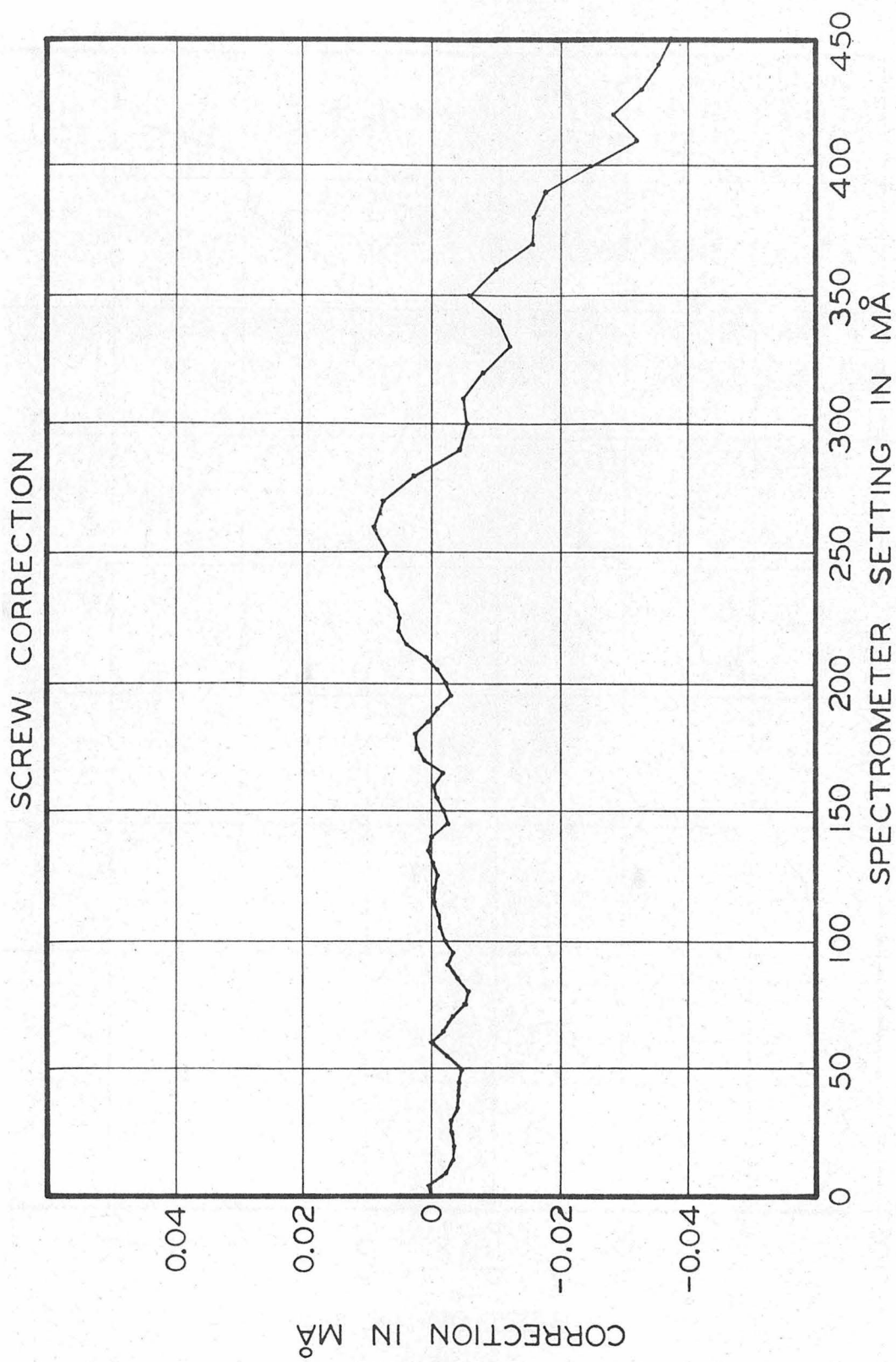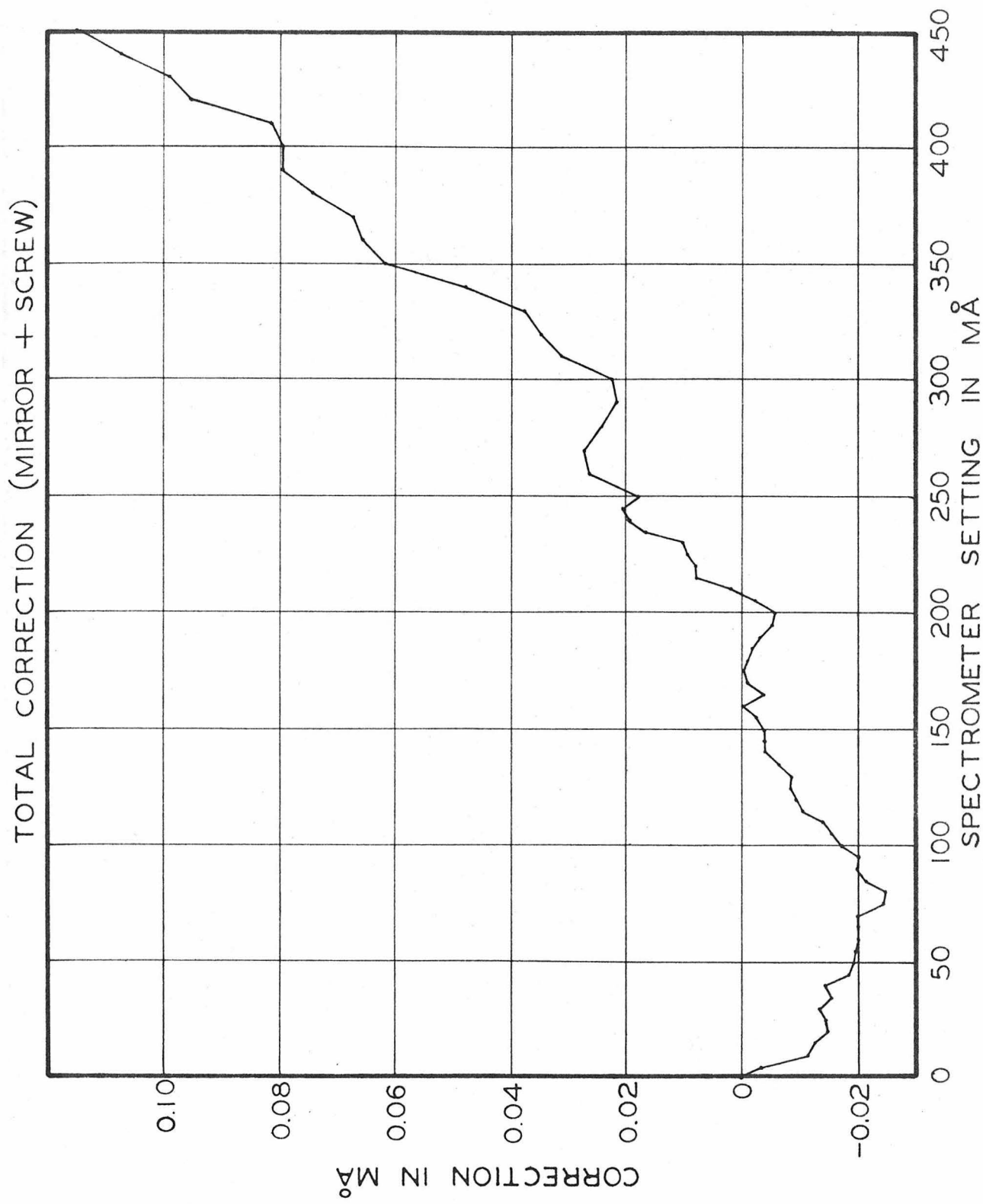
SPECTROMETER SETTING IN mÅ

FIG. 17

Fig. 18 - Showing the permanent provision now made for mounting
the 6" concave mirror above the crystal holder. Using
the mirror and its corresponding microscope, the
minute deflections due to the bending of the $1\frac{1}{4}$ inch
bar can be measured whenever line profiles are being
delineated.
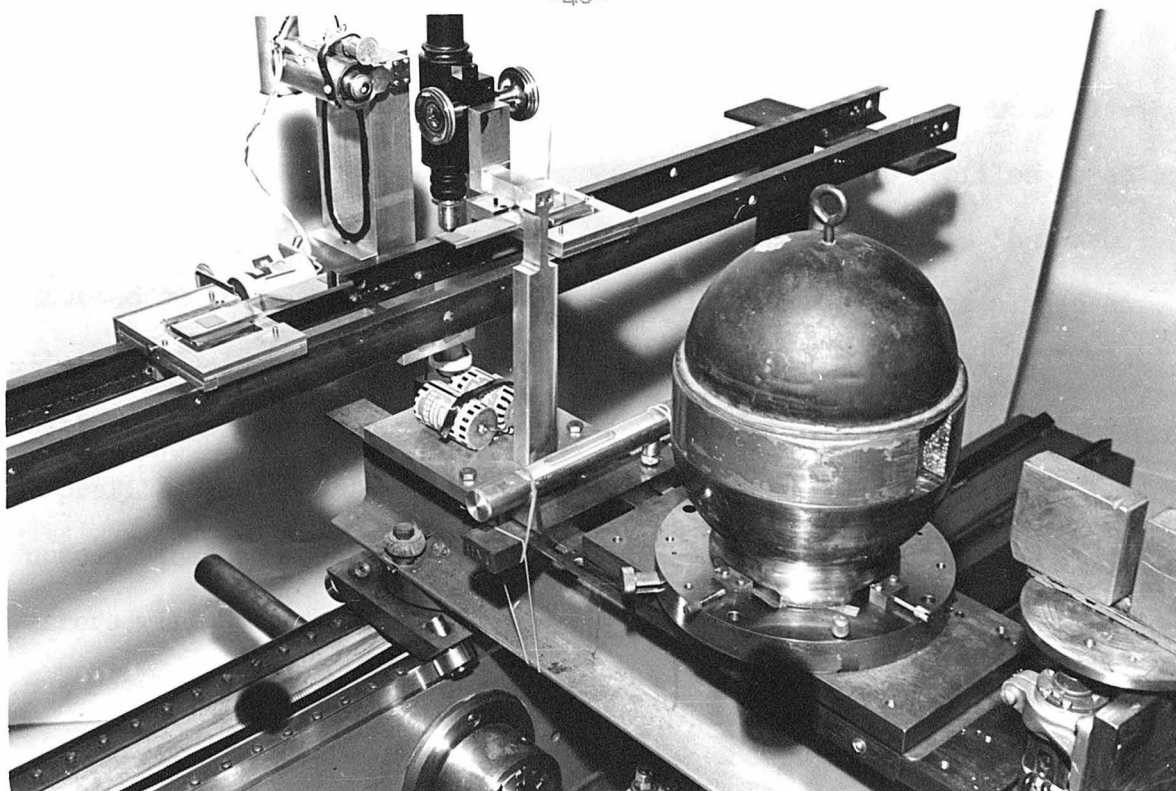
Fig. 19 - Showing the microscope arrangements as now actually used
when delineating profiles. The horizontal elbow
microscope used in conjunction with the 6" concave
mirror has been raised so that the optical path will
clear the lead bomb shielding the source. Two glass
scales are mounted on the steel rails so that fiducial
marks ruled on them will correspond to definite points
on the profiles obtained on opposite sides of the
instrument. These scales are viewed with the vertical
microscope. In this way repeated runs across the line
profiles become unnecessary.

the same way.

Finally, the following procedure was devised by Muller to eliminate the necessity for repeated runs across a given pair of profiles to obtain greater accuracy. Two glass scales with scratches ruled on them are mounted on the steel rails used in the calibration, and are placed so that one scale corresponds to each profile. These scales may be viewed with the microscope mounted on the source carriage. Before running across a profile, the screw reading corresponding to the scratch on the scale is noted. Thus the profile may be located with respect to this mark. Screw errors will be very small in the short distance from peak to mark (about one revolution). The distance between the marks may be established very accurately by repeated measurements, which occupy a very short time compared to the time required for a second run across the profiles. Thus a considerable saving in time is achieved. This is especially valuable with short-lived sources. The arrangement of glass scales and microscope can be seen in Fig. 19. Unfortunately the procedure has not as yet proved successful, chiefly due to inadequate means for clamping the scales rigidly to the steel rails on which they rest. This difficulty will be remedied shortly, and the method is then expected to prove successful.

D. Errors

Most of the processes carried out during the performance and analysis of an experiment contribute in some way to the uncertainty of the final result. In order to get an estimate of this uncertainty, and thus the precision of the experiment, all of these factors must be carefully considered and their contributions to the total uncertainty determined as accurately as possible. Such an analysis of the errors usually begins by assuming that the errors follow a normal distribution. We shall do this here. This assumption of a normal distribution enables one to combine the so-called standard deviations of the different error-contributing factors to obtain the standard deviation of the final result. This is a measure of precision, and if the result is to be combined with the results of other experiments it is assigned a weight inversely proportional to the square of its standard deviation (The square of the standard deviation is often called the variance; this practice will be followed here).

The exact meanings of the terms "normal distribution", "standard deviation", etc., will not be discussed here, since they have been dwelt on at great length in the many texts and articles on probability and statistics. It will suffice for our purposes to state the general rule for combining standard deviations. Suppose that we wish to find the standard deviation σ_f of a function $f = f(x_1, x_2, ---, x_n)$ of the n quantities $x_1, x_2, ---, x_n$, each of which has its own standard deviation. Let these standard deviations be $\sigma_1, \sigma_2, ---, \sigma_n$, respectively. If the quantities $x_1, x_2, ---, x_n$ are observationally independent the rule for propagation of errors then gives

$$\sigma_f^{\ 2} = \sum_{i=1}^{n} \left(\frac{\partial f}{\partial x_i}\right)^2 \sigma_i^{\ 2} \qquad (1)$$

From this relation we see that it is the variance which is the important quantity in the propagation of errors.

There are two methods for obtaining values for the variance. These are referred to as internal consistency and external consistency. The method of internal consistency is that in which the variance due to each error-contributing factor is estimated and these variances are combined according to the above formula to give the variance of the final result. The method of external consistency, on the other hand, estimates the variance by considering the variations between several different measurements of the same quantity. First the mean of the observations is determined; then the sum of the squares of the deviations of the individual measurements from the mean divided by the number of measurements less one gives the variance for a single observation. If the ratio of the variance by external consistency to the variance by internal consistency is near one, the results are considered satisfactory. A large deviation from one in the ratio is usually taken as evidence of an unsuspected systematic error. It should be noted in this connection that one must be extremely careful at which point in the analysis one uses the variances by external and internal consistency for comparison and for weighting measurements. This point will be discussed more fully later in connection with the specific cases which arise here. It can be seen from the definition of variance by external consistency that such a value cannot be obtained if

there is only one measurement; in such a case the variance by internal
consistency is used to give the standard deviation of the final result.
If both kinds of variances can be calculated, it is customary to use
the larger to get the standard deviation which is stated with the final
result.

There are essentially seven error-contributing factors which
appear during the determination of a gamma-ray wavelength with the gamma-
ray spectrometer. These are listed below:

1. Indeterminacy of a Line Profile due to Counting Statistics

2. Error Introduced by the Observer in Matching Profiles

3. Random Variation in Screw Readings

4. Mirror Correction

5. Main Screw Correction

6. Quasi-Periodic Error Correction

7. Conversion Factor from Screw Divisions to $m\overset{\circ}{A}$

These factors and their contributions to the total variance will be dis-
cussed and evaluated in the following sections.

1. Indeterminacy of a Line Profile due to Counting Statistics

Under favorable circumstances it is possible to adjust the time
for running across a profile so that the error due to this source is
negligible in comparison to the errors from other sources. Although the
choice of time spent in accumulating counts at each point of the profile
can be made reasonably well by "feel", there are times when it is advisable
to know exactly what the counting statistics contribute to the total error.
For example, with short-lived sources it is very desirable to know the

minimum time which can be spent on a profile with no appreciable loss in precision or, with weak sources, the point beyond which no useful information can be obtained with the spectrometer. With these criteria in mind Muller[6] has analyzed the errors introduced by counting statistics. A brief resumé of this analysis will be presented here.

Two different processes may be used to determine corresponding positions on the two profiles obtained by reflections from opposite sides of the crystal planes. (The difference between these two positions gives twice the wavelength.) First, the two profiles may be superimposed on each other and the corresponding positions noted; second, each profile may be compared with a composite profile (made from many different runs over different lines) and the positions corresponding to a fiducial mark on the composite noted. The second of these two methods is believed preferable, and is the method currently used. Theoretically, then, all that is needed to determine the position of the line profile is one point and the composite profile. We shall first determine the error from this ideal case. The figure below will be useful for this. If N_i is the total

$$\sqrt{N_i}$$

$$\lambda = \lambda_i$$
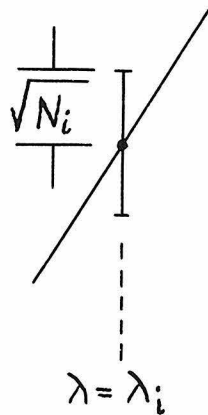
N_i = total number of counts at wavelength position λ_i.

S_i = slope of profile at wavelength position λ_i.

number of counts at a given wavelength position λ_i, the standard deviation associated with N_i is $\sqrt{N_i}$. The uncertainty in the position of the profile depends on both this number and the slope of the profile at this point. This uncertainty, stated as a standard deviation, is given by

$$\sigma_i = \frac{\sqrt{N_i}}{S_i} \quad , \tag{2}$$

where σ_i is the standard deviation in position of the profile and S_i is the slope at wavelength position λ_i. If, now, counts are taken for equal time intervals at several points, we may combine the various σ_i to obtain a standard deviation σ for the whole. The formula for such a combination is

$$\frac{1}{\sigma^2} = \sum_{i=1}^{n} \frac{1}{\sigma_i^2} \quad . \tag{3}$$

Hence σ is given by

$$\frac{1}{\sigma^2} = \sum_{i=1}^{n} \frac{S_i^2}{N_i} \quad , \tag{4}$$

if counts are taken at n different wavelength settings. From (2) and (4) it is clear that only those points on the sides of the profile, where the slope is appreciably different from zero, contribute to σ. Furthermore, the steeper the sides (i.e., the greater the value of S_i) of the profile the smaller is the value of σ. Equation (4) can be used to estimate the variance σ^2 due to this source of error. This variance

varies from about 0.1×10^{-6} $(m\overset{\circ}{A})^2$ to 25×10^{-6} $(m\overset{\circ}{A})^2$, depending on the individual circumstances of the experiment. In the process of taking the difference between the positions of two profiles, the variance will be doubled; but since the difference gives twice the wavelength, the above value is divided by two to get the variance for the wavelength λ.

2. Error Introduced by the Observer in Matching Profiles

Although this source of error cannot be completely resolved from that discussed in Section 1, if we assume that once we have the points on a profile its position is fixed, then the effort of the observer to match a single experimental profile to the composite profile will contribute its own variance to the total. This effect has been estimated by having several different observers match the profiles. The variance found from the deviations of the individual readings from the mean is the desired estimate. Comparison of a large number of cases indicates that 4.5×10^{-6} $(m\overset{\circ}{A})^2$ is a good value for this variance (for a single profile). Again this must be doubled when applied to the difference in positions, or divided by two when applied to the wavelength λ .

3. Random Variation in Screw Readings

If the screw is set to the same setting a number of times in succession, the actual positions of the instrument should exhibit a normal distribution about the "true" setting. Or, looking at the situation from another viewpoint, if the spectrometer is set to the same position (judged by means other than the screw) several times, the screw readings should exhibit a normal distribution about the true value. This effect has been estimated by use of the scales shown in Fig. 19 of Section C. 10 successive

runs were made between the marks on the two scales. The variance of the difference between the two positions as given by the screw readings is the desired estimate. This was found to be $4.8 \times 10^{-6} \ (\text{m\AA})^2$. This refers to the difference 2λ and must be divided by 4 to refer to the wavelength λ.

4. Mirror Correction

This uncertainty stems mainly from deflections of the light beam produced by air movements in the light path. As a result of these deflections the position of the image in the mirror microscope can be uncertain to as much as one scale division, which corresponds to 0.004 m\AA on the screw. However, for the most part, an uncertainty of half this seems to be a good value. Using this, the variance is $8 \times 10^{-6} \ (\text{m\AA})^2$ for 2λ or $2 \times 10^{-6} \ (\text{m\AA})^2$ for λ.

5. Main Screw Correction

In Fig. 14 of Section C, the results of 4 separate (intensive) calibration runs over a typical 10 cm region are plotted together. These plots show a definite tendency to spread out as the distance from the base point is increased. This "spreading out" is essentially the same as that appearing in the analysis of the random walk. The random walk analysis was therefore used to determine the variance associated with the main screw correction. Briefly, the process of finding the variance was to find the variance for each screw setting, divide this by the distance travelled, sum all the values so obtained, and divide by n, the number of points along the scale at which readings were taken. The variance for a distance of travel D is then found by multiplying the above

result by D. In formula form the variance is

$$\sigma^2 = \frac{D}{n} \sum_{j=1}^{n} \frac{1}{d_j \, (m-1)} \sum_{i=1}^{m} \sigma^2_{ij} \, , \qquad (5)$$

where σ^2_{ij} is the square of the deviation of the ith run from the mean at distance d_j, m the number of runs, n the number of points in each run, and D the distance of travel for which the variance is required. A complete analysis of the calibration data reduces (5) to the numerical form

$$\sigma^2 = 0.15D \times 10^{-6} \; (m\mathring{A})^2 \; , \qquad (6)$$

where D is in screw divisions $(m\mathring{A})$. An additional term must be added to (6) to account for the uncertainties of the positions of the base points used as the starting points in the intensive calibration. We then have

$$\sigma^2 = (9n + 0.15D) \times 10^{-6} \; (m\mathring{A})^2 \; , \qquad (7)$$

where D is the distance of travel between the two profiles of a pair, and n is the number of base points passed during this motion. The variance given by (7) refers to twice the wavelength or 2λ.

6. Quasi-Periodic Error Correction

The contribution of this source of error has been determined in a somewhat arbitrary manner to avoid the lengthy and tedious calculations otherwise required. Minimum and maximum values for the variance were calculated from the many sets of periodic error curves (see Fig. 15). These are $\sigma^2 = 3 \times 10^{-6} \; (m\mathring{A})^2$ and $\sigma^2 = 18 \times 10^{-6} \; (m\mathring{A})^2$, respectively.

From these it seems that $\sigma^2 = 10 \times 10^{-6}$ (m$\overset{\circ}{A}$)^2 is a reasonable value for the variance, and this is the value used. It refers to a single point; the variances for 2λ and λ are $\sigma^2 = 20 \times 10^{-6}$ (m$\overset{\circ}{A}$)^2 and $\sigma^2 = 5 \times 10^{-6}$ (m$\overset{\circ}{A}$)^2, respectively.

7. Conversion Factor from Screw Divisions to m$\overset{\circ}{A}$

The multiplicative factor which must be used to convert the wavelength in screw divisions is made up of 3 parts: (1) the known wavelength of the WK$_{\alpha_1}$ x-ray line in x.u.[10], (2) the wavelength of this x-ray line in screw divisions, and (3) the ratio λ_g/λ_s[11] for converting wavelengths in x.u. to m$\overset{\circ}{A}$. The factor is found from the relation

$$ f = \frac{\lambda(\text{x.u.})}{\lambda(\text{screw div.})} \left(\frac{\lambda_g}{\lambda_s} \right) \tag{8} $$

where the λ's in the first fraction refer to the WK$_{\alpha_1}$ x-ray line. Since the different terms appear as multipliers or divisors, equation (1) shows that it is the relative errors which add in quadrature. These relative errors are:

(1) WK$_{\alpha_1}$ x-ray wavelength in x.u. - 56.7 parts per million (ppm)

(2) WK$_{\alpha_1}$ x-ray wavelength in screw divisions - 52.3 ppm

(3) λ_g/λ_s - 16.3 ppm

The resultant relative error for f is 78.6 ppm, and the corresponding variance is $\sigma^2 = 6180 \times 10^{-12}$. Before using this variance it should be emphasized that f is a multiplicative factor, and that the variances of Sections 1 through 6 refer to additive factors. The method for finding the total variance for the wavelength must take this into account.

The results of this section are summarized in Table III. In referring to this table (and to Sections 1 - 7) it must be remembered that the first 4 error-contributing factors apply to the individual runs across the profiles, whereas the last 3 factors apply to the average of the runs (since the correction is the same for all runs). Hence in establishing the weights for determining a weighted average, the process of weighting and averaging must be carried out after the corrections of Sections 1 - 4 have been carried out and before those of Sections 5 - 7 are applied. This weighting process gives the variance by internal consistency which is to be compared with the variance by external consistency (which is also determined after the corrections of Sections 1 - 4 only have been applied). In the event that reflections from different orders have been obtained, the above arguments apply to the measurements in each order. Then the corrections of Section 5 and 6 must be applied before weights are assigned to the measurements in the different orders.

Table III

Section	Error-Contributing Factor	Variance in $(m\overset{\circ}{A})^2$	
		2λ	λ
1.	Counting Statistics	$(0.2\text{-}50) \times 10^{-6}$	$(0.05\text{-}12.5) \times 10^{-6}$
2.	Matching Profiles	9×10^{-6}	2.3×10^{-6}
3.	Random Variation in Screw Readings	4.8×10^{-6}	1.2×10^{-6}
4.	Mirror Correction	8×10^{-6}	2×10^{-6}
5.	Main Screw Correction	$(0.15D + 9n) \times 10^{-6}$	$\frac{1}{4}(0.15D + 9n) \times 10^{-6}$
6.	Quasi-Periodic Error Correction	20×10^{-6}	5×10^{-6}
7.	Conversion Factor from Screw Divisions to $m\overset{\circ}{A}$	78.6 ppm relative error	78.6 ppm relative error

E.   The Line Profile

Before progressing to a detailed discussion of the factors con-
tributing to the line profile, it will be advantageous to review the
basic processes in the determination of a gamma-ray wavelength. Such a
review will help to emphasize the more important properties of the pro-
file. The first step in a wavelength determination is, of course, to
locate the position of the gamma-ray line which is to be measured. This
line may be one which has been investigated previously by other methods;
in this case a crude value of the wavelength is known and a short search
in a region about this value is sufficient to locate the line. A second
procedure, necessary for locating new lines, is to set the spectrometer
for a search run covering the interesting region. In such a search
counts are taken for one minute periods at intervals of 0.1 x.u. along
the screw. Any gamma-ray line which can be measured with the spectro-
meter definitely will appear during the search. After the line is located,
a run is made across it on <u>both</u> sides of the spectrometer, i.e., using
reflections from both sides of the crystal planes. The two profiles thus
obtained are then corrected for background and decay, and are normalized
to unit height. Comparison with a composite profile, made by superposi-
tion of all normalized profiles from a single source, gives a screw read-
ing corresponding to a fiducial mark on the composite. The difference in
the two screw readings for the members of a pair equals twice the wave-
length when all corrections have been made.

The most obvious property to be desired in a gamma-ray line is
intensity. In terms of the line profile, the height of the profile peak

above background is a measure of the intensity. Thus we wish to obtain

the maximum height above background commensurate with any restrictions

which may be imposed. The intensity of the line will govern, to some

extent, the accuracy with which the wavelength may be measured. This is

particularly true with weak sources of short half-life. Reference to

equation (4) of Section D, however, shows that the slope of the sides of

the profile, in addition to the total number of counts, is important.

Admittedly the slope of the side of the profile is dependent on the inten-

sity of the source, but it also is dependent on several other factors

such as the diffraction pattern of the crystal for monochromatic radiation

and the size and shape of the source. Any adjustment which may be made

in these factors to steepen the sides of the profile will increase the

precision of the measurement. It may be that several gamma-ray lines lie

close together. In such a case the resolution of the instrument is im-

portant, good resolution being essential to accurate wavelength deter-

mination. The property of the profile which fixes the possible resolu-

tion is the width; thus for the case of several gamma-ray lines whose

wavelengths are nearly equal, the profile should be made as narrow as

possible. On the other hand, for a search run a wide profile is desir-

able, since then several of the rather widely spaced points will fall on

the profile. It should be emphasized that, except for the cases where

good resolution is required, the width of the profile has little to do

with the precision of the measurement; it is principally the steepness

of the sides of the profile which matters. From this brief discussion

we see that the properties of the profile which are of interest are (1)

height above background, (2) width, and (3) the slopes of the sides.

We shall now turn to the factors which determine the line profile and
which might be used to alter the characteristics of the profile.

The factors which determine the shape of the line profile are
essentially three in number: the crystal window, the source window, and
the natural line profile. The line profile as observed is the so-called
fold of these three factors. For the most part, the profiles for nuclear
gamma-radiation studied with the spectrometer are determined entirely
by the crystal and source windows. The notable exception to this is
the annihilation radiation, to be more fully discussed in the next
section. X-radiation, too, has a natural width which contributes to the
observed profile. The shape of the line profile has been discussed ex-
tensively in the literature[2,6,7,12,13,14]. Nevertheless, for a com-
plete understanding of the work presented in this thesis, it is advisable
that portions of this material be reiterated.

Before discussing the different windows contributing to the line
profile, the exact meaning of the term "window" should be made clear. In
analyzing a line profile, the interesting property is the amount of radia-
tion detected at each wavelength setting. Now the crystal responds to
monochromatic radiation (i.e., radiation of a single wavelength) not at
a single reflection angle, but over a small range of angles. Thus the
crystal might be said to spread out the radiation, since different angles
should correspond to different wavelengths. The plot of crystal response
versus angular setting, or the wavelengths corresponding to the angular
settings, is called the crystal window. It is what the crystal "sees"
when placed in the path of monochromatic radiation. In a somewhat
similar sense the source sends radiation toward the crystal from different

points along the focal circle, and this source distribution means that
the crystal must turn through a small angle in order to present itself
in the proper reflecting position to the different portions of the
source. Thus again we have a distribution of radiation (accepted for
reflection by the crystal) with respect to angle or corresponding wave-
length. This distribution is called the source window. The response of
the instrument as a whole is the fold of the crystal and source windows.

The Crystal Window: There are two principal contributors to the
crystal window: deviations of the front surface of the crystal from a true
cylinder and the intrinsic diffraction pattern of the crystal. The first
of these has resulted in the extensions of the crystal planes not inter-
secting in a line at the β -point. Sensitive x-ray tests have shown
that the width of the best focus is about 0.05 mm. This value is about
one-third the width of the diffraction pattern of the crystal (see below),
and it is doubtful whether any attempts to reduce the width at best focus
would be worth the great care and effort required. The second contributor,
the intrinsic diffraction pattern of the crystal, has been found to be
considerably wider than that for an unstressed crystal. Studies by
Lind[12,13] have indicated that the stressed (bent) crystal lamina seems
to behave like a mosaic crystal. Furthermore, it has been found that the
intensity of the reflected beam is proportional to the thickness of the
crystal lamina; thus doubling the thickness of the crystal increases the
over-all luminosity of the spectrometer by a factor of two. Unfortunately
the spectral width of the crystal window is doubled at the same time,
thereby limiting the resolving power of the instrument somewhat more severely.
In the sources studied to date, however, this has not been a serious diffi-

culty, and consequently the original 1 mm lamina has been replaced by one of 2 mm thickness. The intrinsic diffraction pattern of the 2 mm crystal has a width at half-maximum of about 0.16 mÅ, corresponding to 0.16 mm of travel of the source carriage relative to the screw carriage. This value was found from the experimental profiles obtained with a very thin (0.025 mm) source of Au^{198}. With such a thin source, practically all of the width of the instrumental window is due to the crystal window, contributions from the source size and natural breadth of the gamma-ray line being negligible. More recent measurements of the 662 Kev gamma-ray line from a thin source of Cs^{137} have corroborated this value. For the purposes of calculation, the function $e^{-h^2 x^2}$ may be used to re-present the crystal window. The constant h is chosen so that the curve has a 0.16 mÅ width at half-maximum. The only significant deviation of this Gaussian function from the true window is in the "tails" of the curve, where the Gaussian is considerably higher than the actual window curve. For discussion of the more important properties of the profile, however, this can be ignored.

The Source Window: Ideally the radiation reaching the crystal should appear to come from a line on the focal circle. There are two methods of approximating this ideal situation: confining the source to a small volume approximating such a line, or using a narrow slit on the focal circle to define the source as seen by the crystal. Both of these methods are used in the spectrometer. In either case the radiation will appear to come from a small section of the focal circle instead of a line. A plot of the fraction of the total radiation reaching the crystal due to a small element of this section of the focal circle versus the position

of the element on the focal circle is called the source window. The
shape of this window curve depends on either the shape and position of
the source or the design of the slit.

Let us first consider the case where the source is to be defined
by its own dimensions. The usual practice is to make the source rectan-
gular in shape (see Fig. 20a) and place it with its narrowest dimension
facing the crystal and its center on the focal circle. This is illus-
trated in the somewhat exaggerated drawing of Fig. 20b. As the angle η
is varied so that the line CP sweeps across the source, the length of
the section of the line passing through the source gives a number pro-
portional to the ordinate of the source window for that angle, if self-
absorption of radiation in the source is neglected. The window thus
obtained is shown in Fig. 20c. In this figure the ordinate scale has
been compressed considerably to show the detail. It should be realized
that this is the source window as seen by a small portion of the crystal
near C; a portion of the crystal at C' sees a slightly different window.
Such differences, however, are negligible so long as the depth of the
source is not too large in comparison to the width. Furthermore, the range
of η which produces the slanting sides of Fig. 20c is extremely small, and
the window can be represented by a rectangle with no appreciable error.
Now for maximum intensity in the reflected beam all portions of the crystal
must see the radiation as coming from the same section of the focal circle.
Thus placing a larger source at some distance beyond the focal circle
would not appreciably increase the height of the observed profile but
would merely cause a broadening of the line, since different portions of
the crystal would see different sections of the focal circle as the source

of radiation. It is clear from Fig. 20b that the width of the source

window, as given by the change in η as CP sweeps across the source, is

dependent on both the width w of the source and the depth d. A small

change in w, however, is much more effective in changing the width of

the source window than a small change in d. Consequently, in any attempt

to increase the source strength by increasing its size one should first

consider increasing the depth. Unfortunately the result of such a change

is limited by self-absorption of the radiation, which becomes quite marked

for low energies. To increase the intensity of low energy radiation, then,

one must make the source wider. Further inspection of Fig. 20b shows that

the initial positioning of the source along CR is not a critical adjustment.

Also, a slight lateral displacement to one side or the other merely effec-

tively shifts the β -point, and this cancels out when the difference in

the positions of the two profiles of the pair is taken. The important

thing is not to place the source at an exactly predetermined position,

but to know precisely where it is at all times subsequent to its installa-

tion in the spectrometer. Some care should be taken to align the source

so that its longest axis intersects the line CR, but adjustments in the

direction of CR can be made with sufficient accuracy with an ordinary meter

stick. This fact is to be incorporated in a new spectrometer now being

designed.

It has already been emphasized that for accurate wavelength deter-

minations the sides of the line profile should be as steep as possible.

From the discussion so far it is apparent that the only factor contributing

to the line profile over which the experimenter has any reasonable degree

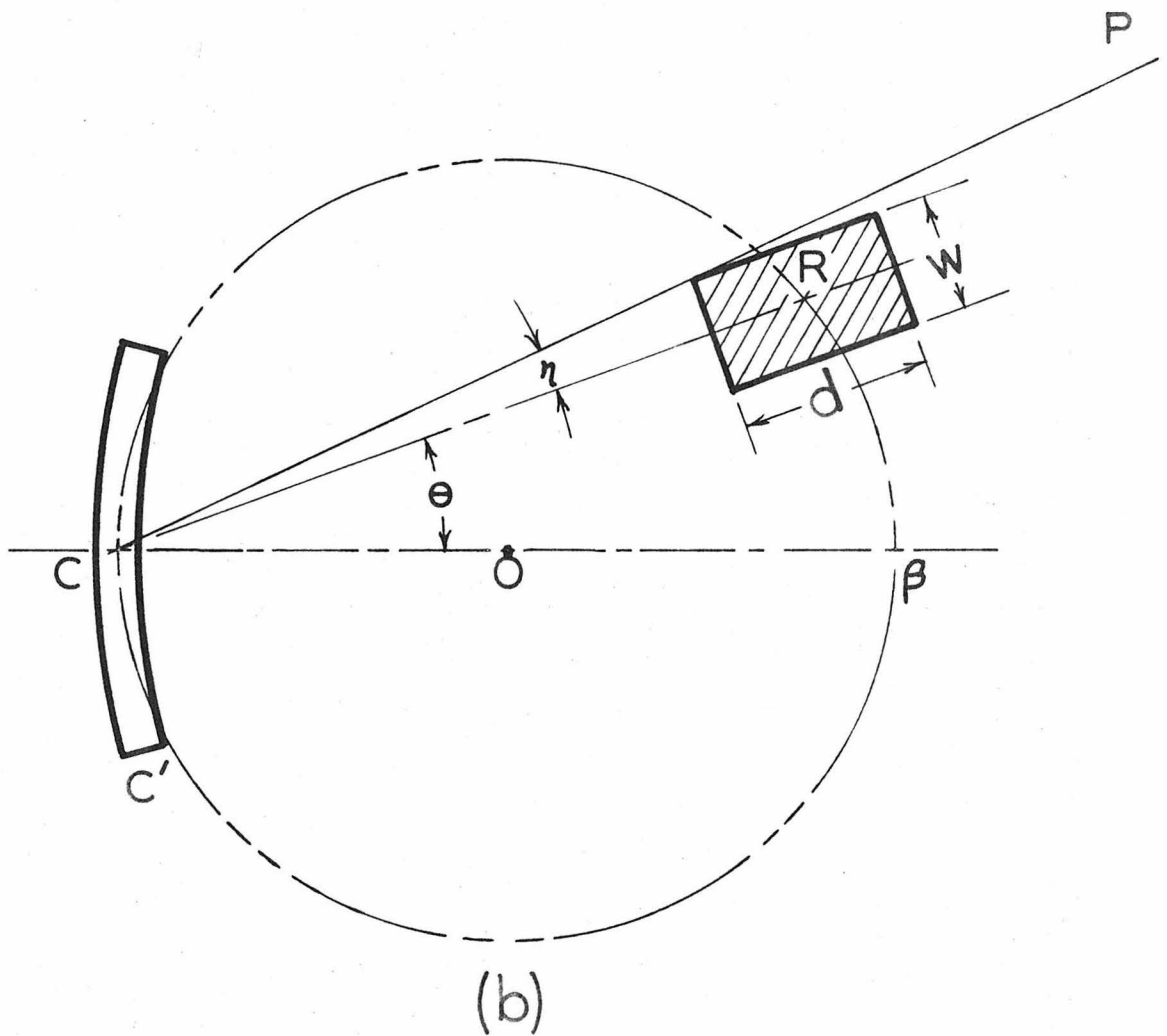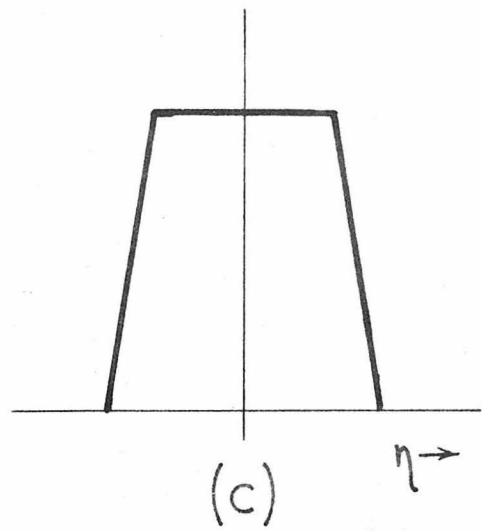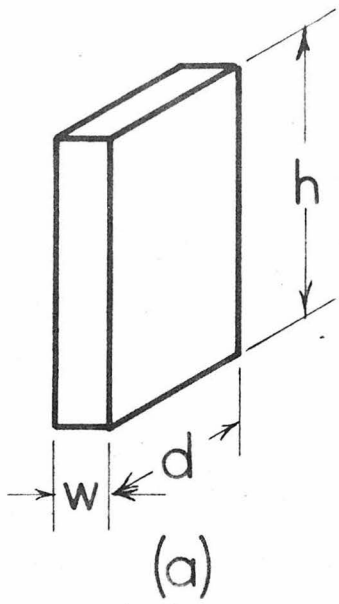of control is the source window. Hence every effort should be made to

Fig. 20 — Illustrating the Source Window

TYPE I

SOURCE

TO CRYSTAL

α

(a)

TYPE II

SOURCE α
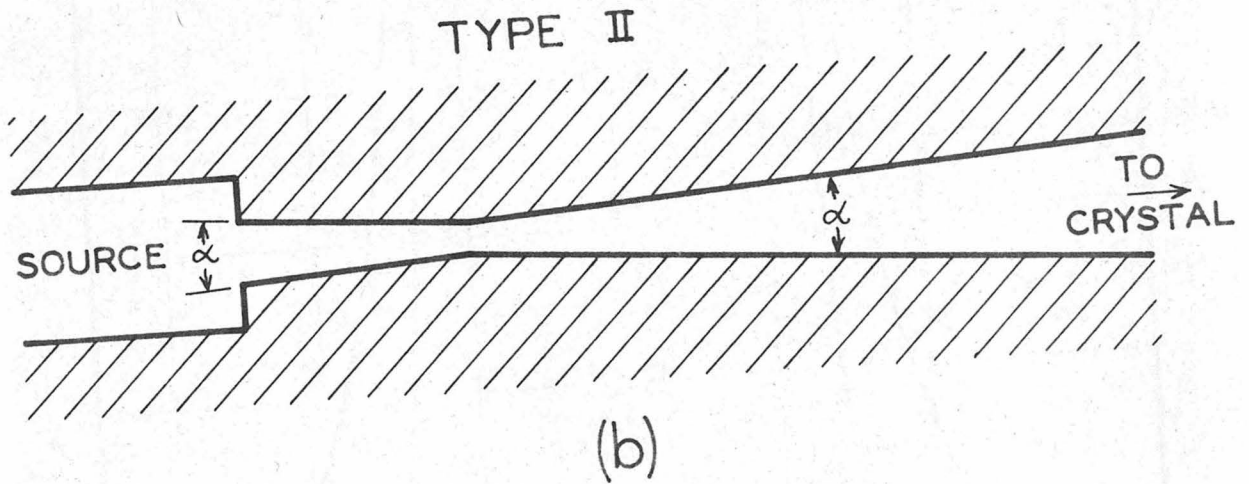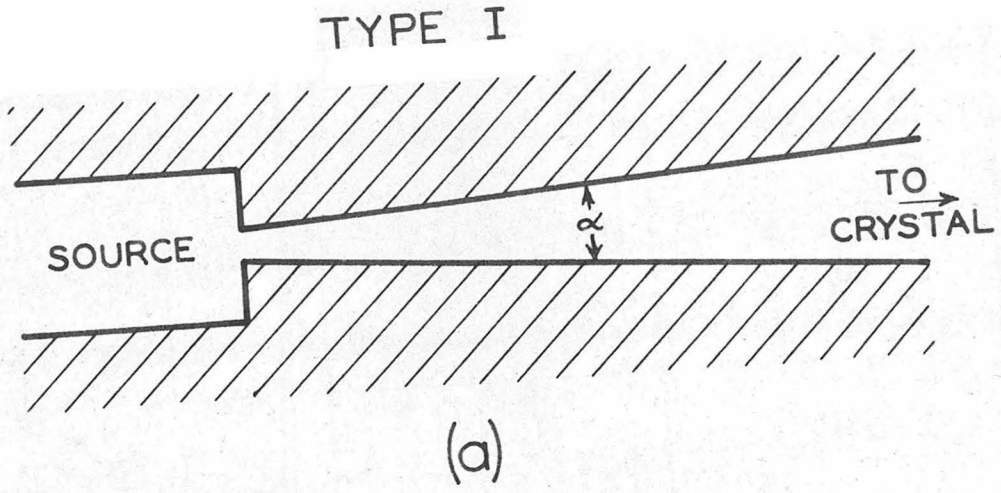
TO CRYSTAL

α

(b)

FIG. 21 - TWO DESIGNS FOR SLIT JAWS
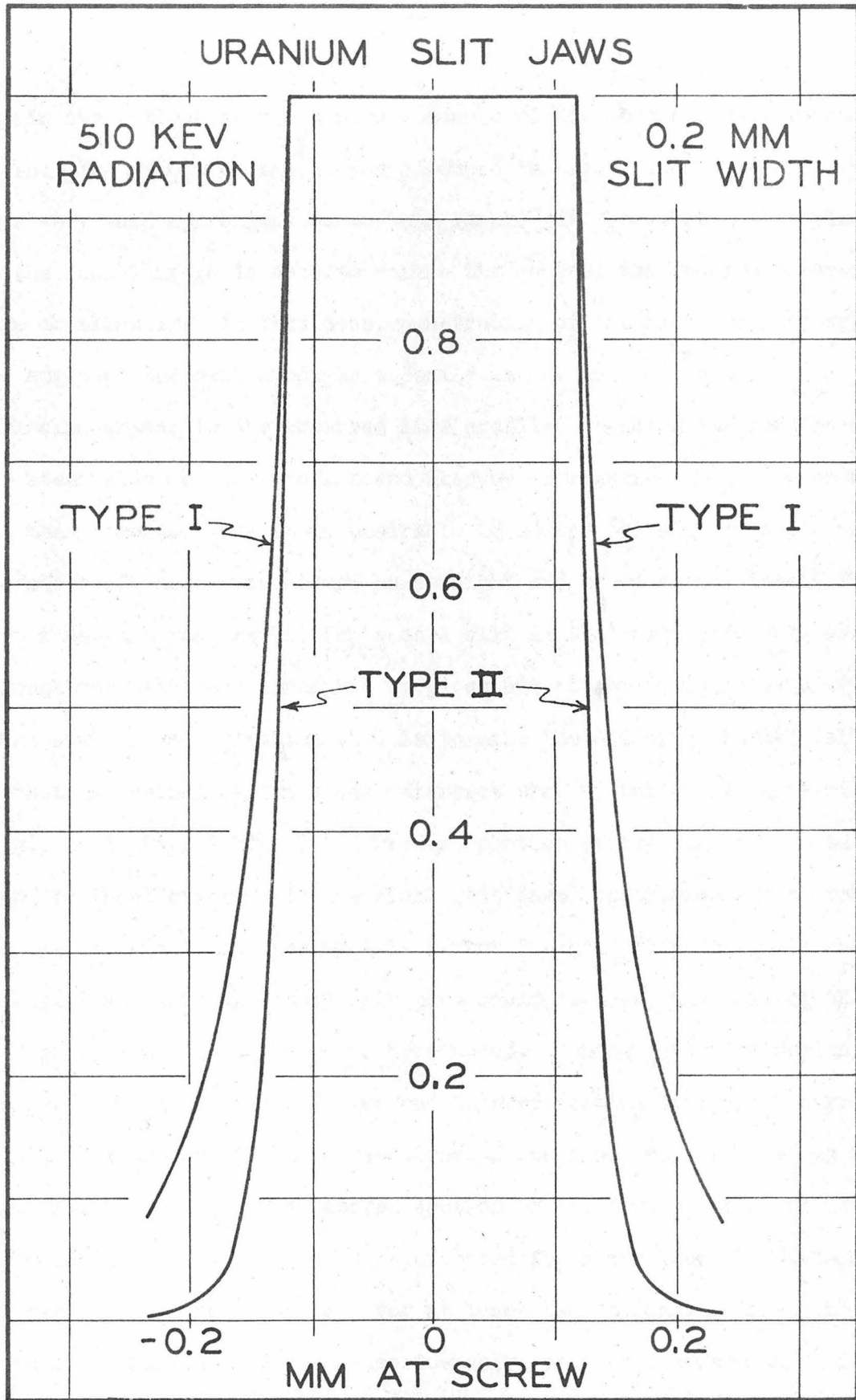THE SKETCHES ARE NOT TO SCALE.

FIG. 22 - SOURCE WINDOWS

obtain the optimum source window. Such a window should have vertical
sides. The window of the source pictured in Fig. 20 and discussed above
is a very good approximation to this ideal. If, however, a slit placed
on the focal circle is used to define the source, the problem becomes
more complicated. In this case, penetration of the radiation through
the edges of the slit produces a "tail" in the source window. This tail
will also appear in the observed line profile, reducing the lengths of
the steep sides of the profile and thereby decreasing the precision of
the measurement. Thus it is desirable to design the slit so as to make
the sides of the source window as straight and steep as possible. The
most important requirement for such a slit is that radiation not passing
through the slit pass through a large amount of absorbing material. The
first step in accomplishing this is to make the defining channel (slit)
so that extensions of its sides intersect the crystal at its extremities
(e.g., C' in Fig. 20b). The narrowest portion of the slit is placed at
R on the focal circle. In the first slit jaws constructed the source
was placed immediately behind this narrow "neck". This design is shown
in Fig. 21a. Although these slit jaws could be used, the tail of the
line profile proved to be quite pronounced. Consequently the design was
improved by the addition of a second tapered section behind the narrowest
point. The tapers of the two sections of the jaws are the same, as in
Fig. 21b. Supposedly the tapered section of the jaws between the narrow-
est point and the source could be extended for a considerable distance.
However, this is not practical for at least two reasons. First, the
source size must be increased considerably, and the increase in luminosity
is roughly proportional to the increase in depth rather than to the increase

in volume. This is a result of the fact that each element of the crystal
views a very small portion of the entire source. The size of this
source element is essentially determined by the width of the narrowest
portion of the slit jaws and the depth of the source. Second, the space
available for the source and source jaws is limited in the present spec-
trometer by the size of the lead bomb used for shielding. Nevertheless,
even a 1 cm tapered section behind the narrowest point produces a marked
improvement. This can be seen in Fig. 22, which shows the source windows
for the two designs of Fig. 21. These windows are for 510 Kev radiation
and slit jaws of uranium. The slit width is 0.2 mm and the angle α is
1.455°. The material to be used in construction of the slit jaws should
be chosen to give the greatest absorption coefficient for the particular
energy of the radiation being studied.

Thus far little has been said about the actual dimensions of
sources used in the spectrometer. The height of the source has not been
considered at all here, since aberrations caused by radiation traveling
in a plane not parallel to the focal circle are slight. The usual height
of sources is about 1.25 inches (31.8 mm). The depth has not proved to
be too critical either, except when self-absorption is appreciable. Values
for self-defining sources normally range from 1 mm to 5 mm; with a defining
slit, sources as deep as 12.5 mm (0.5 inch) have been used. As stressed
before, it is the width of the source or defining slit that is the most
critical dimension. It is desirable to keep the width of the source
window of the same general magnitude as that of the crystal window (0.16 m$\overset{o}{A}$).
The normal range of widths in use is from 0.025 mm to 0.3 mm (i.e., 0.001
inch to 0.012 inch). Wider sources produce a line profile which is not

SOURCE WIDTH = 0.004 INCH
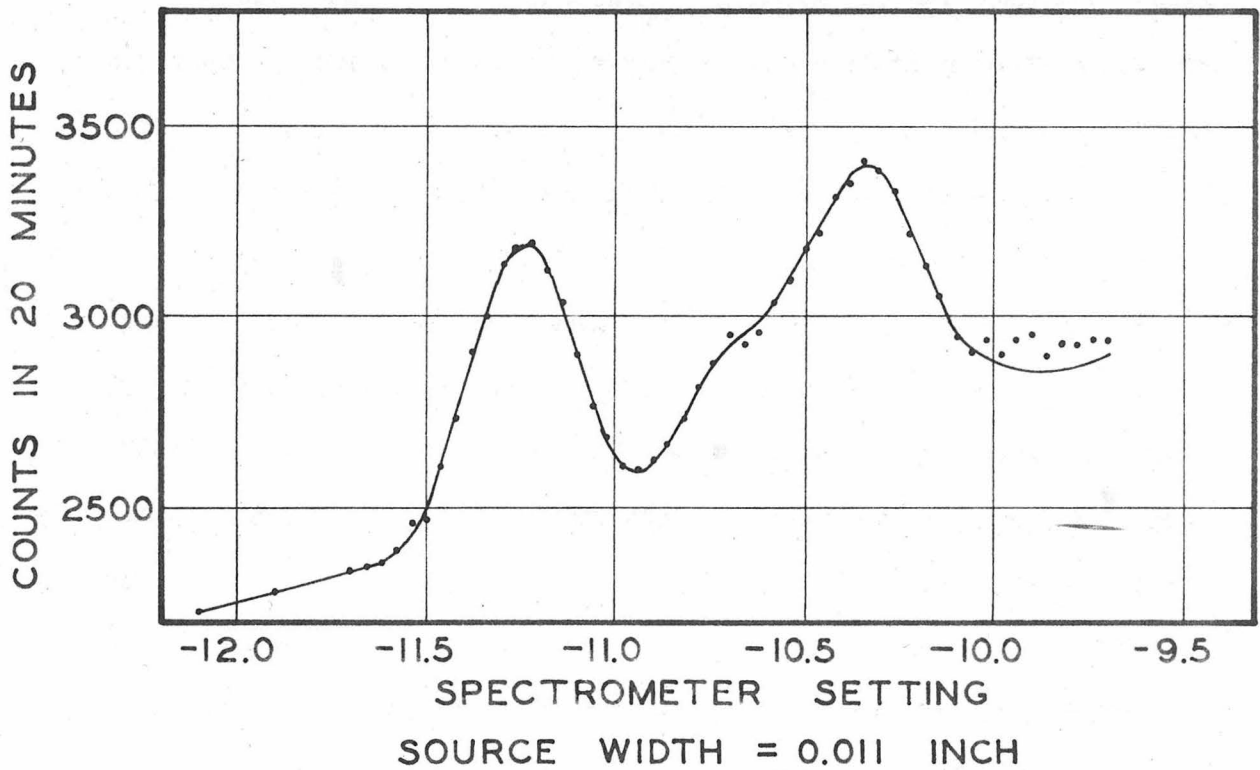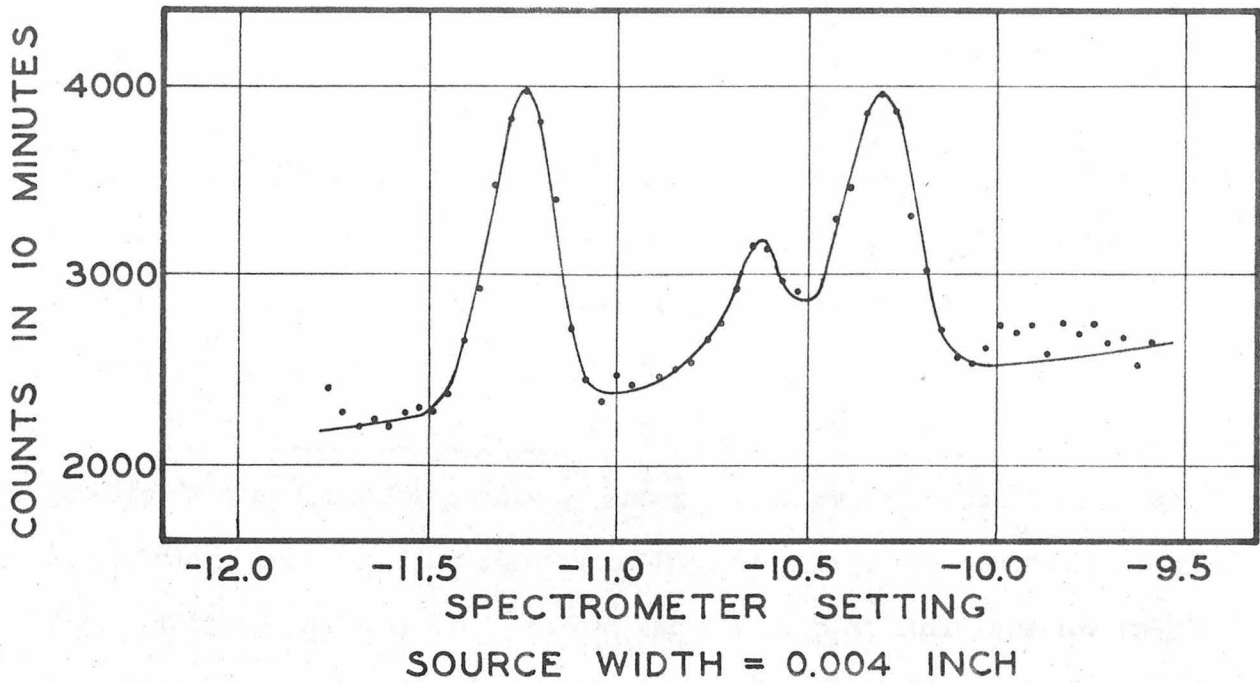
SOURCE WIDTH = 0.011 INCH

FIG. 23 - SHOWING THE EFFECT OF SOURCE WIDTH
ON RESOLUTION. GAMMA - RAY LINES OF
ABOUT 1.2 MEV ARE SHOWN.   THESE
FOLLOW DECAY OF TA 182.

appreciably higher but which has a flat top. Also, resolution is seriously impaired with wide sources. If it is known that good resolution is required, the narrowest source consistent with adequate intensity should be used. Fig. 23 illustrates very well the effect of source width on resolution.

The Natural Line Profile: We include in this category any inhomogeneity in the radiation studied. Among the causes of inhomogeneity are natural line breadth, line structure, Doppler shift, and Compton scattering. Of these, natural line breadth and the Doppler shift are the only two which have produced readily observable effects in line profiles obtained with the gamma-ray spectrometer. Although nuclear gamma-ray lines are supposed to have breadth, those line profiles studied to date have not had sufficient width to indicate appreciable natural line breadth. This has been ascertained by comparison of the experimental line profile with a line profile calculated solely from the crystal and source windows, and by comparison of the experimental profiles obtained from 1st, 2nd, and 3rd order reflections in the crystal. The case for x-rays, however, is different, since x-ray lines are known to have natural breadth. Experimental profiles for x- and gamma-ray lines produced during decay of the same source of Ta^{182} are shown in Fig. 24 to illustrate the effects of natural breadth. It can be seen both as an increase in line width and as the presence of a pronounced tail. In the case of the annihilation radiation, the motion of the center of mass of the annihilating electron-positron pair with respect to the crystal (i.e., in the LAB coordinate system) produces a Doppler shift in the observed wavelength. This appears as a symmetric broadening of the line profile, since positive and negative
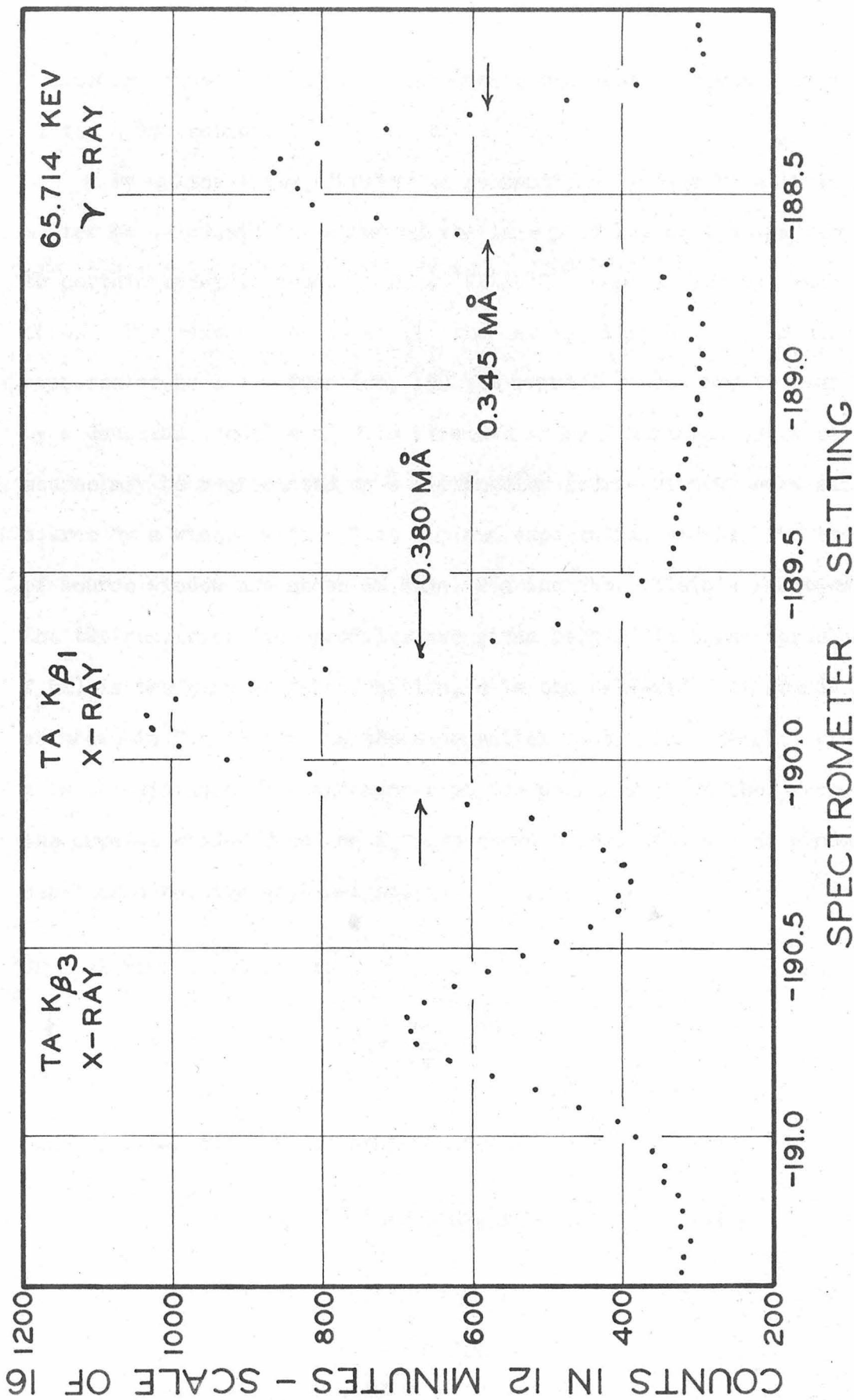
FIG. 24 – SHOWING THE EFFECT OF NATURAL LINE BREADTH. THIS RADIATION FOLLOWS DECAY OF TA 182.

shifts are equally likely. This Doppler broadening is shown in Fig. 29 of the next section.

By making a few simplifying assumptions it is a relatively easy matter to calculate the shape of the line profile, or that part of it due to certain specific causes. D. J. Klein[14] has carried out such calculations. His assumptions were: (1) the natural line has no width and may be represented by a δ-function, (2) the crystal window may be represented by a Gaussian function of 0.16 mÅ width at half-maximum, (3) a self-defining source may be represented by a rectangular source window and a slit-defined source by a window with a flat top and exponential sides. The two types of source window are shown in Figs. 25a and 25b. Klein's functions for the two resultant line profiles are given below. In these formulae $f_p(x)$ is the line profile function, d is the half-width of source or slit as shown in Fig. 25, a is the exponential factor for the slit window, and x is the distance from the center of the profile. h is the parameter of the crystal window function f_c also shown below. The source windows were taken to have unit height.

Crystal Window Function:

$$f_c = \frac{h}{\sqrt{\pi}} \, e^{-h^2 x^2} \tag{1}$$

Line Profile for Self-Defining Source:

$$f_p(x) = \frac{2}{\pi} \left[\text{erf } h(d + x) + \text{erf } h(d - x) \right] \tag{2}$$

Line Profile for Slit-Defined Source:

$$f_p(x) = \frac{2}{\pi}\left[\text{erf } h(d+x) + \text{erf } h(d-x)\right]$$

$$+ \tfrac{1}{2}\left\{\exp\left[a(d+x)+\frac{a^2}{4h^2}\right]\right\}\left\{1-\text{erf}\left[h(d+x)+\frac{a}{2h}\right]\right\}$$

$$+ \tfrac{1}{2}\left\{\exp\left[a(d-x)+\frac{a^2}{4h^2}\right]\right\}\left\{1-\text{erf}\left[h(d-x)+\frac{a}{2h}\right]\right\} \qquad (3)$$

These functions may be used to study the effect of source or slit width on the line profile or to get some idea of the natural line profile, if appreciable. The composite and calculated (using eq. (2)) profiles for a source of Ta^{182} are compared in Fig. 26. The more pronounced tail of the calculated line profile is due to the tail of the Gaussian function (eq. (1)) assumed for the crystal window.
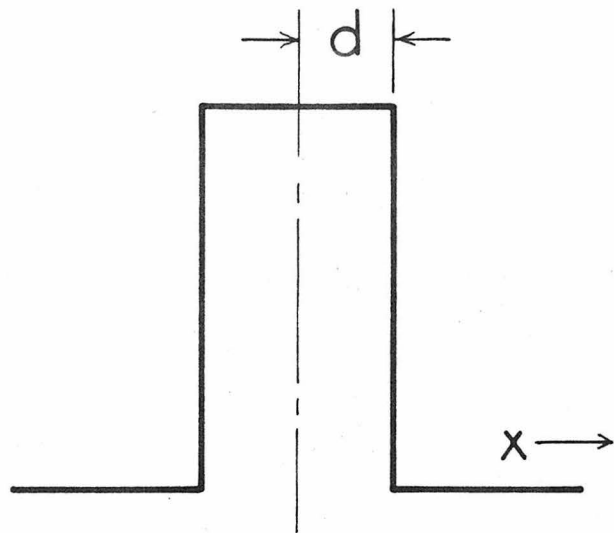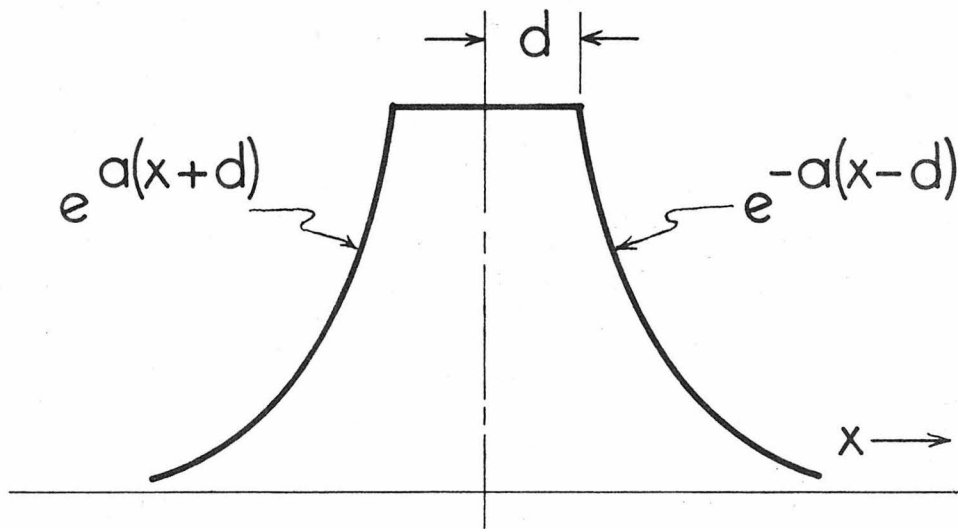
FIG. 25 – SOURCE WINDOWS USED IN CALCULATING THE LINE PROFILE.

FIG. 26 – COMPARISON OF COMPOSITE AND CALCULATED LINE PROFILES

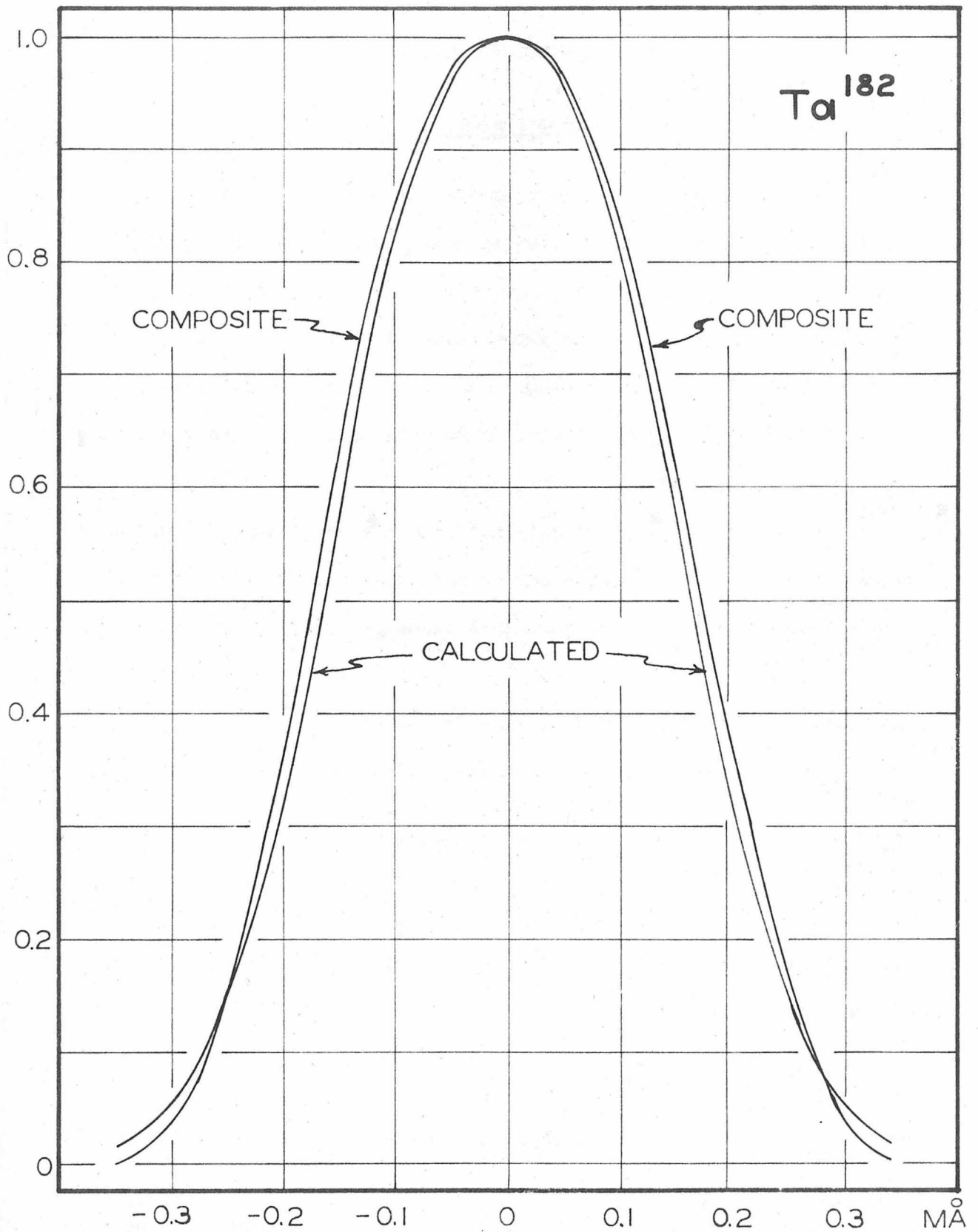## II. WAVELENGTH MEASUREMENTS

A. The Annihilation Radiation

It is well known that the positron decays by the process of annihilation of positron-electron pairs. The energy released by the disappearance of the masses of the positron and the electron appears as radiation. If we view the positron-electron system in the center of mass coordinate system, two or more quanta must be produced in order to conserve momentum. If an atom or nucleus is available to absorb the residual momentum, one-quantum annihilation also is possible. Of one-, two-, and three-quantum annihilation, the two-quantum process is the most prevalent. Studies with the curved crystal gamma-ray spectrometer have been limited to two-quantum annihilation, principally because of intensity requirements.

If both positron and electron are at rest in the CM system, the equivalence of mass and energy yields equation (1) below.

$$(m_+ + m_-)c^2 = 2h\nu = 2\frac{hc}{\lambda_A} \tag{1}$$

In this relation m_+ and m_- are the rest masses of the positron and electron, respectively, c is the velocity of light, h is Planck's constant, ν is the frequency of the annihilation radiation, and λ_A is the wavelength. Rearranging (1), the wavelength is found to be

$$\lambda_A = \frac{2h}{(m_+ + m_-)c} \tag{2}$$

Now this is the wavelength in the CM system; in the LAB coordinate system

the observed wavelength will be altered by a Doppler shift due to the
motion of the center of mass. However, there is no reason to assign
a preferred direction to the motion of the center of mass; and therefore,
when one considers all of the electron-positron pairs annihilating in a
given time interval, the effect is a broadening of the observed line
rather than a shift in the center of the line. If there should be a
residual kinetic energy in the CM system, or if the potential energies
of the two particles should not be equal in magnitude and opposite in
sign, a shift in wavelength would result. It has been shown[7] that
such effects, if present, are negligible, and so may be neglected. The
observed wavelength, then, is that given by equation (2).

A measurement of the annihilation radiation wavelength may be
interpreted in two different ways, depending on the initial assumptions
made. First, if the constants h, c, and m_- are considered to be known
from other sources, such as a least-squares adjustment of constants,[11]
the wavelength measurement yields the mass of the positron. In such a
case, the result cannot be entered as an input datum in a least-squares
adjustment of constants unless the positron mass is taken as an additional
output datum. On the other hand, if one feels sufficiently certain that
the masses of the positron and the electron are equal, the wavelength is
a measure of h/m_0c (here m_0 is the rest mass of the electron or positron)
and is a suitable input datum for a constants adjustment. The successes
of the Dirac relativistic wave equation and the "hole" theory of the
electron have supported the belief that the masses m_+ and m_- are equal.
However, since Dirac theory, in common with many theories, has its

difficulties,* a comparison of electron and positron masses which is
independent of the theory is highly desirable. The first interpretation
of the wavelength measurement, then, seems to be the preferable one.
This is the viewpoint which we shall adopt here.

One of the principal problems in the measurement of the annihilation
radiation wavelength with the curved crystal spectrometer is the source of
positrons to be used. First, a fairly strong source of radiation is
necessary; the radiation should correspond to an activity of 10 millicuries
or better at all times. Second, only naturally radioactive or neutron-
activated materials are economically feasible because of the source strength
requirement. On this basis Cu^{64} was selected as the source material.
Even with this most advantageous choice, however, additional difficulties
are encountered. These are: (1) Cu^{63} comprises only 69 percent of
natural copper; (2) the neutron absorption cross-section of Cu^{63} is rela-
tively low - 2.82 barns; (3) Cu^{64} has a short half-life - 12.8 hours;
(4) Cu^{64} decays by three competing processes - K-capture, β^- emission,
and β^+ emission - and positron emission occurs in only 17.5 percent of
all cases; (5) the relatively long range of positrons before annihilation
requires that the source be defined by a slit, thereby severely limiting
the effective volume of the source. The steps taken to make the most of
the available activity will be described in the discussions of the experi-
ments.

The first measurement of the annihilation radiation wavelength

* For example, see W. Heitler, Quantum Theory of Radiation (Oxford
University Press, London, 1944), p. 191 ff.

using the curved crystal spectrometer was made in the summer of 1948
and is reported in reference 7. To compensate as much as possible for
the difficulties listed above, arrangement was made with the Atomic
Energy Commission to have the source irradiated at a very high neutron
flux level, and a special pair of slit jaws was constructed. These slit
jaws were made of lead; their design was that shown in Fig. 21a. The
narrowest point of the slit jaws was adjusted to a width of 0.1 mm and
was placed on the focal circle. The tapered section in front of the
source was about 2.5 inches long. The source itself was a solid piece
of copper 1 mm x 10 mm x 30 mm. On arrival the activity of the source
was 2.5 curies (1 curie equals 3.7 x 10^{10} disintegrations per second);
the useful activity was equivalent to that of an 88 millicurie source
producing a single gamma-ray with each disintegration. Seven pairs of
profiles were obtained, which, on analysis, gave the wavelength

$$\lambda_A = 24.271 \pm 0.010 \text{ m\AA} \tag{3}$$

As mentioned in Part I, Section C, the standard deviation assigned here
was 4 times that obtained from the external consistency of the 7 indivi-
dual measurements. This larger error was assigned to take care of the
possible presence of an unknown systematic error. The mass of the positron
may be compared with that of the electron by means of the relation

$$\frac{m_- - m_+}{m_-} = 2 \frac{\lambda_A - \lambda_c}{\lambda_A} , \tag{4}$$

where λ_A is the observed wavelength of the annihilation radiation,
$\lambda_c = h/m_- c$ is the Compton wavelength of the electron, and m_- and m_+ are

the electron and positron rest masses, respectively. Using the 1947 DuMond-Cohen[8] value for λ_c, (4) gave

$$\frac{m_- - m_+}{m_-} = (4.0 \pm 8.8) \times 10^{-4} \tag{5}$$

From these values one could only conclude that the mass of the positron seemed to be the same as that of the electron to 4 parts in 10,000.

With the completion of a new least-squares adjustment of the fundamental constants[11] the data of the 1948 experiment was examined again.[15]* Using the new value for λ_c, (4) gave

$$\frac{m_- - m_+}{m_-} = (8.5 \pm 8.2) \times 10^{-4} . \tag{6}$$

This result raised the question as to whether the positron and electron masses are the same. Furthermore, if one did not use the large value 0.010 mÅ for the error in λ_A, but used the actual value obtained from the data, 0.0025 mÅ, the result was changed to

$$\frac{m_- - m_+}{m_-} = (8.5 \pm 2.1) \times 10^{-4} . \tag{7}$$

This new value for the error definitely seemed to indicate a difference in the masses, if one assumed that all appreciable systematic errors were known. At this time it was decided to repeat the experiment with the gamma-ray spectrometer, since new developments had greatly increased the luminosity of the instrument.

In 1950, Hedgran and Lind[16] at Stockholm measured the energy

---

* Some numerical errors in reference 15 have been corrected here.

difference between the annihilation radiation and the 411 Kev gamma-ray line from Au^{198}, obtaining a value of 99.15 ± 0.06 Kev. This, when combined with a weighted average of determinations of the gold gamma-ray energy yielded the annihilation radiation energy. Their value was

$$E_A = 510.37 \pm 0.16 \text{ Kev.} \tag{8}$$

Comparison with the 1950 constants value of $m_- c^2$ gave

$$\frac{m_- - m_+}{m_-} = (2.35 \pm 0.63) \times 10^{-3} \ , \tag{9}$$

an even more striking result than that of equation (7). It should be noted, however, that the Stockholm value was based primarily on the curved crystal spectrometer value for the gold gamma-ray energy; and therefore it cannot be classed as a completely independent measurement.

Shortly after the publication of the Hedgran-Lind paper, a systematic non-linearity in the gamma-ray spectrometer was discovered. The error this non-linearity introduced was of the right magnitude and sign to account for the mass discrepancy of equations (7) and (9). At the same time, by independent means, Lindström[17] showed that the curved crystal spectrometer value for the Au^{198} gamma-ray line seemed to be too low and that m_+ and m_- appeared to be equal. The subsequent calibration of the spectrometer and the installation of adequate facilities to determine the correction for the non-linearity have been described in Part I. Repetition of the 1948 experiment now was deemed even more desirable, since the mirror (non-linearity) correction is best determined at the time of measurement.

A more careful analysis of the slit jaw problem has shown that the optimum design is that of Fig. 21b. This change in design produces a

marked increase in the steepness of the sides of the source window. Proper
choice of the absorbing material to be used in the slit jaws should in-
crease the steepness even more. Several different materials - lead,
tungsten, heavy-met (90% W, 6% Ni, 4% Cu), and uranium - were compared.
The respective linear absorption coefficients are shown in Table IV.

Table IV

Linear Absorption Coefficients for 510 Kev Gamma-Radiation

Material	μ in cm^{-1}
Pb	1.68
W	2.37
Heavy-met	1.97
U	3.53

Clearly uranium is the most desirable of the materials considered. Through
the cooperation of the Atomic Energy Commission, sufficient uranium was
made available to this project, and the slit jaws were made according to
the required design at the Brookhaven National Laboratory. This design
follows that of Fig. 21b, with a 1 cm tapered section between the source
and the narrowest point, and a tapered section of about 5 cm length
between this point and the crystal. The angle α is 1.455°. The width
of the narrowest point was made adjustable; a width of 0.2 mm was chosen
for the experiment. The source window for these slit jaws is that
labeled Type II in Fig. 22.

The source was a piece of copper 0.080" x 0.497" x 1.25" weighing

7.17 grams. The reactor at the Argonne National Laboratory near Chicago was chosen for the irradiation. Both Chalk River and Brookhaven were considered, but were rejected because almost all of the additional activity produced by the higher neutron flux density would be lost in transit. For this irradiation the Argonne reactor was operated at high level (about 3.2×10^{12} neutrons/cm^2/sec). The source was flown from Chicago to Burbank, California, by a special U. S. Navy plane. In this way it was possible to begin measurements in less than 12 hours from the time the source was removed from the reactor. The source activity was about 7 curies at the time the source was installed in the spectrometer; the useful activity was equivalent to about 250 millicuries.

It had been hoped that the annihilation radiation line could be measured by a 2nd or 3rd order reflection from the crystal planes. The precision of the measurement would be increased considerably if this were possible, since the distance measured by the screw would be doubled or trebled while the instrumental errors remained essentially constant. However, preliminary calculations had shown that if the line were detected at all it would be too weak to use successfully. Measurements made immediately after the installation of the source confirmed this. Consequently, all measurements were confined to 1st order reflections.

A 5 minute counting interval at each wavelength setting was chosen as a satisfactory value. This interval was kept fixed throughout the entire experiment. Thus all of the profiles obtained were subject to the same distortion due to decay of the source. Since the important quantity is the difference in wavelength setting between corresponding points on the two members of a pair of profiles, the decay correction then was not

necessary for proper interpretation of the data. This eliminated possible errors due to additional arithmetic operations. Furthermore, the decay correction for the 3-hour interval required to cross a single profile is quite small. A total of nine pairs of profiles was obtained before the source had decayed below its useful limit (in fact, Run #9 was made with a useful activity of about 5 millicuries equivalent). The profiles for Runs #2 and #9 are shown in Figs. 27 and 28, respectively. The results of the experiment are shown in Tables V, VI, and VII.

Table V illustrates the slight variation in results due to mechanical hysteresis in the spectrometer. It was stated in Section C of Part I that this hysteresis effect, which can be detected with the mirror and microscope attached to the crystal and screw carriage, respectively, depends on the previous history of the spectrometer settings. Since the exact nature of the hysteresis effect is not known, proper correction can be made only by taking the data for the mirror correction at the time the wavelength measurements is being made.

The first column of the table gives the value of the difference 2λ between settings for reflections from opposite sides of the crystal planes, after all corrections except the mirror correction have been made (the values have not been converted from screw divisions to $m\overset{\circ}{A}$, however). The second column gives the values after the mirror correction has been applied. These values are in much better agreement than those of the first column. The values of 2λ (in screw divisions) from the 1948 experiment are also included in the table to indicate the improvement in reproducibility which has been made during the intervening four years.
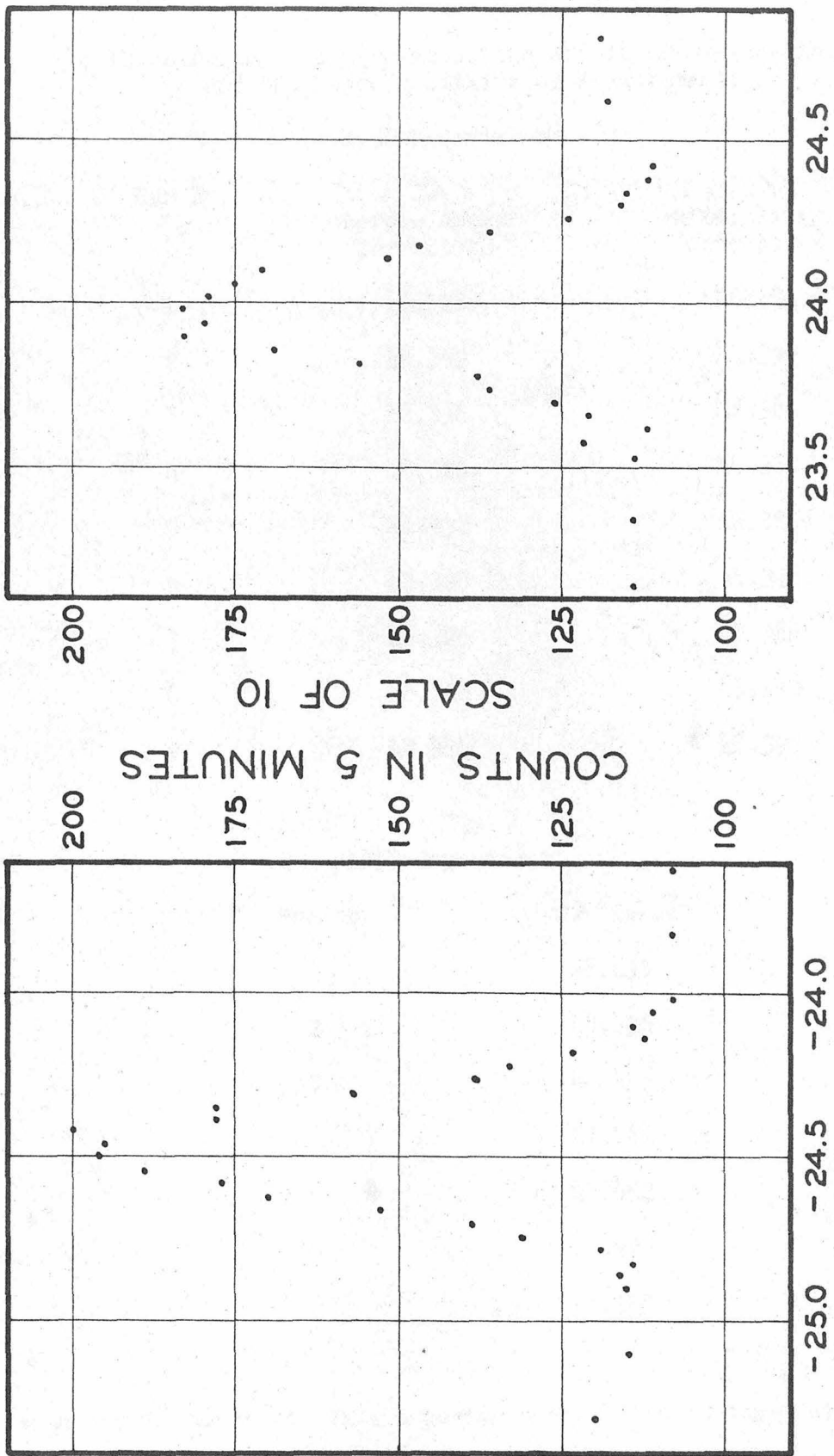
Table VI shows the results of the error analysis for this experiment.
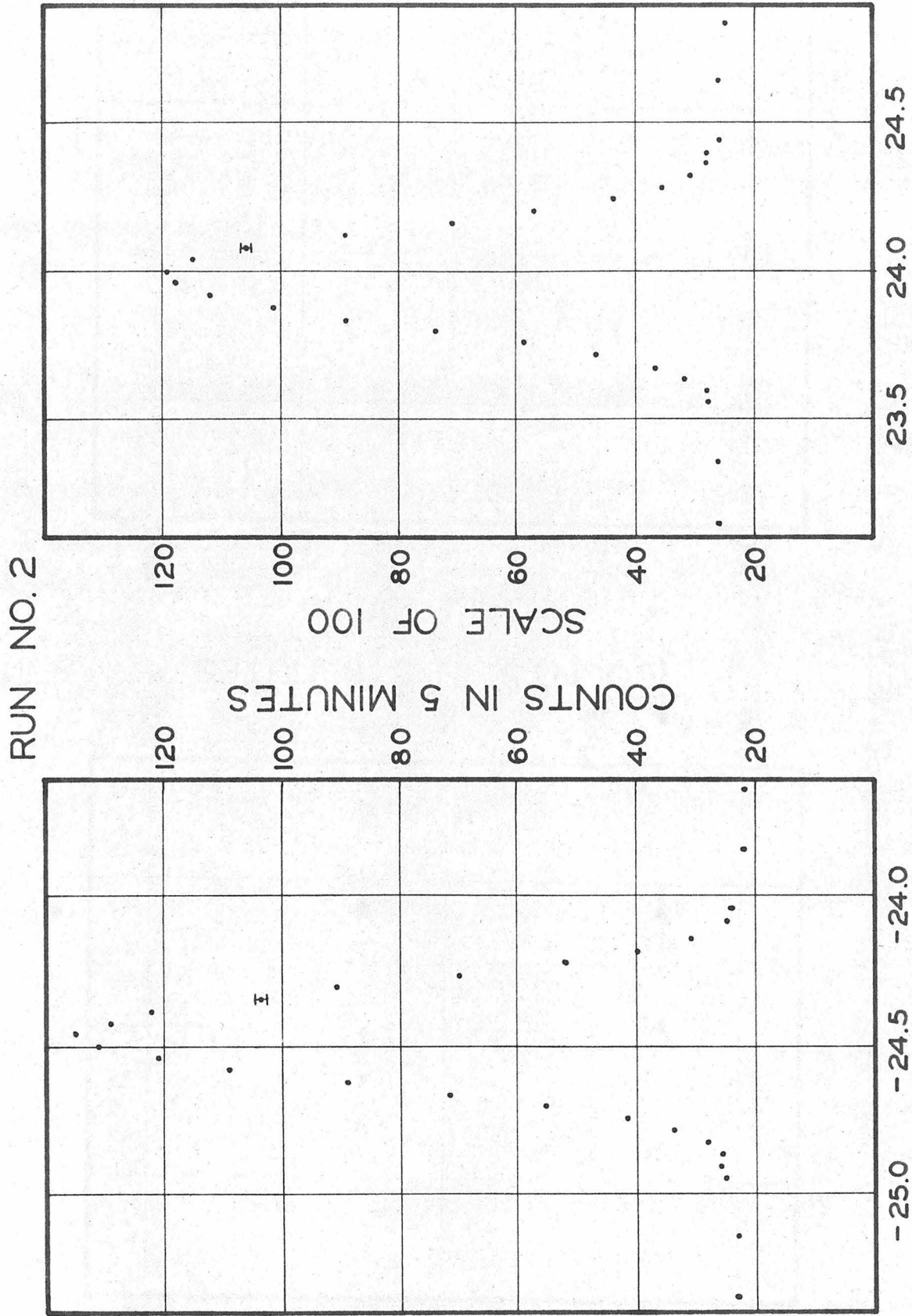
FIG. 27—OBSERVED LINE PROFILES FOR ANNIHILATION RADIATION

FIG. 28 – OBSERVED LINE PROFILES FOR ANNIHILATION RADIATION

TABLE V

Illustrating the Removal of the Effect of Hysteresis and the Reproducibility of Measurements

1952 Experiment*

Run No.	2λ Before Mirror Correction	2λ After Mirror Correction
1	48.328	48.383
2	48.352	48.390
3	48.338	48.388
4	48.320	48.381
5	48.332	48.385
6	48.328	48.378
7	48.326	48.384
8	48.336	48.390
9	48.344	48.392

1948 Experiment

Run No.	2λ in m$\overset{o}{A}$
1	48.453
2	48.436
3	48.455
4	48.464
5	48.452
6	48.423
7	48.465

* Wavelength values for this experiment are given in screw divisions.

TABLE VI

I	II	III	IV	V	VI	VII	VIII
Run No.	λ in Screw Div.	Variances in $(\overset{o}{mA})^2 \times 10^6$					
		Counting Statistics	Matching Profiles	Random Variation in Screw Readings	Mirror Readings	$\sum \sigma_\lambda^2$	Weight
1	24.192	0.17	2.3	1.2	2.0	5.7	2.18
2	24.195	0.19	"	"	"	5.7	2.18
3	24.194	0.27	"	"	"	5.8	2.14
4	24.190	0.51	"	"	"	6.0	2.07
5	24.193	0.71	"	"	"	6.2	2.00
6	24.189	1.22	"	"	"	6.7	1.85
7	24.192	2.19	"	"	"	7.7	1.61
8	24.195	3.94	"	"	"	9.4	1.32
9	24.196	6.92	"	"	"	12.4	1

Weighted Mean of Column II:

$$\lambda = 24.193 \text{ screw divisions}$$

Variance by Internal Consistency from Column VII:

$$\sigma_\lambda^2 = \left[\sum_i \frac{1}{\sigma_i^2} \right]^{-1} = 0.75 \times 10^{-6} \ (\overset{o}{mA})^2$$

Variance by External Consistency from Column II:

$$\sigma_\lambda^2 = 5.46 \times 10^{-6} \ (\overset{o}{mA})^2 \text{ for a single run}$$

$$\sigma_\lambda^2 = 0.61 \times 10^{-6} \ (\overset{o}{mA})^2 \text{ for the mean of 9 runs}$$

Additional Factors Yet to be Applied:

Variance of Main Screw Correction: $\sigma_\lambda^2 = 1.8 \times 10^{-6} \ (\overset{o}{mA})^2$

Variance of Quasi-Periodic Correction: $\sigma_\lambda^2 = 5 \times 10^{-6} \ (\overset{o}{mA})^2$

Conversion of Screw Divisions to $\overset{o}{mA}$:

$$\lambda(\overset{o}{mA}) = \lambda(\text{screw divisions}) \times (1.00286 \pm 0.0000786)$$

TABLE VII

RESULTS ON ANNIHILATION RADIATION

The uncertainties given after each ± are standard
deviations. These are given to one extra place to
avoid incorrect weighting when combining these values
with those of other experimenters.

WAVELENGTH:

1. λ_A = 24.262 ± 0.0033 mÅ Cu^{64} direct measurement of λ_A

2. λ_A = 24.263 ± 0.0033 mÅ Au^{198} expt. + Hedgran & Lind

3. λ_c = 24.26067 ± 0.00048 mÅ   DuMond & Cohen L. S. analysis

ENERGY:

1. E_A = 510.941 ± 0.067 Kev Cu^{64} direct measurement of λ_A

2. E_A = 510.920 ± 0.070 Kev Au^{198} expt. + Hedgran & Lind

3. m_-c^2 = 510.969 ± 0.015 Kev   DuMond & Cohen L. S. analysis

POSITRON MASS:

1. $\dfrac{m_- - m_+}{m_-}$ = (1.01 ± 1.85) x 10^{-4} Cu^{64} direct measurement of λ_A

2. $\dfrac{m_- - m_+}{m_-}$ = (1.92 ± 2.80) x 10^{-4} Au^{198} expt. + Hedgran & Lind

This analysis was carried out as indicated in Section D, Part I. The corrected values of λ, in screw divisions, are given in Column II. The contributions to the total variance for λ due to counting statistics, matching profiles, random variation in screw readings, and mirror readings are given in Columns III-VI. Since these are the only error-contributing factors which vary for the different runs, they are the ones which must be used to assign the proper weights to the individual measurements. The sums of the variances of Columns III-VI are given in Column VII, and the weights obtained from these sums are given in Column VIII. The weighted mean of the values of Column II is given below the table. That part of the variance of this mean which is due to the 4 causes listed in the table is also given. This is the variance by internal consistency. The variance by external consistency can be computed from the values of Column II, this is also given below the tabulated data. Comparison of the variances by internal and external consistency shows a very satisfactory agreement. It has already been mentioned that at the time of the experiment it was felt that data obtained after Run #9 would be of dubious value because of the poor counting statistics. This conclusion is supported by the values of Columns III and VII. The additional factors which must be applied to get the final wavelength value in m$\overset{\circ}{A}$ and its standard deviation are also listed below the table. The multiplicative factor for converting from screw divisions was determined from an average of measurements on the WK_{α_1} x-ray line which were made both before and after the experiment.

The final results of the experiment are given in Table VII. The wavelength of the annihilation radiation, the corresponding energy, and the quantity $(m_- - m_+)/m_-$ are listed. For comparison, the values of the

same quantities as obtained from the Hedgran and Lind experiment and a new measurement of the Au^{198} 411 Kev line (discussed in the next section) are given. The DuMond-Cohen least squares analysis values for $\lambda_c = h/m_-c$ and m_-c^2 are also included. The uncertainties given are standard deviations. The factor (12396.44 $\pm$ 0.25) Kev-mÅ$^{(11)}$ was used to change from wavelengths to energies and vice versa.

The values of Table VII indicate that the rest masses of the positron and the electron are equal to 1 part in 10,000.

Theoretically it is possible to unfold the instrumental window from the experimental line profile to obtain the natural line profile. Then an analysis of the shape of the natural line profile should give the momentum distribution for the centers of mass of the annihilating pairs. This information tells which atomic electrons take part in the annihilation process, and to what extent they enter into the reaction. Unfortunately, a complete analysis of the line profile is difficult because of the incomplete knowledge of all of the factors making up the instrumental window. One can, however, obtain some useful information by a rudimentary form of analysis.

The major sources of the instrumental window, the crystal window and the source window, have been discussed in detail in Section E of Part I. In the concluding paragraph of this section it was stated that an appropriate relation for the instrumental window can be obtained by assuming (1) that the crystal window can be represented by a Gaussian function whose width at half-maximum is 0.16 mÅ, and (2) that for a slit-defined source the source window has a flat top and exponential sides.

This relation is

$$f(x) = g(x + d) + g(x - d), \qquad (10)$$

where

$$g(u) = \frac{2}{\pi} \text{ erf } hu + \frac{1}{2}\left\{\exp(hu + \frac{a^2}{4h^2})\right\}\left\{1 - \text{erf}(hu + \frac{a}{2h})\right\}. \qquad (11)$$

The crystal and source windows used to derive (10) and (11) are given below by $f_c(x)$ and $f_s(x)$, respectively.

$$f_c(x) = \frac{h}{\sqrt{\pi}} e^{-h^2 x^2} \qquad (12)$$

$$f_s(x) = e^{a(x+d)} \quad , \quad -\infty < x \leq -d,$$

$$= 1 \quad , \quad -d \leq x \leq d,$$

$$= e^{-a(x-d)} \quad , \quad d \leq x < \infty. \qquad (13)$$

The value for h can be found from the width (0.16 mÅ) at half-maximum, and the values of a and d can be found from the plot labeled Type II in Fig. 22. Thus we find $h = 10.407 \text{ (mÅ)}^{-1}$, $d = 0.1175 \text{ mÅ}$, and $a = 65(\text{mÅ})^{-1}$ when all three quantities are expressed in terms of wavelength values. Using these values and (10) and (11), the instrumental window has been calculated. The plot of equation (10), normalized to unit height, is shown in Fig. 29. The composite profile made from the 18 observed profiles (without the decay correction) is also plotted here. The broadening of the profile is quite evident.

Now if the natural line profile and the instrumental window could be represented by Gaussian functions, their widths at half-maximum could
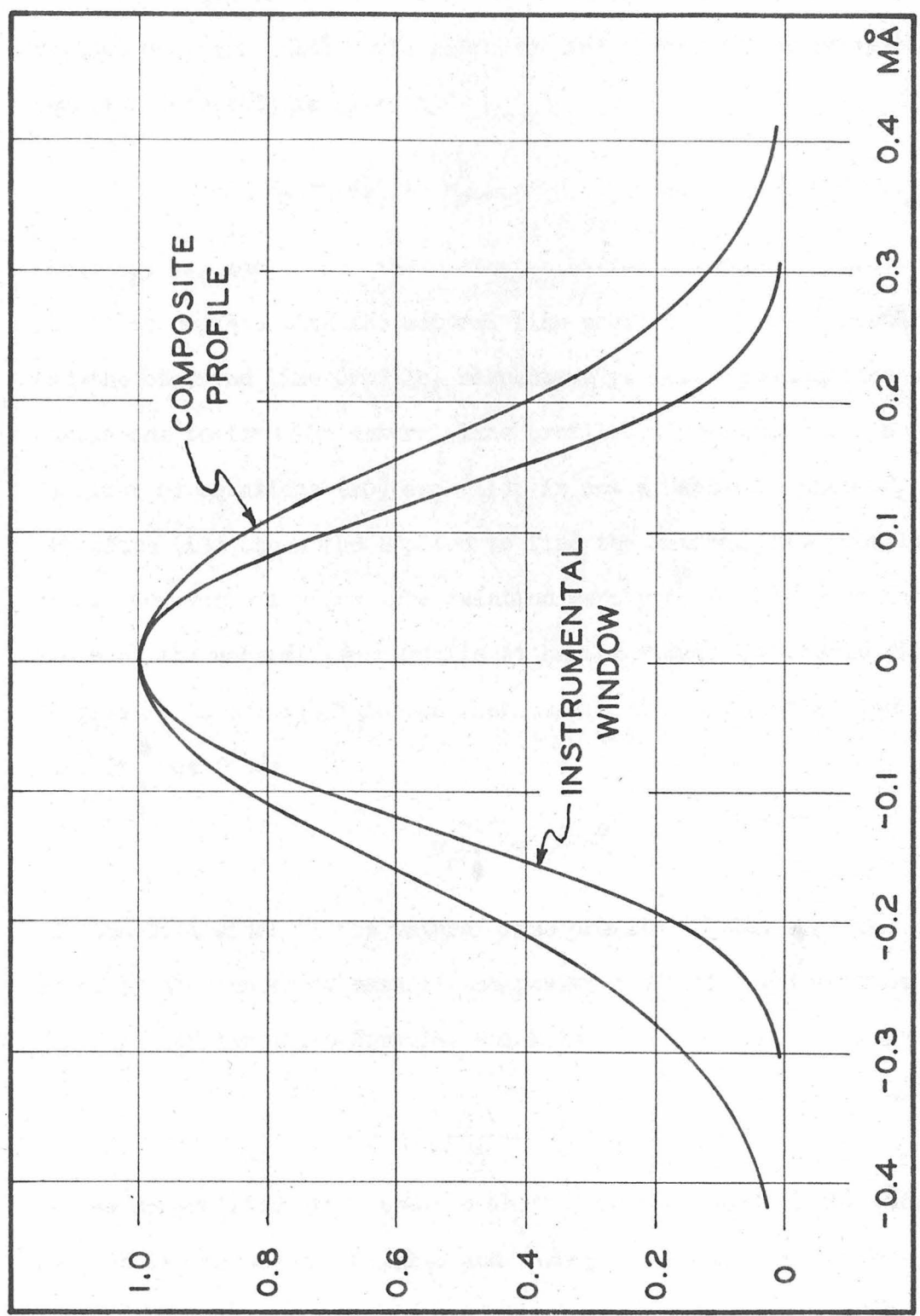
WIDTH OF COMPOSITE PROFILE AT HALF-MAXIMUM = 0.360 MÅ
WIDTH OF INSTRUMENTAL WINDOW AT HALF-MAXIMUM = 0.270 MÅ

FIG. 29 - COMPARISON OF INSTRUMENTAL WINDOW AND COMPOSITE PROFILE

be added in quadrature to obtain the width at half-maximum of the resultant Gaussian which would represent the observed line profile. In equation form this is given by

$$w_n^2 + w_i^2 = w_o^2 , \qquad (14)$$

where w_n, w_i, and w_o are the widths at half-maximum of the Gaussian functions representing the natural line profile, the instrumental window, and the observed line profile, respectively. This equation then would enable one to find the natural line profile. Obviously the window curve, as given by equations (10) and (11), is not a Gaussian function, and therefore (13) cannot be applied to find the natural line profile in toto. However, if we use the relation merely to find a value for the width of the natural line profile at half-maximum, the result will not be greatly in error. This has been done; using the widths given in Fig. 29, one finds

$$w_n = 0.238 \text{ m\AA} \qquad (15)$$

for the full width of the natural line profile at half-maximum. The speed of the center of mass of the positron-electron pair can be found from the Doppler shift formula, which is

$$\frac{\Delta\lambda}{\lambda} = \frac{v}{c} = \beta \qquad (16)$$

in the non-relativistic case. v in (16) is the speed of the center of mass, c is the speed of light, and $\Delta\lambda = \frac{1}{2} w_n$. Substituting for $\Delta\lambda$ and λ in (16) gives

$$\beta = 0.0049 , \qquad (17)$$

corresponding to a momentum

$$p = 9.8 \times 10^{-3} \, m_-c \ . \tag{18}$$

This result is in good agreement with that of the 1948 experiment[7] and the results of De Benedetti, et al,[18] which were obtained by an independent method. (Comparison of (17) and (18) with the 1948 experiment is valid, since the shape of the line profile observed at that time was not affected by the recently discovered systematic non-linearity.) The values of (17) and (18) indicate that, for the most part, only the conduction electrons take part in the annihilation process. M electrons might also play a small role in the process. These conclusions are discussed in more detail in references 7 and 18.

The half-life of Cu^{64} can also be determined from the observed profiles. To do this, the height of the profile peak above background and the corresponding time at which the peak was reached were used. Writing the exponential decay function,

$$N = N_o e^{-\lambda t} , \tag{19}$$

in its logarithmic form,

$$\log N = \log N_o - \lambda t , \tag{20}$$

we obtain a linear relation. Then, using the standard least-squares procedure for finding the straight line best fitting the observed data, we obtain the half-life. Because of a slight asymmetry in the profiles obtained on opposite sides of the spectrometer (the heights are not

equal), there are two separate sets of data to be analyzed. The average of the two values is

$$\tau_{\frac{1}{2}} = 12.77 \pm 0.14 \text{ hours.} \tag{21}$$

This is in good agreement with the results of Silver.[19]

B. Gamma-Radiation Following Decay of Au[198]

The discovery of the systematic non-linearity in the spectrometer,
and the method for making the necessary correction, made it advisable to
redetermine the wavelength of the 411 Kev gamma-ray line which follows
the decay of Au[198]. This experiment serves essentially three purposes:
(1) it provides a precise energy value for the calibration of β-ray
spectrometers; (2) it enables one to make a new determination of
$(m_- - m_+)/m_-$ from the data of Hedgran and Lind;[16] and (3) with the
high intensity possible with this source, high order reflections could
be used to find the wavelength, thus affording a check on the removal of
the systematic non-linearity.

Au[198] decays by β^- emission to Hg[198] in an excited state, which
then decays to its ground state by the emission of gamma-rays.[20-24]
The half-life for the process is 2.7 days. The decay scheme is given
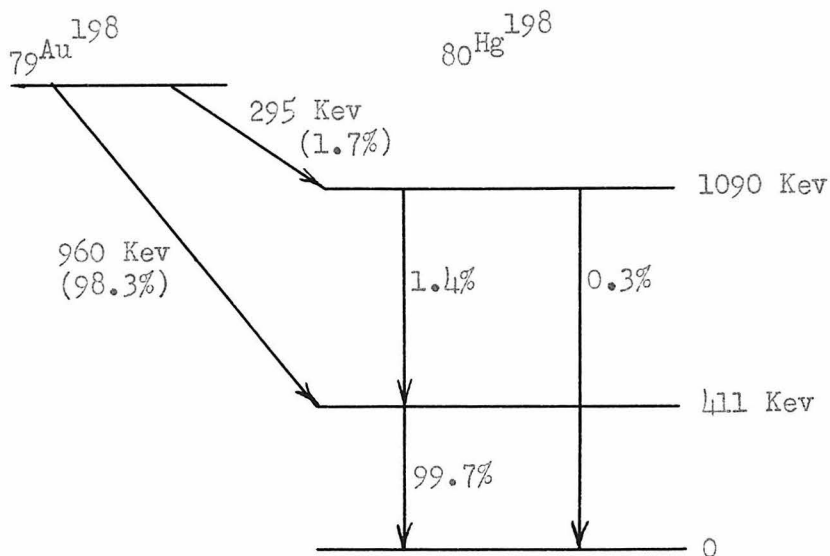below in Fig. 30. The 411 Kev gamma-ray is produced in 99.7 percent of

Fig. 30   Decay Scheme for Au[198]

all decays. This, together with the large neutron absorption cross-section (96.4 barns) of Au^{197}, assures the detection of high order re-flections if a large enough source is used.

The source was a piece of 24 carat gold foil, 0.006" x 0.197" x 1.25". This was held rigidly in an aluminum sandwich made from a piece of aluminum tubing squeezed flat. The front part of the sandwich was cut away so that there would be no absorbing material between the source and the crystal. The reactor at the Argonne National Laboratory was used for irradiation. The source had approximately 5 curies of activity on arrival in Pasadena.

Preliminary searches showed that the 2nd and 3rd order reflections could be detected. In addition, the 159 Kev line following the decay of Au^{199}(25) was detected. Au^{199} is produced by double neutron capture in Au^{197}. The 159 Kev line was intense enough for a wavelength measurement, but such a measurement was not possible because of the loss of almost two half-lives of activity because of electronic difficulties. These difficulties made it necessary to confine all measurements to the 411 Kev line.

A total of 2 runs in the 3rd order, 1 run in the 2nd order, and 10 runs in the 1st order was made. A counting interval of 20 minutes at each wavelength setting was used for the 2nd and 3rd order line profiles; this interval was sufficient to assure one percent counting statistics or better at the peak of the profile. For the 1st order runs, counting intervals of 2 to 4 minutes were used, depending on the source strength when the runs were made. A typical pair of profiles for the 1st order is shown in Fig. 31. To determine the composite profile, only the profiles obtained from the 1st order runs were used. Decay corrections were not

necessary, since only $2\frac{1}{2}$ hours or less was required to cross each profile. The 2nd and 3rd order profiles were also matched to this composite, after decay corrections had been made.

The final results of the experiment are given in Table VIII. The errors given in the last column were found by the procedure discussed in Section D, Part I. This error analysis is given in Table IX. The multiplicative factor used to convert from screw divisions was determined from an average of measurements made on the WK_{α_1} x-ray line immediately after the experiment. The factor (12396.44 ± 0.25) Kev - m$\overset{o}{A}$ [11] was used to change from wavelength to energy. The good agreement between the values obtained from the different orders of reflection indicates that the mirror correction has satisfactorily removed the effect of the systematic non-linearity. The variance due to counting statistics was essentially the same for all runs in the 1st order; therefore these runs were assigned equal weight. The values of the variances due to the 4 different factors which affect each run individually are given in Columns III-VI in Table IX. The appropriate mean of the sum of these values for all runs is given in Column VIII. The final variance, after the screw corrections which affect all runs identically have been applied, is given in Column XI. Column XII contains the weights to be assigned to the measurements in the different orders. The variance by internal consistency for the 1st order from Column VIII, $\sigma^2 = 0.52 \times 10^{-6}$ $(m\overset{o}{A})^2$, agrees well with the variance by external consistency, $\sigma^2 = 0.82 \times 10^{-6}$ $(m\overset{o}{A})^2$, computed from the values of Table VIII.

The half-life of Au^{198} was calculated from the data for the 1st

order profiles in the same way as from the Cu^{64} data. The average of the two values obtained (for reflections from opposite sides of the crystal planes) is

$$\tau_{\frac{1}{2}} = 2.74 \pm 0.04 \text{ days} \ .$$

This agrees with Silver's[19] value of 2.69 ± 0.015 days.

TABLE VIII

WAVELENGTH VALUES FOR THE 411 KEV GAMMA-RAY LINE
FOLLOWING DECAY OF AU 198

Order	Run No.	Wavelength in Screw Divisions	Average Wavelength in Screw Divisions*
1	1	30.018	
	2	30.016	
	3	30.017	
	4	30.017	
	5	30.010	
	6	30.015	
	7	30.014	
	8	30.013	
	9	30.019	
	10	30.019	30.016 ± 0.0028
2		30.019	30.019 ± 0.0023
3	1	30.021	
	2	30.021	30.021 ± 0.0016

Weighted Average*:

$$\lambda = 30.019 \pm 0.0012 \text{ screw divisions}$$

To get m$\overset{\circ}{A}$, multiply by 1.00285 ± 0.0000786.

Final Results*:

$$\lambda = 30.105 \pm 0.0026 \text{ m}\overset{\circ}{A}$$

$$E = 411.770 \pm 0.036 \text{ Kev}$$

* All errors are standard deviations. These are given to an extra place to avoid incorrect weighting when combining these results with those of other experimenters.

TABLE IX

ERROR ANALYSIS FOR THE 411 KEV GAMMA-RAY LINE FOLLOWING DECAY OF AU 198

Variances for λ in 10^6 $(m\overset{\circ}{A})^2$

| I	II	III	IV	V	VI	VII	VIII	IX	X	XI	XII
Order	No. Runs	Counting Statistics	Matching Profiles	Random Variation in Screw Readings	Mirror Correction	$\sum$ Columns III-VI	σ_λ^2 for mean of all runs before screw corrections	Main Screw Correction	Quasi-Periodic Correction	Total of Columns VII-X	Weight
1	10	0.025	2	1.2	2	5.225	0.522	2.25	5	7.77	1
2	1	0.323	0.5	0.3	0.5	1.623	1.623	2.25	1.25	5.12	1.52
3	2	0.028	0.222	0.133	0.222	0.605	0.302	1.25	0.556	2.11	3.68
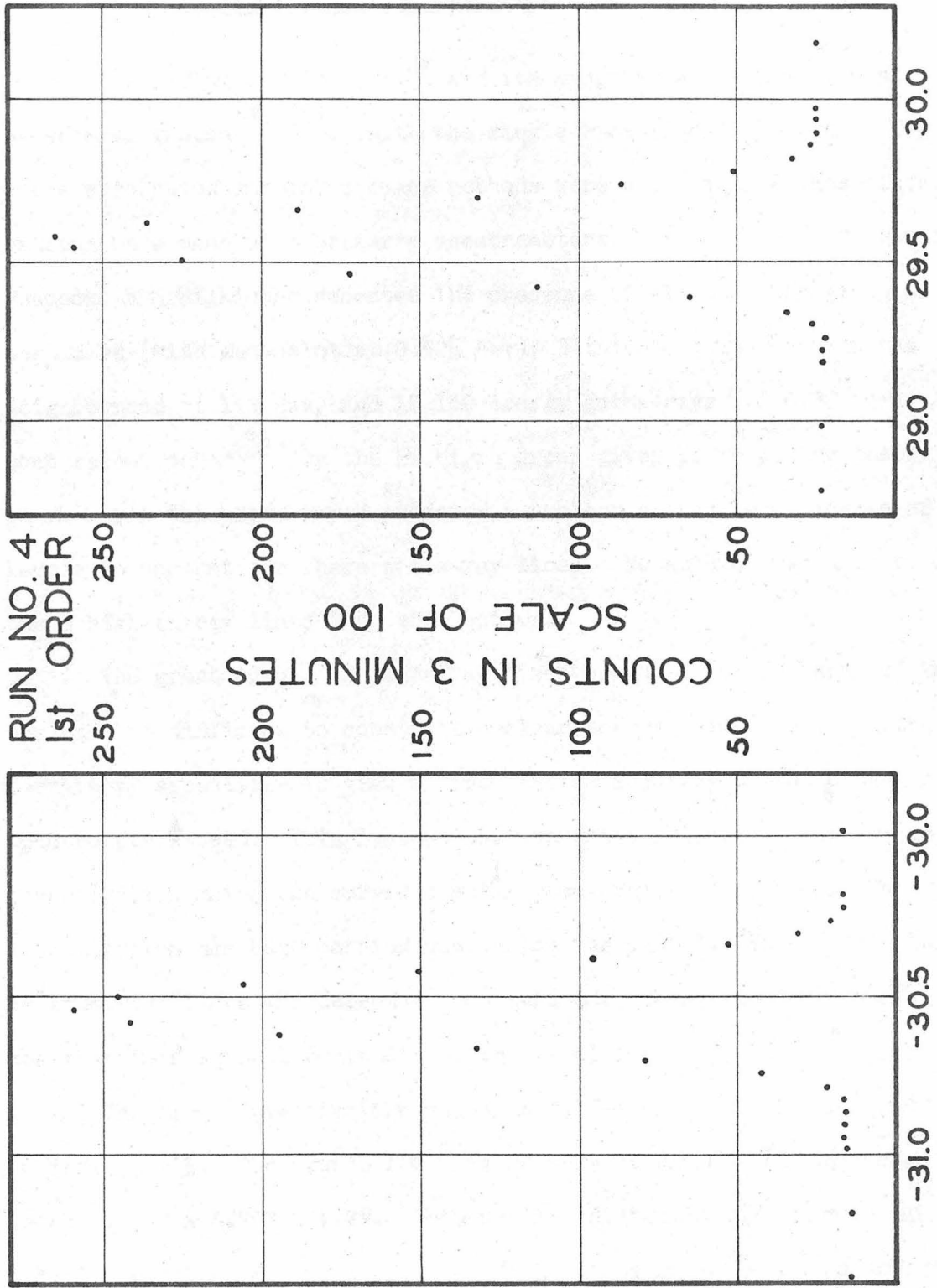
FIG. 31 – 411 KEV GAMMA–RADIATION FOLLOWING DECAY OF AU^{198}

C. Gamma-Radiation Following Decay of Ta^{182}

The radiations from Ta^{182} and its daughter W^{182} have been studied by several groups[26-33]. With the single exception of reference 29, where absorption and coincidence methods were used, all of these investigations were made with beta-ray spectrometers. In reference 32 Beach, Peacock, and Wilkinson reported the presence of at least one group of beta particles (with end-point at 0.525 Mev), 3 intense gamma-rays in the neighborhood of 1.2 Mev, and 17 low energy gamma-rays (< 0.33 Mev). The most recent paper[33] by the Michigan group gives 14 to 18 low energy gamma-rays; this same paper proposes a nuclear energy level scheme of 8 levels to account for these gamma-ray lines. No attempt was made to fit the 3 high energy lines into this scheme.

The great number of gamma-ray lines produced in the decay of Ta^{182} has made it difficult to construct nuclear energy level schemes with certainty, especially in view of the limited accuracy of the beta-ray spectrometers used. This isotope was therefore selected for a precision investigation using the curved crystal gamma-ray spectrometer. This investigation has been carried out during the past two years. A total of 16 gamma-ray lines was detected and measured. These lines can be fitted together into several tentative energy level schemes.

The first investigation was made by James Brown, and is reported in reference 5. The source for this experiment was a strip of tantalum metal 0.004" x 0.20" x 1.2". This was irradiated at Oak Ridge to an activity of about 500 millicuries. With this source the 3 high energy lines and 6 low energy lines were detected and measured. Lines below about 125 Kev could not be detected for two reasons: (1) self-absorption

in the source limited the useful activity at these energies to a very thin section at the front of the source, and (2) the multi-cellular Geiger counter in use at the time of the experiment had an extremely low efficiency in this energy region. One line (at 156 Kev) was accidentally missed in the initial search run. The 9 lines measured were insufficient, in themselves, for the formulation of an energy level scheme.

In an attempt to increase the amount of information obtainable with the spectrometer a second source, 0.011" x 0.054" x 1.2", was prepared. The width was increased over that of the first source to increase the intensity of the low energy radiation; the depth was decreased to remove the essentially useless portion. Irradiation in the Argonne reactor for one half-life (120 days) produced an activity of 300 millicuries. During the interval between the two experiments the scintillation counter was completed and installed in the spectrometer. Thus an increase in over-all luminosity was achieved by a redesign of the source and an improvement in the detector. With this source 18 gamma-rays were detected in the search runs. In addition, the $K\alpha_1$, α_2, β_1, β_3, and β_2 x-rays of tungsten and the $K\alpha_1$, α_2, β_1, and β_3 x-rays of tantalum were detected. The x-rays of hafnium were not detected; thus there is no evidence for K-capture in Ta^{182}. The detection of the $WK\alpha_1$ x-ray line permitted the instrument to be calibrated without the installation of the heavy x-ray tube and its stiff high voltage cables, which could easily produce mechanical flexures in the spectrometer. Such a calibration was performed both before and after the gamma-ray measurements, and the method has been used in connection with every subsequent experiment.

Satisfactory measurements were obtained for 16 of the gamma-ray lines.

The final results are presented in Table XI. One of the remaining two lines, at about 108 Kev, was so weak that it could not be detected sufficiently well for a good measurement. The other line, at about 250 Kev, appeared as a strong line during two different search runs, but decayed below the minimum intensity for measurement during the one month interval between the searches and the measurements. This is definitely contrary to the known half-life of 120 days of Ta^{182}. Since the two searches in which the line was detected were about a week apart and on opposite sides of the instrument, it is difficult to explain this effect by a freakish behavior of the spectrometer. Comparison with the adjacent 264 Kev line in the two search runs indicates a half-life of about 7 - 10 days for the 250 Kev line. This effect is to be investigated with a new source of Ta^{182} in the near future.

The wavelengths of the 16 lines as measured in the different runs made with the second source are given in Table X. These values are in screw divisions, and include all the necessary corrections up to the final conversion to mÅ. The corrections are those determined by the new calibration (discussed in Section C, Part I), which was performed after the measurements had been made. For this reason, a calibration curve was necessary for the mirror correction. Since hysteresis effects cannot be included in such a curve, the measurements might be more in error than is indicated by their external consistency. Consequently, the arbitrary value of 0.010 screw divisions was assigned as the error. This value is believed to be large enough to account for errors due to hysteresis. In the case of the line designated by the letter B, the source was so wide that although the line could be resolved from the adjacent line A

TABLE X

OBSERVED WAVELENGTHS IN SCREW DIVISIONS FOR 16
GAMMA-RAY LINES FOLLOWING DECAY OF TA 182

Identification Letter	Run No.	Wavelength	Average Wavelength	Assigned Error
A		10.108	10.108	0.010
B*		10.411	10.411	0.015
C		11.028	11.028	0.010
D		46.819	46.819	0.010
E		53.930	53.930	0.010
F		55.682	55.682	0.010
G		62.350	62.350	0.010
H		68.936	68.936	0.010
I	1	79.070		
	2	79.072	79.071	0.010
J		81.126	81.126	0.010
K	1	106.230		
	2	106.226		
	3	106.224	106.226	0.010
L	1	108.788		
	2	108.788	108.788	0.010
M	1	123.528		
	2	123.533	123.530	0.010
N	1	146.030		
	2	146.038	146.034	0.010
O	1	182.538		
	2	182.532	182.535	0.010
P	1	188.143		
	2	188.166	188.154	0.010

* λ_B was determined by adding the difference $\lambda_B - \lambda_A = 0.303$, as found by J. R. Brown[5], to the value of λ_A above. For this reason the larger error 0.015 has been assigned to λ_B.

TABLE XI

WAVELENGTHS, ENERGIES, AND RELATIVE INTENSITIES*
OF GAMMA-RADIATION FOLLOWING DECAY OF TA 182

Identification Letter	Wavelength in mÅ	Energy in KEV	Relative Intensity*
A	10.134 ± 0.010	1223.25 ± 1.21	334
B#	10.437 ± 0.015	1187.74 ± 1.70	157
C	11.057 ± 0.010	1121.14 ± 1.02	352
D	46.941 ± 0.011	264.086 ± 0.060	27
E	54.070 ± 0.011	229.266 ± 0.046	24
F	55.827 ± 0.011	222.051 ± 0.044	45
G	62.512 ± 0.011	198.305 ± 0.036	9
H	69.115 ± 0.011	179.360 ± 0.030	19
I	79.277 ± 0.012	156.369 ± 0.024	14
J	81.337 ± 0.012	152.408 ± 0.023	43
K	106.500 ± 0.013	116.398 ± 0.014	2
L	109.071 ± 0.013	113.655 ± 0.014	9
M	123.851 ± 0.014	100.092 ± 0.012	46
N	146.414 ± 0.015	84.667 ± 0.009	6
O	183.010 ± 0.018	67.736 ± 0.007	100
P	188.643 ± 0.018	65.714 ± 0.006	9

* All factors except internal conversion have been taken into account
in calculating the relative intensities.

The wavelength of line B was found by adding to the wavelength of
line A given above the difference in the wavelengths of lines B and
A as found by J. R. Brown.

with the aid of the composite profile, the accuracy of the determination
was seriously impaired. Therefore the following procedure was adopted:
the wavelength of line A was determined from the data obtained with the
second (wide) source; then the difference, $\lambda_B - \lambda_A$, determined with
the first source, for which the lines were clearly resolved, was added
to the wavelength of line A to get the wavelength of line B. This
difference in resolution is shown in Fig. 23 (Section E, Part I). The
value obtained in this manner is believed to be more reliable; however,
a larger error (0.015 screw divisions) has been assigned to this line.

Originally it was intended to combine the measurements made with
the second source with those made with the first source. Therefore,
only one run was made for each of the lines previously measured. Com-
parison of the data from the two experiments, however, showed a dis-
couraging apparent lack of reproducibility in the measurements of the
first experiment. A variation in results of this magnitude occurred in
none of the cases where several measurements were made with the second
source. A review of the procedures followed in the first experiment
showed that several lines were measured during a single run. The lines
were run (in order of decreasing wavelength) on one side of the instrument,
and then (in opposite order) on the opposite side. As much as two weeks
elapsed between delineations of the two members of a pair of profiles.
There could easily be slight changes in the instrument during a period of
several days which would be sufficient to cause the observed variations.
This procedure was not used with the second source; profiles from opposite
sides of the instrument for a given line were determined in immediate
succession. The results from the first experiment have been rejected

principally for this reason. Only the results from the second experiment are reported and discussed here.

The final values for the experiment are given in Table XI. The energies were found from the wavelengths by using the conversion factor 12396.44 ± 0.25 Kev - mÅ.[11] Errors were computed from the assigned error for the wavelength and the errors of the conversion factors. To determine the relative intensities, the observed intensities (measured by the heights of the peaks above background) were corrected for (1) the reflection coefficient of the crystal, which is proportional to λ^2, (2) self-absorption in the source, and (3) counter efficiency. Internal conversion could not be taken into account because neither the nature of the radiation nor the internal conversion coefficients (for the lower energies) are known.

Because of the complexity of any nuclear energy level scheme containing more than 10 gamma-ray lines, it is desirable to use a systematic method for determining possible level schemes. Such a method has been devised by D. E. Muller[6,9]. A brief description will be given here. The initial process is to form a matrix containing the sum and difference of each pair of gamma-ray energies. Then, according to the Ritz Combination Principle, one can select those quantities which seem to obey equations of the form $X + Y = W$, $X + Y = U + V$, and $X + Y = U - V$, where X, Y, U, V, and W are gamma-ray energies. All of the equations obtainable from the matrix will not be independent; however, it is a relatively easy matter to select those which can be considered independent. Furthermore, it is likely that there will be some "accidental" equations, that is,

some equations which do not fit into the final scheme at all. It is
very probable that there are equations which agree with the actual level
scheme (as yet unknown) which cannot be found from the matrix of sums
and differences. Nevertheless, a good start can be made with the matrix.
Seventeen equations obtained from the matrix for the 16 measured gamma-
rays are listed in Table XII. The criteria used in selecting the equations
are explained in the footnotes to the table. Both the actual discrepancy
and the standard deviation for each equation are given in the table.

The second step is to construct a topological "map" using these
equations. The first 5 equations were chosen as a starting nucleus,
since none of them has a discrepancy of more than 100 electron-volts.
The resulting map for the 10 lines contained in these equations is shown
in Fig. 32. The gamma-ray lines are indicated by capital letters and
the energy levels by lower case letters. It is important to note that
this map is not a unique assignment for these 10 lines. For example,
lines I and F can be interchanged without affecting equation (2). For
simplicity we shall refer to this interchange as a rotation about P.
Similarly, J and O can be rotated about N. Thus there are 4 permutations
of this map, each representing a different energy level arrangement.
These 4 maps and their associated energy level schemes are given in
Figs. 33 - 36. If these 10 lines represented the totality of lines from
this source, each of the 4 level schemes could be inverted without altering
the equations, thus doubling the number of possible schemes. Clearly the
topological map can only enumerate the possible level schemes; selection of
the proper scheme must be made on the basis of additional information.
Relative intensities, known beta-rays associated with the decay process,

TABLE XII

EQUATIONS* FOR DETERMINING THE ENERGY LEVEL SCHEME FOR W 182

I		II	III Discrepancy: Column I - Column II in KEV#	IV Standard Deviation in KEV	V Identification Number
G + P	=	D	- 0.067	0.070	(1)
I + P	=	F	- 0.059	0.068	(2)
L + N	=	G	0.017	0.039	(3)
L + P	=	H	0.009	0.034	(4)
N + O	=	J	- 0.005	0.025	(5)
C + O	=	B	1.14	1.99	(6)
M + C	=	A	- 2.02	1.58	(7)
A + G	=	B + E	4.55	2.09	(8)
A + K	=	B + I	- 4.46	2.09	(9)
A + K	=	B + J	- 0.50	2.09	(10)
A + E	=	B + D	0.69	2.09	(11)
A + L	=	B + J	- 3.24	2.09	(12)
A + N	=	B + K	3.78	2.09	(13)
A + M	=	C + G	3.90	1.58	(14)
B + J	=	C + F	- 3.04	1.99	(15)
B + K	=	C + H	- 3.64	1.99	(16)
C + P	=	B	- 0.89	1.99	(17)

* Only independent equations are listed here.

\# Equations containing two of lines A, B, and C have been rejected
if the discrepancy was over 5 KEV. Equations not containing any
of the lines A, B, and C have been rejected if the discrepancy
was more than 5 times the standard deviation.
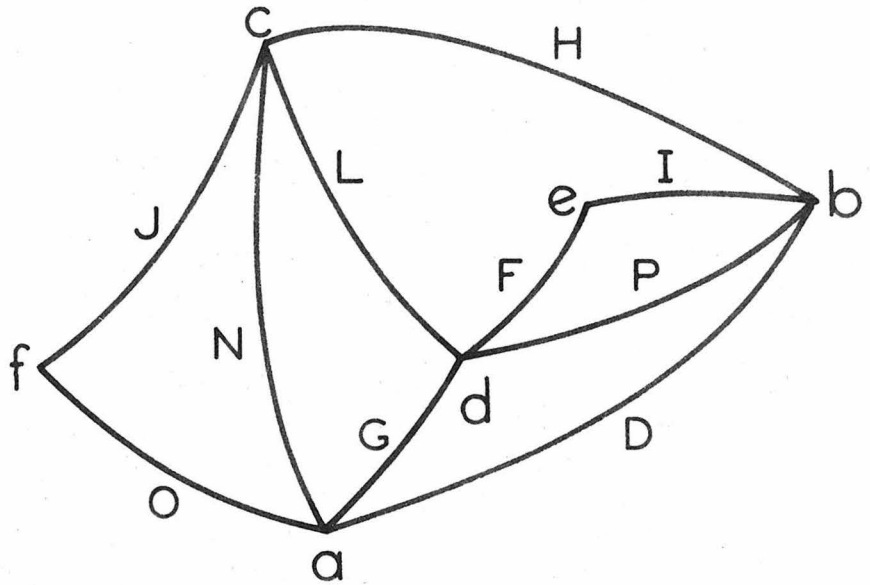
FIG. 32 - A TOPOLOGICAL MAP FOR
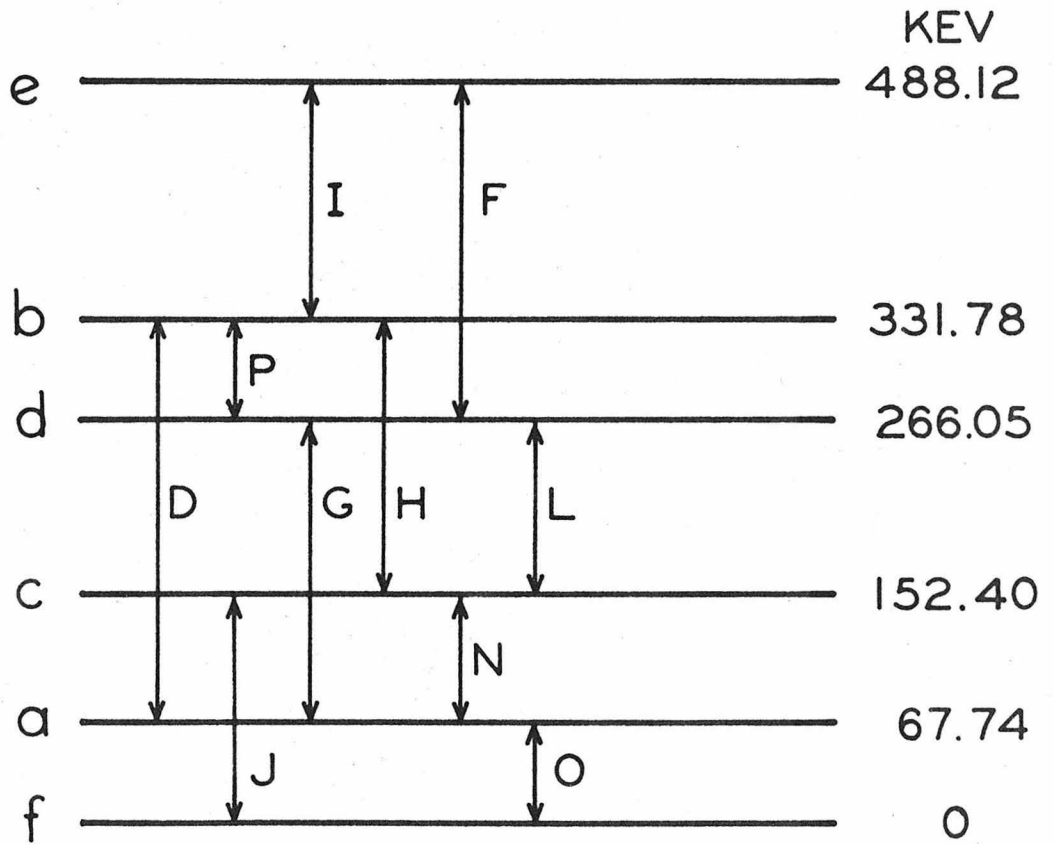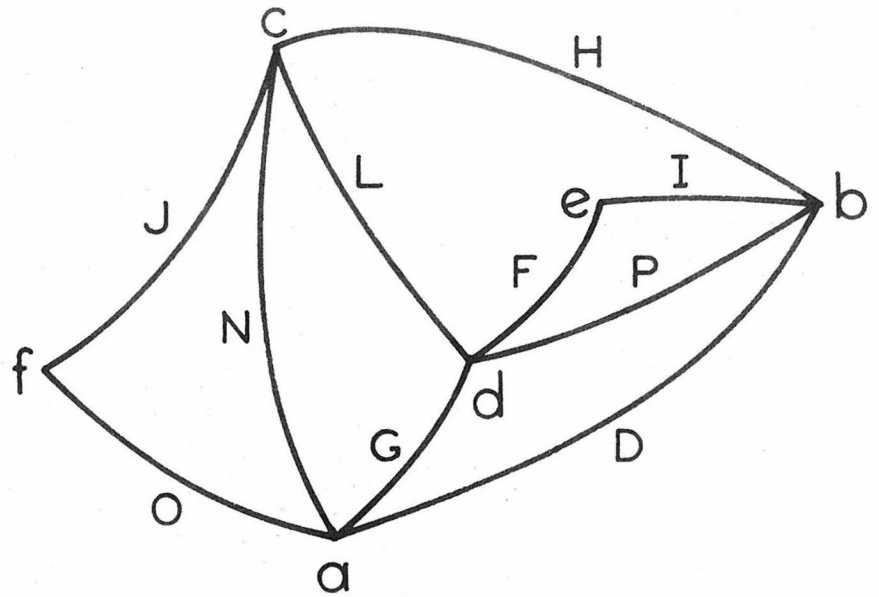THE FIRST FIVE EQUATIONS
OF TABLE XII

FIG. 33- A POSSIBLE ENERGY LEVEL
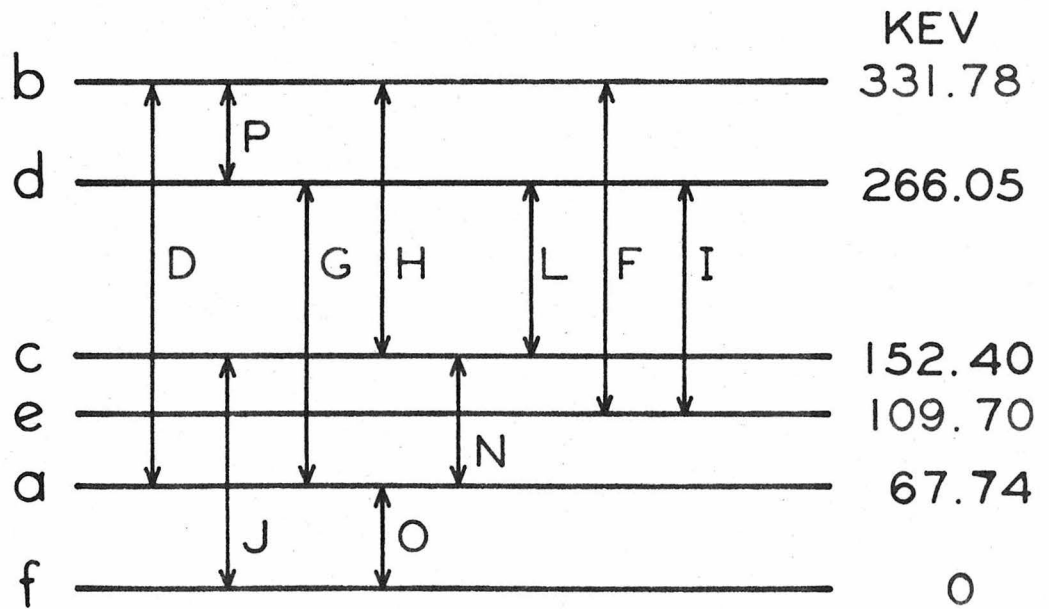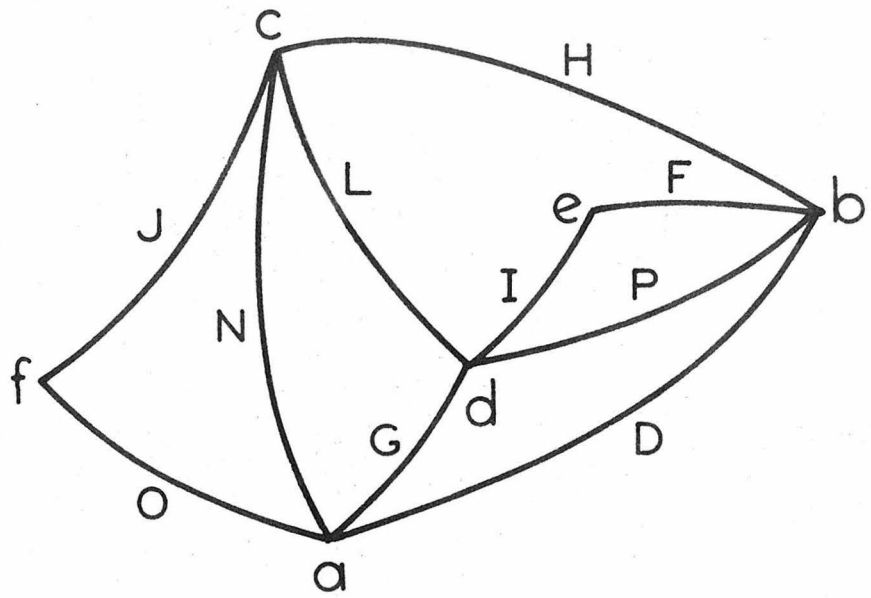SCHEME FOR 10 GAMMA-RAY
LINES FROM W 182

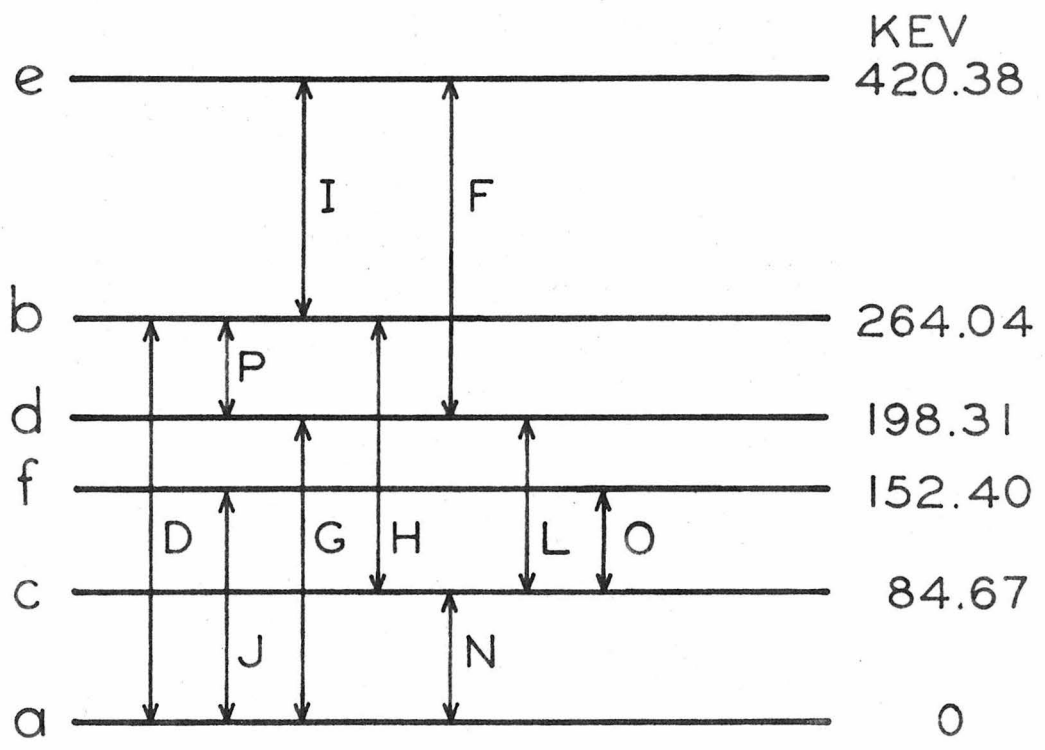FIG. 34 — A POSSIBLE ENERGY LEVEL
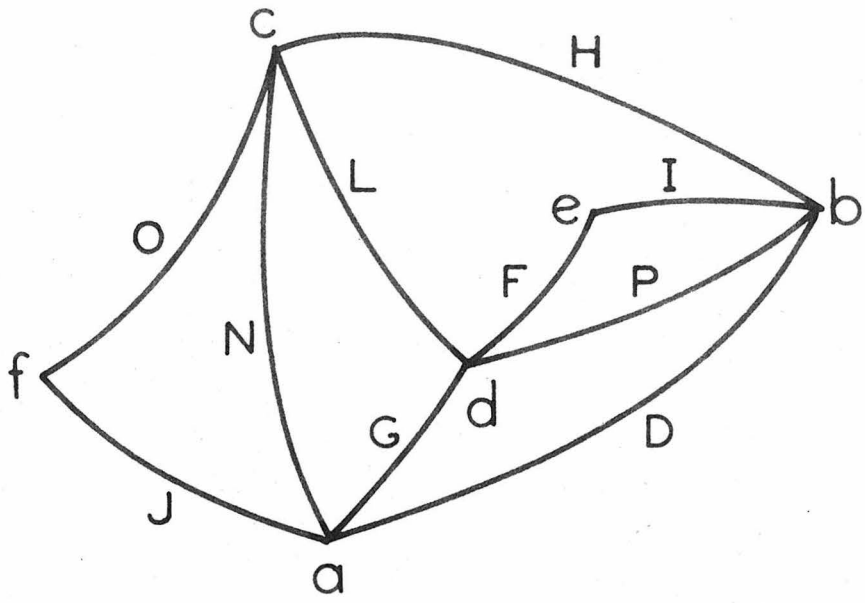SCHEME FOR 10 GAMMA-RAY
LINES FROM W 182

FIG. 35 — A POSSIBLE ENERGY LEVEL
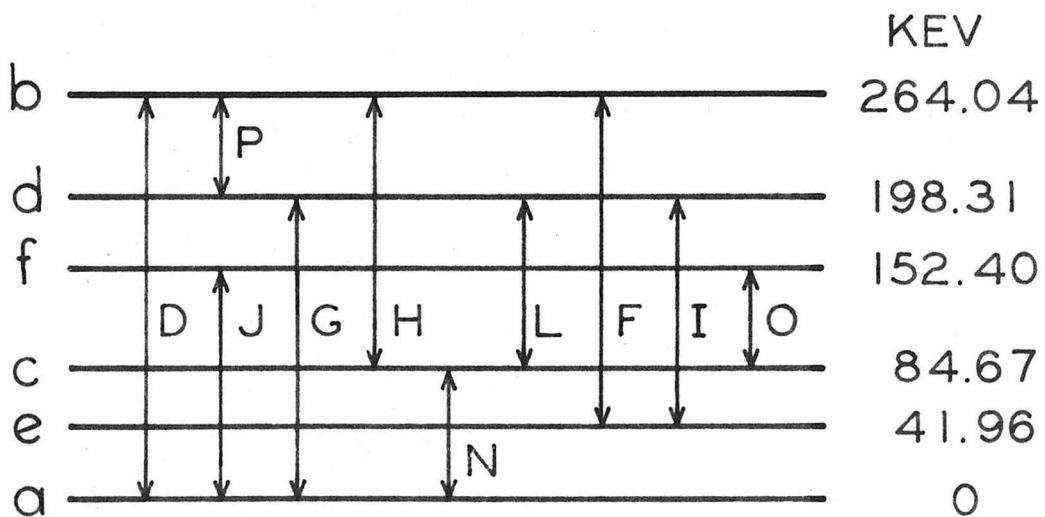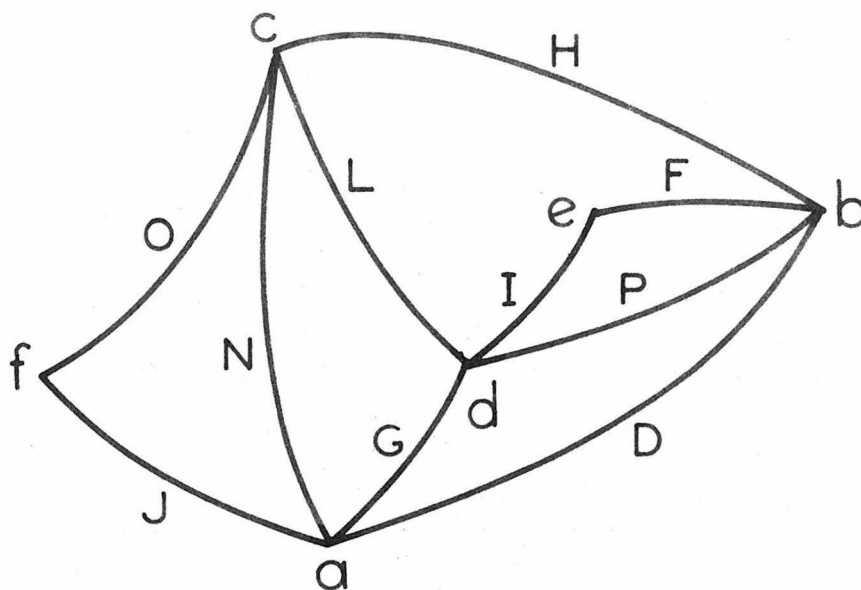SCHEME FOR 10 GAMMA-RAY
LINES FROM W 182

FIG. 36-A POSSIBLE ENERGY LEVEL
SCHEME FOR 10 GAMMA-RAY
LINES FROM W 182

internal conversion coefficients, etc., are part of such information.

Unquestionably the 16 measured lines are not the only lines produced during the decay of Ta^{182} and its daughter W^{182}. For this reason it is conceivable that some of the observed lines might not fit into a level scheme devised solely on the basis of the 16 lines measured with the gamma-ray spectrometer. This indeed turns out to be the case. The difficulty arises with lines E and K; it seems impossible to include both of these lines in a level scheme based on the data now available. Furthermore, the more satisfying of the seemingly possible schemes contain neither E nor K. A second obstacle is the low precision of the measurements of the high energy lines A, B, and C. These are known at best to only 1.2 Kev (about 0.1%), whereas all of the remaining lines are known to 0.06 Kev or better (< 0.03%). This lack of precision makes it difficult to select the proper equations from equations (6) - (17) of Table XII. The value of the discrepancy is not too reliable here; nevertheless, since it is practically all that is available to aid in making a decision, it must be used.

The only data available on line intensities is that obtained from this experiment. This is given in Table XI. These values have not been corrected for internal conversion, and such a correction might alter the values drastically. This must be kept in mind when using the relative intensities to eliminate schemes. The experiment of Beach, Peacock, and Wilkinson[32] furnishes some information about the beta-rays emitted during the decay process. A very definite end-point was found at 525 Kev. There were no observed beta-rays above this energy. There were some slight indications of beta-rays with end-points at 300 Kev or less, but this

evidence was not conclusive. Nevertheless, the possibility cannot be
ruled out entirely.

The arguments which are used to eliminate level schemes are essential-
ly two in number: (1) One or more fairly strong lines will end on a level
above ground state from which there are no observed gamma-rays. If we
assume that a strong line should beget an observable line (except when
going to ground state), such a "hanging" level seems unlikely. (2) One
or more fairly strong lines will leave a level to which there are neither
observed gamma-rays nor possible beta-rays. Such "unfed" levels also
seem unlikely. On the basis of these two arguments one can eliminate a
large number of the schemes corresponding to permutations of the original
topological map.

A large number of attempts have been made to obtain a satisfactory
level scheme containing a maximum number of lines. On the whole the
results have been rather unsatisfactory. First, there are a large number
of maps containing 14 or 15 lines to start from, each map having 24 or
more permutations. Second, the reasons for selecting a single preferred
permutation of a given starting map become rather nebulous in several
cases. Only two of these possibles are presented here, in Figs. 37 and
38. The energy level schemes have been omitted, and only the proper
permutations of the respective topological maps are given in the figures.

The unsatisfactory nature of the final results clearly indicates
a need for further precision work on the decay of Ta^{182}. A program of
joint experiments with the gamma-ray spectrometer, the newly developed
axial focussing homogeneous magnetic field beta-ray spectrometer[34,35],
and coincidence equipment is now being planned. Measurements with these

three different types of equipment will give (1) the high energy values
to less than 0.1 Kev, (2) many additional gamma-ray lines, (3) the
β-rays emitted by Ta^{182}, and (4) the internal conversion coefficients
for many of the gamma-rays. With this information there is a reasonable
possibility that the actual energy level scheme can be found.

In spite of the fact that a final level scheme for W^{182} cannot be
determined on the basis of the information now available, a considerable
advance has been made. The remarkable agreement of equations (1) - (5)
in Table XII makes it reasonably certain that one of the level schemes of
Figs. 33 - 36 will form the nucleus of the final level scheme, when it
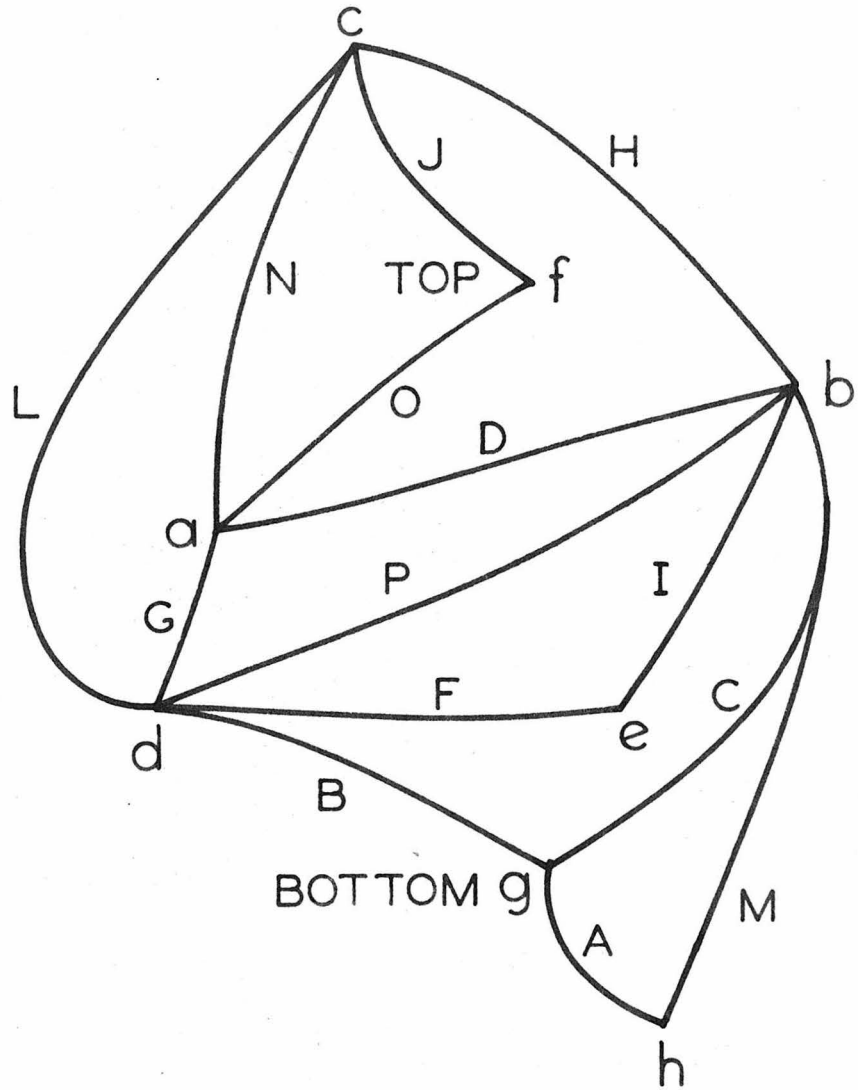is found.

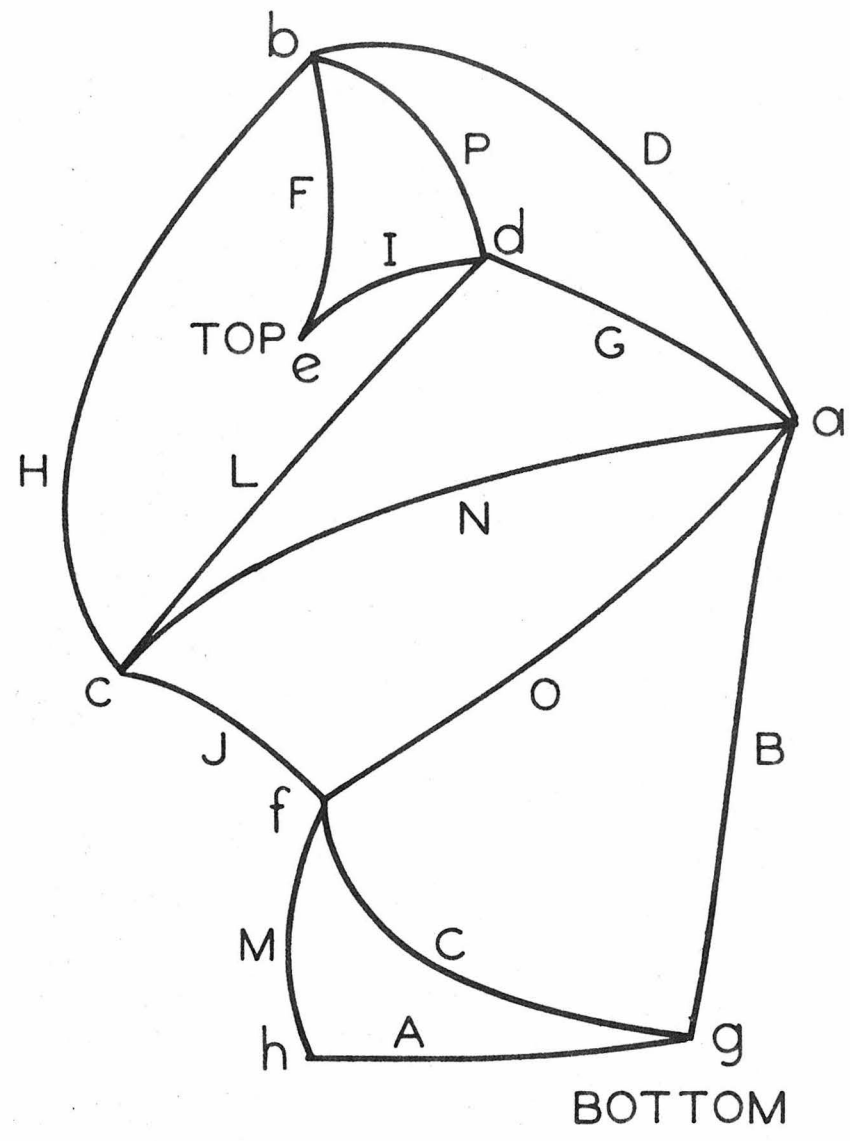FIG. 37 - A POSSIBLE ENERGY
LEVEL SCHEME FOR W 182

FIG. 38 — A POSSIBLE ENERGY
LEVEL SCHEME FOR W 182

BIBLIOGRAPHY

1. Jesse W.M. DuMond and Harry A. Kirkpatrick, Review of Scientific Instruments $\underline{1}$, 88 (1930)

2. Jesse W.M. DuMond, Review of Scientific Instruments $\underline{18}$, 626 (1947)

3. Y. Cauchois, Journal de Physique et le Radium, Series 7, No. 3, 320 (1932)

4. David A. Lind, Review of Scientific Instruments $\underline{20}$, 233 (1949)

5. James R. Brown, Thesis, California Institute of Technology (1951)

6. David E. Muller, Thesis, California Institute of Technology (1951)

7. Jesse W.M. DuMond, David A. Lind, and Bernard B. Watson, Physical Review $\underline{75}$, 1226 (1949)

8. Jesse W.M. DuMond and E. Richard Cohen, Reviews of Modern Physics $\underline{20}$, 82 (1948); (21), 651 (1949)

9. David E. Muller, Harry C. Hoyt, David J. Klein, and Jesse W.M. DuMond, Physical Review (to be published)

10. Bernard B. Watson, William J. West, David A. Lind, and Jesse W.M. DuMond, Physical Review $\underline{75}$, 505 (1949)

11. Jesse W.M. DuMond and E. Richard Cohen, Report to the National Research Council Committee on Constants and Conversion Factors of Physics, December, 1950; Physical Review $\underline{82}$, 555 (1951)

12. D. A. Lind, W. J. West, and J.W.M. DuMond, Physical Review $\underline{77}$, 475 (1950)

13. David A. Lind, Thesis, California Institute of Technology (1948)

14. David J. Klein, Thesis, California Institute of Technology (1951)

15. Jesse W.M. DuMond, Physical Review $\underline{81}$, 468 (1951)

16. Arne Hedgran and David A. Lind, Physical Review $\underline{82}$, 126 (1951)

17. Gunnar Lindström, Physical Review $\underline{83}$, 465 (1951)

18. S. DeBenedetti, C. E. Cowan, and W. R. Konneker, Physical Review $\underline{76}$, 440 (1949); S. DeBenedetti, C. E. Cowan, W. R. Konneker, and H. Primakoff, Physical Review $\underline{77}$, 205 (1950)

19. L. M. Silver, Physical Review $\underline{76}$, 589A (1949)

20. R. W. Pringle and S. Standil, Physical Review 80, 762 (1950)

21. L. G. Elliott and J. L. Wolfson, Physical Review 82, 333A (1951)

22. A. R. Brossi, B. H. Ketelle, H. Zeldes, and E. Fairstein, Physical Review 84, 586 (1951)

23. Cavanagh, Turner, Booker, and Dunster, Proceedings of the Physical Society (London) A64, 13 (1951)

24. Patrick E. Cavanagh, Physical Review 82, 791 (1951)

25. P. M. Sherk and R. D. Hill, Physical Review 83, 1097 (1951)

26. R. V. Zumstein, J. D. Kurbatov, and M. L. Pool, Physical Review 63, 59 (1943)

27. W. Rall and R. G. Wilkinson, Physical Review 71, 321 (1947)

28. J. M. Cork, Physical Review 72, 581 (1947)

29. C. E. Mandeville and M. V. Scherb, Physical Review 73, 340 (1948)

30. J. M. Cork, H. B. Keller, J. Sazynski, W. C. Rutledge, and A. E. Stoddard, Physical Review 75, 1778 (1949)

31. C. H. Goddard and C. S. Cook, Physical Review 76, 1419 (1949)

32. L. A. Beach, C. L. Peacock, and R. G. Wilkinson, Physical Review 76, 1585 (1949)

33. J. M. Cork, H. B. Keller, W. C. Rutledge, and A. E. Stoddard, Physical Review 78, 95 (1950)

34. J. W. M. DuMond, L. Bogart, J. L. Kohl, D. E. Muller, and J. R. Wilts, Special Technical Report No. 16, California Institute of Technology, March 1952

35. James R. Wilts, Thesis, California Institute of Technology (1952)